ISTANBUL TECHNICAL UNIVERSITY ★ GRADUATE SCHOOL

AN EXPERIMENTAL STUDY ON THE BEHAVIOR OF SQUARE SHORT CONCRETE COLUMNS CONFINED WITH HYBRID FRP UNDER MONOTONIC AXIAL COMPRESSION STRESS

M.Sc. THESIS

Bilal Ibrahim Majeed AL-OUBAIDI

Department of Civil Engineering

Structural Engineering Programme

FEBRUARY 2024

ISTANBUL TECHNICAL UNIVERSITY ★ GRADUATE SCHOOL

AN EXPERIMENTAL STUDY ON THE BEHAVIOR OF SQUARE SHORT CONCRETE COLUMNS CONFINED WITH HYBRID FRP UNDER MONOTONIC AXIAL COMPRESSION STRESS

M.Sc. THESIS

Bilal Ibrahim Majeed AL-OUBAIDI
(501201007)

Department of Civil Engineering

Structural Engineering Programme

Thesis Advisor: Assoc. Prof. Dr. Medine İSPİR ARSLAN

FEBRUARY 2024

İSTANBUL TEKNİK ÜNİVERSİTESİ ★ LİSANSÜSTÜ EĞİTİM ENSTİTÜSÜ

MONOTONİK EKSENEL BASINÇ YÜKLEMESİ ALTINDA HİBRİT LİFLİ POLİMER MALZEME İLE SARGILANMIŞ KARE BETON KOLONLARIN DAVRANIŞI ÜZERİNE DENEYSEL BİR ÇALIŞMA

YÜKSEK LİSANS TEZİ

Bilal Ibrahim Majeed AL-OUBAIDI
(501201007)

İnşaat Mühendisliği Anabilim Dalı

Yapı Mühendisliği Programı

Tez Danışmanı: Assoc. Prof. Dr. Medine İSPİR ARSLAN

ŞUBAT 2024

Bilal Ibrahim Majeed AL-OUBAIDI, a M.Sc. student of ITU Graduate School student ID 501201007 successfully defended the thesis entitled "AN EXPERIMENTAL STUDY ON THE BEHAVIOR OF SQUARE SHORT CONCRETE COLUMNS CONFINED WITH HYBRID FRP UNDER MONOTONIC AXIAL COMPRESSION STRESS", which he/she prepared after fulfilling the requirements specified in the associated legislations, before the jury whose signatures are below.

Thesis Advisor :	**Assoc. Prof. Dr. Medine İSPİR ARSLAN** Istanbul Technical University	.....
Jury Members :	**Prof. Dr. Abdullah Gedikli** Istanbul Technical University	.....
	Assoc. Prof. Dr. Hasan Özkaynak Beykent University	.....
		.....

Date of Submission : **8 FEBRUARY 2024**
Date of Defense : **6 FEBRUARY 2024**

By the name of Allah, The Merciful

FOREWORD

The thesis is realized as part of the project 221M159, supported by TÜBİTAK. This support was crucial in helping me achieve this work. TÜBITAK's backing not only made my research possible but also inspired me to work harder and contribute meaningful solutions to our field.

I would like to thank my advisor Assoc. Prof. Dr. Medine İspir Arslan for her guidance and understanding. Prof. Alper Ilki and Dr.Korhan Deniz Dalgıç deserve my sincere gratitude for their outstanding aid and direction during my research path. I am grateful to Res. Ass. Ali Gürkan Genç for his advice and guidance. I'd also want to thank my colleague, Ismail Sencar, for being a constant companion and support during this study trip. Sharing this journey with Ismail has not only made it more pleasurable, but has also helped greatly to the success of our project.

I'd like to thank Mustafa Khattab, Feras Abla, şhabeddin Rifai and Mohammed Tareq for their crucial psychological support and aid along this journey. Their unselfish and compassionate contribution, which went far beyond professional advise, gave me the strength and support I needed to navigate through difficult circumstances.

I especially thank my friend Aristo Taufiq, who had made it possible for me to finish this thesis by the time I needed it. With his deeds I am now become aware of the kindness that a person could possess and make difference.

Last but not least, my heartfelt thanks go to my family, whose unflinching faith in me has been the foundation of my path. Their unwavering financial and psychological support has been the cornerstone of my strength and resolve through thick and thin. Their unwavering support and trust in my talents has kept my spirits high throughout this trip, serving as a continual source of strength and drive. I am eternally grateful to them for their love and support, which have been critical to my achievement.

February 2024 Bilal Ibrahim Majeed AL-OUBAIDI

TABLE OF CONTENTS

	Page
FOREWORD	**ix**
TABLE OF CONTENTS	**xii**
ABBREVIATIONS	**xiii**
SYMBOLS	**xv**
LIST OF TABLES	**xvii**
LIST OF FIGURES	**xxiii**
SUMMARY	**xxv**
ÖZET	**xxix**
1. INTRODUCTION	**1**
1.1 Background	1
1.2 Research Objective	3
1.3 Thesis Organization	3
2. LITERATURE REVIEW	**5**
2.1 General Introduction	5
2.2 Concrete Columns Strengthened With CFRP	5
2.3 Concrete Columns Reinforced With PET-FRP	11
2.4 Concrete Columns Reinforced With Hybrid FRP	14
3. METHODOLOGY	**19**
3.1 Objective of Experimental Program	19
3.2 Design of Test Specimens	20
3.3 Material Properties	23
3.3.1 Concrete	23
3.3.1.1 28-Day strength test for concrete	26
3.3.2 FRP materials	29
3.4 Applying External FRP Confinement to the Specimen	29
3.5 Cap	31
3.6 Test Setup	35
3.6.1 Strain gauges	35
3.6.2 LVDTs	37
3.6.3 Setup and calibration of specimens in the testing machine	40
4. COUPON TEST	**43**
4.1 Test Background	43
4.2 Experimental Details	44
4.2.1 Materials and specimens	44
4.2.2 Tensile test on composite	47
4.3 Coupon Test - Result	49
4.3.1 Mechanical properties of FRP laminates	54
5. UNCONFINED CONCRETE PROPERTIES	**57**
5.1 Overview	57
5.2 Test Result & Stress-Strain Curves	57
5.3 Compressive Strength Prediction	59
5.4 Test Outcome	59
6. COMPRESSION TESTS OF FRP-WRAPPED SQUARE SPECIMENS	**63**
6.1 Overview of Experimental Findings	63
6.2 Stress-Strain Response	64
6.2.1 R Group	65
6.2.2 Group 1C & 2C	65
6.2.3 Group 1P & 2P & 3P	66
6.2.4 Group 1C1P & 1C2P & 1C3P	68
6.3 Insights Into Failure Mechanisms and Strain Distribution	74
6.3.1 Group R	74
6.3.2 Group 1C & 2C	78

6.3.3 Group 1P & 2P & 3P 82
6.3.4 Group 1C1P & 1C2P & 1C3P 92
6.4 Test Results 101
6.4.1 Analysis and discussion of test results 105
7. ANALYTICAL EXPLORATION 115
7.1 Introduction 115
7.2 Evaluation Methodology 115
7.3 Theoretical Analysis 116
7.3.1 Estimation of peak axial stress and strain in CFRP-wrapped specimens 116
7.3.2 Estimation of peak axial stress and strain in PET-wrapped specimens 120
7.3.3 Estimation of peak axial stress and strain in hybrid-wrapped specimens. 125
8. CONCLUSION AND RECOMMENDATION 133
REFERENCES 137
CURRICULUM VITAE 145

ABBREVIATIONS

CFRP	**:** Carbon Fiber Reinforced Polymer
FRP	**:** Fiber Reinforced Polymer
PET	**:** Polyethylene Terephthalate
PEN	**:** Polyethylene Naphthalate
PIV	**:** Particle Image Velocimetry
ESPI	**:** Speckle Pattern Interferometry
ANN	**:** Artificial Neural Networks
LRS	**:** Large rupture strain
CDPM	**:** Concrete Damage Plasticity Module
FEA	**:** Finite Element Analysis
FE	**:** Finite element
RC	**:** Reinforced concrete
HSC	**:** High-strength concrete
SRS-FRP	**:** Small rupture strain FRP
CFFT	**:** Concrete filled fiber tubes
RAC	**:** Recycled aggregate concrete
CBA	**:** Clay bricks as aggregate
BE	**:** Basalt and glass fibers
PP	**:** Polypropylene
GFRP	**:** Glass Fiber Reinforced Polymer
BFRP	**:** Basalt Fiber Reinforced Polymer
LVDT	**:** Linear Variable Differential Transformers
R	**:** References specimen without wrapping FRP
1C	**:** Specimen wrapped with one layer of CFRP
2C	**:** Specimen wrapped with one layer of CFRP
1P	**:** Specimen wrapped with one layer of PET FRP
2P	**:** Specimen wrapped with two layer of PET FRP
3P	**:** Specimen wrapped with three layer of PET FRP
1C1P	**:** Specimen wrapped with one layer of CFRP and one layer of PET FRP
1C2P	**:** Specimen wrapped with one layer of CFRP and two layer of PET FRP
1C3P	**:** Specimen wrapped with one layer of CFRP and three layer of PET FRP
SD	**:** Standard deviation
LSC	**:** Low-strength concrete
AAE	**:** Average Absolute Error.

SYMBOLS

P	: Maximum load applied to the specimen
D	: Diameter of the cylinder
L	: Length of the cylinder
E	: Modulus of elasticity
ε_o	: Transition strain
fc	: Concrete's compressive strength
ε_{co}	: Axial strain at peak stress
ε_{cu85}	: Axial strain at 85% of the peak after the peak
E_{cs}	: Secant modulus of elasticity
E_{cc}	: Chord modulus
f_{ct}	: Compressive strength at t-day
fcc	: Confined strength in concrete
ε_{cc}	: Confined strain in concrete
fcc/fco	: Strength enhancement ratio
$\varepsilon_{cc}/\varepsilon_{co}$	: Strain enhancement ratio
$fccp1$	: First peak strength of confined concrete with PET FRP
$fccp2$	: Second peak strength of the confined concrete with PET FRP
$fccp3$	: Strength of the confined concrete (with PET FRP) at the ultimate strain
ε_{ccp1}	: Corresponding strain to the first peak strength (PET FRP)
ε_{ccp2}	: Corresponding strain to the second peak strength (PET FRP)
ε_{cu}	: Ultimate strain of the confined concrete with PET FRP
$fhcc1$	: Strength at CFRP rupture (hybrid FRP)
$fhcc2$	: Ultimate strength after CFRP rupture (hybrid FRP)
$fhcc3$	: Strength of confined concrete at ultimate strain (hybrid FRP)
ε_{hcc1}	: Axial strain at CFRP rupture (hybrid FRP)
ε_{hcc2}	: Strain corresponding to the ultimate strength after CFRP ruptures (hybrid FRP)
ε_{hcc3}	: Ultimate strain (hybrid FRP)
ER	: Experimental value
MP	: Predicted result
$\varepsilon_{r,s.f}$	: Rupture hoop strain measured on a flat face
$\varepsilon_{r,s.c}$	: Rupture hoop strain measured in the corner
f_{MP}	: Predicted maximum compressive strength of confined concrete
f_{al}	: Lateral pressure provided by confinement
$\varepsilon_{f.rup}$	: Lateral strain in FRP sheets at rupture

LIST OF TABLES

Page

Table 3.1 : The test matrix. **23**
Table 3.2 : The weight proportions of concrete mixes for low-strength concrete. **24**
Table 3.3 : Concrete temperatures and flow test results during casting. **24**
Table 3.4 : Compressive strength of concrete cylinders. **26**
Table 3.5 : Splitting tensile strength of concrete cylinders. **28**
Table 3.6 : Standard properties of CFRP and PET FRP materials provided by the manufacturer. **30**
Table 3.7 : Number of CFRP ring layers. **31**
Table 4.1 : Nominal thicknesses of the coupon specimens. **47**
Table 4.2 : Mechanical properties of FRP from the coupon test. **55**
Table 5.1 : Compression test results of LSC. **58**
Table 6.1 : Ultimate strength and strain characteristics of unconfined concrete. .. **103**
Table 6.2 : Test results of CFRP-wrapped concrete. **103**
Table 6.3 : Test results of PET-FRP-wrapped concrete. **104**
Table 6.4 : Test results of hybrid-FRP-wrapped Concrete. **104**
Table 7.1 : Compressive strength functions of the models. **117**
Table 7.2 : Ultimate strain functions of the models. **117**
Table 7.3 : Model predictions for ultimate strength of CFRP-specimens **118**
Table 7.4 : Model predictions for ultimate strain of CFRP-specimens **118**
Table 7.5 : Compressive strength functions of the models. **121**
Table 7.6 : strain functions of the PET models. **122**
Table 7.7 : Model predictions for strength at point 1 of PET-specimens **122**
Table 7.8 : Model predictions for strength at ultimate strain of PET-specimens .. **123**
Table 7.9 : Model predictions for strain at point 1 of PET-specimens **123**
Table 7.10 : Model predictions for strain at point 3 of PET-specimens **123**
Table 7.11 : Model predictions at point 1 of hybrid-specimens. **127**
Table 7.12 : Model predictions at the ultimate strain of hybrid-specimens. **128**

LIST OF FIGURES

Page

Figure 3.1 : Concrete columns wrapped with different configurations of FRP sheets where (a) is the reference: unwrapped concrete column, (b) CFRP confinement: columns wrapped with 1C and 2C FRP layers. **21**

Figure 3.2 : Concrete columns wrapped with different configurations of FRP sheets : (a) columns wrapped with 1P, 2P, and 3P FRP layers, (b) the hybrid confinements: columns wrapped with 1C1P, 1C2P, and 1C3P FRP Layers. **22**

Figure 3.3 : Stages of concrete preparation (a) wooden molds, (b) manual compaction of concrete using a steel rod, (c-d) flow test and temperature measurements, (e) cylindrical concrete samples for 28-day strength assessment..... **25**

Figure 3.4 : Comprehensive Overview of the monotonic uniaxial compression test setup of the unconfined concrete cylinder: (a) dimensions of the cylinder specimen, (b) positioning of the strain gauge, (c) 3D view of the setup and instrumented cylinder, (d) the set-up. **27**

Figure 3.5 : Splitting tensile test process: (A) splitting test machine, (B) concrete cylinder specimen (15 cm x 30 cm), (C) image capturing the test in progress. **29**

Figure 3.6 : Types of Fiber-Reinforced Polymers (FRP) used in the study:(a) Carbon Fiber Reinforced Polymer (CFRP), (b) Polyethylene Terephthalate (PET) Fiber Reinforced Polymer **30**

Figure 3.7 : Cross-sections of FRP confined columns showing overlap..... **31**

Figure 3.8 : Preparation process of the concrete specimens for confinement: (a) cutting the FRP material to size, (b) epoxy resin and hardener cans, (c) homogenizing epoxy components, (d) surface cleaning of columns, (e) application of epoxy to column surface, (f) adhering FRP wrap for confinement, (g) installation of CFRP rings, (h) final appearance of the confined column. **32**

Figure 3.9 : Steps in capping process of concrete column specimens: (a) preparing surface with angle grinder, (b) Surface post-roughening, (c) bag of Sika MonoTop-2400 mortar, (d) mixing mortar with electric hand mixer, (e) Oiling glass plate for leveling, (f) applying mortar to column top, (g) leveling mortar with glass plate, (h) Ensuring level surface with bubble level..... **34**

Figure 3.10 : Comprehensive visualization of strain gauge implementation: (a) the strain gauges utilized, (b) placement of strain gauges on column, (c) 3D view of a column with attached strain gauges. **36**

Figure 3.11 : Detailed stages of strain gauge installation on FRP-wrapped columns: (a) applying epoxy to FRP surface, (b) thinning epoxy layer with sander machine, (c) Evobond 502 super Japanese adhesive, (d) marking strain gauge locations, (e) applying adhesive on strain gauges, (f) securing strain gauges with pressing for one minute. **38**
Figure 3.12 : Illustration of LVDT setup in axial displacement measurement: (a) 3D view of steel frame with mid-positioned LVDTs, (b) placement of full-length LVDTs. **39**
Figure 3.13 : 3D View of the instrumented specimen in testing setup. **40**
Figure 3.14 : Sequential stages in setting up the testing apparatus: (a) verifying base level of testing machine, (b) Marking specimen tops for centering guidance, (c, d) leveling steel frame and LVDTs, (e) connecting strain gauges to data logger, (f) connecting LVDTs to switch box, (g) overall view of the experimental setup. **41**
Figure 4.1 : Carbon and PET Fiber rectangular cut for FRP plate preparation. ... **44**
Figure 4.2 : Fiber layup arrangement for producing composite plates: (a) one-layer carbon, (b) two-layer carbon, (c) one-layer PET, (d) one-layer carbon and one-layer PET, (e) two-layer PET, (f) one-layer carbon and two-layer PET, (g) three-layer PET, (h) one-layer carbon and three-layer PET. **45**
Figure 4.3 : The procedure to prepare the wet layup materials for flat tensile testing : (a) the application of resin via a paint roller to the foundational layer of acetate . (b) the carbon FRP sheet was placed into the resin, followed by applying the resin (c) placement of the second layer of PET sheet. (d) eliminating the extra resin and air using a floor wiper. **45**
Figure 4.4 : Demonstrates the process of cutting FRP plates with the Kuka KR16 Ultra-F Robot equipped with a water jet pump on the left side, while the resulting cut coupons are displayed on the right side. **46**
Figure 4.5 : the measurements of the test coupons and the placement..... **46**
Figure 4.6 : Setting up of tensile test of coupon/specimen. **48**
Figure 4.7 : Stress-strain curve of the coupon test results of C-1P. **49**
Figure 4.8 : Average stress-strain curve of the coupon test results of C-1P..... **49**
Figure 4.9 : Stress-strain curve of the coupon test results of C-2P. **50**
Figure 4.10 : Average stress-strain curve of the coupon test results of C-2P..... **50**
Figure 4.11 : :Stress-strain curve of the coupon test results of C-3P. **51**
Figure 4.12 : Average stress-strain curve of the coupon test results of C-3P..... **51**
Figure 4.13 : Stress-strain curve of the coupon test results of C-1C. **52**
Figure 4.14 : Average stress-strain curve of the coupon test results of C-1C. **52**
Figure 4.15 : Stress-strain curve of the coupon test results of C-2C. **52**
Figure 4.16 : Average stress-strain curve of the coupon test results of C-2C. **53**
Figure 4.17 : Stress-strain curve of the coupon test. **53**
Figure 4.18 : Average stress-strain curve of the coupon test results of C-3P showing the transition strain..... **54**

Figure 5.1 : (a) 28-Day concrete cylinders: stress-strain response,(b) 312-Day concrete cylinders: stress-strain characteristics, (c) comparative stress-strain curves for 28-Day vs. 312-Day cured concrete cylinders. **60**
Figure 6.1 : Stress-strain behavior of unconfined concrete specimens (R1 & R2). **65**
Figure 6.2 : Stress-strain behavior of confined concrete specimens (1C-1 & 1C-2). **66**
Figure 6.3 : Stress-strain behavior of confined concrete specimens (2C-1 & 2C-2). **67**
Figure 6.4 : Comparative stress-strain curves and hoop strain analysis for unconfined and CFRP-wrapped concrete specimens..... **67**
Figure 6.5 : Stress-strain behavior of confined concrete specimens (1P-1 & 1P-2). **68**
Figure 6.6 : 4.6: Stress-strain behavior of confined concrete specimens (2P-1 & 2P-2). **68**
Figure 6.7 : Stress-strain behavior of confined concrete specimens (3P-1 & 3P-2). **69**
Figure 6.8 : Comparative stress-strain curves for unconfined and CFRP-wrapped concrete and PET-FRP-wrapped concrete specimens. **69**
Figure 6.9 : Stress-strain behavior of confined concrete specimens (1C1P-1 & 1C1P-2)..... **71**
Figure 6.10 : Stress-strain behavior of confined concrete specimens (1C1P-1 & 1C1P-2)..... **71**
Figure 6.11 : Stress-strain behavior of confined concrete specimens (1C3P-1 & 1C3P-2)..... **72**
Figure 6.12 : Stress-strain behavior of confined concrete specimens (1C1P & 1C & 1P). **72**
Figure 6.13 : Stress-strain behavior of confined concrete specimens (1C2P & 1C & 2C & 2P). **73**
Figure 6.14 : Stress-strain behavior of confined concrete specimens (1C3P & 1C & 3P). **73**
Figure 6.15 : Stress-strain behavior of confined concrete specimens (1C1P & 1C2P & 1C3P). **74**
Figure 6.16 : A comparative display of stress-strain curves and corresponding failure states for specimens R-1 and R-2. ..... **75**
Figure 6.17 : Unconfined specimens: (a) R-1 ; (b) R-2 before and after testing.... **76**
Figure 6.18 : Stress-strain characteristics and localized strain distribution in unconfined concrete specimens R-1 and R-2..... **77**
Figure 6.19 : Visual comparison of CFRP-wrapped specimens 1C-1 (a) and 1C-2 (b) before and after axial load testing, highlighting failure modes..... **79**
Figure 6.20 : Visual comparison of CFRP-wrapped specimens 2C-1 (a) and 2C-2 (b) before and after axial load testing, highlighting failure modes..... **80**
Figure 6.21 : Hoop strain analysis for (a) 1C and (b) 2C specimens with CFRP wrapping under axial stress conditions. **81**
Figure 6.22 : Visual comparison of PET-FRP-wrapped specimens 1P-1 (a) and 1P-2 (b) before and after axial load testing, highlighting failure modes..... **83**

Figure 6.23 : Visual comparison of PET-FRP-wrapped specimens 2P-1 (a) and 2P-2 (b) before and after axial load testing, highlighting failure modes. **84**
Figure 6.24 : Visual comparison of PET-FRP-wrapped specimens 3P-1 (a) and 3P-2 (b) before and after axial load testing, highlighting failure modes. **85**
Figure 6.25 : Hoop strain response, stress-strain values, and in-test visuals for PET-wrapped specimens (1P-1) under axial loading. **86**
Figure 6.26 : Hoop strain response, stress-strain values, and in-test visuals for PET-wrapped specimens (1P-2) under axial loading. **87**
Figure 6.27 : Hoop strain response, stress-strain values, and in-test visuals for PET-wrapped specimens (2P-1) under axial loading. **88**
Figure 6.28 : Hoop strain response, stress-strain values, and in-test visuals for PET-wrapped specimens (2P-2) under axial loading. **89**
Figure 6.29 : Hoop strain response, stress-strain values, and in-test visuals for PET-wrapped specimens (3P-1) under axial loading. **90**
Figure 6.30 : Hoop strain response, stress-strain values, and in-test visuals for PET-wrapped specimens (3P-2) under axial loading. **91**
Figure 6.31 : Visual comparison of hybrid-FRP-wrapped specimens 1C1P-1 (a) and 1C1P-2 (b) before and after axial load testing, highlighting failure modes. **93**
Figure 6.32 : Visual comparison of hybrid-FRP-wrapped specimens 1C2P-1 (a) and 1C2P-2 (b) before and after axial load testing, highlighting failure modes. **94**
Figure 6.33 : Visual comparison of hybrid-FRP-wrapped specimens 1C3P-1 (a) and 1C3P-2 (b) before and after axial load testing, highlighting failure modes. **95**
Figure 6.34 : Hoop strain response, stress-strain values, and in-test visuals for hybrid-wrapped specimens (1C1P-1) under axial loading. **96**
Figure 6.35 : Hoop strain response, stress-strain values, and in-test visuals for hybrid-wrapped specimens (1C2P-1) under axial loading. **97**
Figure 6.36 : Hoop strain response, stress-strain values, and in-test visuals for hybrid-wrapped specimens (1C2P-2) under axial loading. **98**
Figure 6.37 : Hoop strain response, stress-strain values, and in-test visuals for hybrid-wrapped specimens (1C3P-1) under axial loading. **99**
Figure 6.38 : Hoop strain response, stress-strain values, and in-test visuals for hybrid-wrapped specimens (1C3P-2) under axial loading. **100**
Figure 6.39 : The investigated points of PET-FRP wrapped samples on the stress vs strain curve. **102**
Figure 6.40 : The investigated points of hybrid-FRP wrapped samples on the stress vs strain curve. **102**
Figure 6.41 : Enhancement ratios of 1C and 2C wrapped concrete columns: (a) strength enhancement ratios ; (b) strain enhancement ratios. **106**
Figure 6.42 : Enhancement ratios of 1P, 2P and 3P wrapped concrete columns: (a) strength enhancement ratios ; (b) strain enhancement ratios. **108**

Figure 6.43 : Enhancement ratios of 1C1P ,1C2P and 1C3P wrapped concrete columns: (a) strength enhancement ratios ; (b) strain enhancement ratios. **109**
Figure 6.44 : Enhancement ratios of 1C, 1P and 1C1P Wrapped concrete columns: (a) strength enhancement ratios ; (b) Strain enhancement ratios. **112**
Figure 6.45 : Enhancement ratios of 1C, 2P and 1C2P wrapped concrete columns: (a) strength enhancement ratios ; (b) strain enhancement ratios. **112**
Figure 6.46 : Enhancement ratios of 1C , 3P and 1C3P wrapped concrete columns: (a) strength enhancement ratios ; (b) strain enhancement ratios. **113**
Figure 7.1 : the investigate point of CFRP-wrapped samples stress vs strain curve **116**
Figure 7.2 : Test results versus model predictions for ultimate axial strength of the CFRP-samples. **118**
Figure 7.3 : Test results versus model predictions for axial strain of the CFRP-samples. **119**
Figure 7.4 : Assessment of Model Accuracy in Predicting Ultimate Strength and Strain: A Comparison Using Average Absolute Error (AAE) of the CFRP-samples. **119**
Figure 7.5 : the investigate point of PET-FRP stress vs strain curve **120**
Figure 7.6 : Test results versus model predictions for axial strength of PET-FRP wrapped columns (point 1). **124**
Figure 7.7 : Test results versus model predictions for axial strain of PET-FRP-wrapped columns (point 1). **124**
Figure 7.8 : Test results versus model predictions of axial strength at ultimate strain of PET-FRP wrapped specimens. **125**
Figure 7.9 : Test results versus model predictions for ultimate axial strain of PET wrapped specimens. **126**
Figure 7.10 : Assessment of Model Accuracy in Predicting First point of PET-FRP Wrapped Specimens **126**
Figure 7.11 : Assessment of Model Accuracy in Predicting second point of PET-FRP Wrapped Specimens **127**
Figure 7.12 : The investigate point of hybrid-FRP stress vs strain curve. **128**
Figure 7.13 : Test results versus model predictions for axial strength of hybrid specimens. **129**
Figure 7.14 : Test results versus model predictions for axial strain of hybrid specimens. **130**
Figure 7.15 : Assessment of model accuracy in predicting ultimate strength and strain at the rupture of the internal CFRP layer: A comparison using AAE. **130**
Figure 7.16 : Assessment of model accuracy in predicting ultimate strength and strain: A comparison using AAE. **131**

AN EXPERIMENTAL STUDY ON THE BEHAVIOR OF SQUARE SHORT CONCRETE COLUMNS CONFINED WITH HYBRID FRP UNDER MONOTONIC AXIAL COMPRESSION STRESS

SUMMARY

Column elements of structural systems are often in need of strengthening due to aging, damage, increased load demands, or adding floors to existing multistory buildings. The potential collapse of these columns necessitates retrofitting to boost their strength and ductility. Consequently, enhancing the resilience of building columns has become a focal point of recent research.

The primary aim of such structural reinforcement is to improve strength and ductility, increasing the structure's ability to bear loads and reducing the risk of damage or failure during catastrophic events like earthquakes.

A common technique for reinforcing such columns involves the application of Fiber Reinforced Polymer (FRP) jackets. This method wraps the concrete member with FRP jackets, which consist of fibers positioned at right angles to the member's longitudinal axis. FRP jackets provide passive confinement pressure to the concrete column and are activated (strain) only when the column faces additional axial load, leading to its expansion.

The degree of strengthening and the overall increase in strength of the reinforced concrete depend on various factors. such as fibers used (modulus, thickness, and rupture strain) and the physical characteristics of the column (size and shape, whether circular, square, or rectangular).

Traditionally, composite structures mainly utilized fibers like carbon, aramid, basalt, and glass for strengthening. However, the introduction of new fibers, such as PET and PEN, has been a game-changer in the construction industry. These materials have led to the development of new building materials that are crucial for strengthening and offer environmental advantages. Compared to traditional fibers, these new fibers exhibit distinctive mechanical properties, including a higher capacity to stretch before breaking (rupture strain) and lower strength values.

Our research is primarily focused on hybrid fiber-reinforced polymers (FRP), particularly the combination of Carbon and Polyethylene Terephthalate (PET) fibers. Hybrid FRP involves using two different types of fibers together, each with its unique set of mechanical characteristics. By using these fibers together, the resulting composite material can show improved mechanical performance and may also be more cost-effective.

The experimental part of our study 18 specimens, with two identical samples for each FRP wrapping configuration. Each sample was 300x300x550 mm in size and had a corner radius of 30 mm. The specimens were categoriaed with respect to the type and number of FRP layers used: a control group without FRP, a specimen group wrapped conventionally, and a hybrid-FRP wrapped specimen group that combined both fiber types. The last specimen group addresses a significant gap in existing research by examining the hybrid use of FRP types and assessing their practical application in real-world settings.

Prior to the sample preparation phase, careful attention was given to the concrete mix design. The aim was to ensure that the produced concrete possessed lower strength characteristics, mimicking the quality commonly found in older buildings.

The second phase of the thesis study is to characterize tensile behavior of CFRP and PET FRP. For each FRP type, five coupon specimens were prepared and tested under tensile loading in accordance to ASTM D3039 [1]. Thanks to these tests, the strength, strain capacity and modulus of elasticity were determined for each FRP type. This methodical approach was intended to provide a clear and comprehensive understanding of how each FRP material behaves when subjected to forces that aim to stretch it, ensuring a robust evaluation of their potential for retrofitting older building structures.

The main variable parameters considered were the type of FRP material, the application of hybridization, and the number of layers used to wrap the columns. This allowed for a detailed comparison of various layer combinations under monotonic compression axial loads. Precise measurements of the hoop strain of the FRP and the longitudinal strain were obtained by strategically positioning strain gauges and LVDTs. Compression tests were conducted utilizing an Instron testing device with a maximum capacity of 5000 KN.

The main goal of this study is to examine the axial strain ductility and strength of a column by using PET-FRP sheets that are wrapped around a carbon FRP layer. The sheets are layered on top of each other. The whole system is expected to exhibit a ductile behavior compared to the brittle behavior seen in concrete wrapped with conventional FRP application. The purpose of this research is carry out the following studies: (a) Investigate the efficiency of hybrid FRP composites in terms of strength and strain enhanchements (b) Conduct comparative studies to evaluate the performance of FRP wrapped and unwrapped specimens. (c) Analyze failure patterns (d) Contribute new insights to the existing knowledge on FRP wrapping techniques. (e) Perform theoretical analyses to predict axial behavior in confined samples and correlate these predictions, with empirical observations.

The test results show that the use of CFRP wrapping greatly improved the mechanical characteristics of concrete, notably enhancing both its strength and strain capacity. It was discovered that employing two layers of CFRP material significantly magnified these effects. While the application of PET-FRP wrapping significantly improved the axial ductility of the specimens, that of CFRP wrapping greatly improved the strength.Additionally, PET FRP ensured that the integrity of the specimens was almost maintained even when the specimens were subjected to severe damages.

The enhancement of concrete columns wrapped with PET-FRP layers reveals a direct correlation between the number of layers and the degree of enhancement in both strength and strain. Specifically, columns wrapped with a single layer of PET-FRP, designated as 1P, exhibit an ultimate strength enhancement of 1.23 and an ultimate strain enhancement of 15.51. When a second layer is added, creating 2P specimens, the strength enhancement increases to 1.29, and strain enhancement shows a more pronounced increase to 27.47. This trend continues with 3P specimens, where three layers of PET-FRP wrapping provide the highest recorded enhancements, with strength enhancement reaching 1.44 and strain enhancement escalating to 30.54. These figures suggest that each additional layer of PET-FRP not only contributes to a higher load-bearing capacity but also significantly improves ductility, allowing the column to undergo larger deformations before failure. This is particularly beneficial in seismic zones where energy absorption and ductility are critical for the structural integrity of buildings.

The key findings of the test results of hybrid-FRP wrapped specimens show that the hybrid wrapping method works well at improving both the strength and axial strain ductility of concrete. Each extra layer of PET-FRP makes a big difference, especially when it comes to strain capacity, which makes the concrete stronger against forces that cause it to deform. PET-FRP significantly contributes to the ductility of the specimens, a desirable property, especially in seismic-prone areas. The hybrid-FRP system, combining the advantages of both materials, emerges as a good solution, striking an optimal balance between strength and flexibility.

The thesis study also looked at existing predictive models and compared them to test results. This showed how hard it is to accurately model the behavior of FRP-confined concrete, especially in hybrid configurations. The discrepancies observed in strain predictions underline the need for more sophisticated models to accurately capture the complexities of material behavior under confinement. Looking ahead, the research opens several promising avenues for future exploration. The adaptability and performance of the hybrid system will be investigated across different column geometries and in conjunction with traditional reinforcement methods such as reinforced concrete (RC) columns. Furthermore, the durability of the hybrid system under various environmental conditions and loads will be a key focus, ensuring its long-term effectiveness and reliability as a structural reinforcement solution.

In the future, researchers could look into the best ways to combine different type of FRP layers for different structural needs and also look into how well hybrid-FRP retrofitted structures work over time.

MONOTONİK EKSENEL BASINÇ YÜKLEMESİ ALTINDA HİBRİT LİFLİ POLİMER MALZEME İLE SARGILANMIŞ KARE BETON KOLONLARIN DAVRANIŞI ÜZERİNE DENEYSEL BİR ÇALIŞMA

ÖZET

Deprem etkileri altında betonarme binaların performansını iyileştirmek/artırmak için kolon elemanların güçlendirilmesi yoluna gidilebilmektedir. Bu tür yapısal güçlendirmenin temel amacı, betonarme yapıların dayanımını ve sünekliğini artırarak deprem gibi etkiler altında hasar/toptan göçme riskini azaltarak can kaybını önlemektir.

Betonarme kolon elemanların güçlendirilmesi için kullanılacak hızlı ve etkin yöntemlerden biri, kolon elemanı Lifli Polimer (LP) kompozitlerle sargılamaktır. LP'nin kolonun çevresine, lifler enine donatılara paralel olacak şekilde, sarılması ve yapıştırılması ile sargılama işlemi tamamlanır. Bu yöntemin uygulanması ile betonarme kolonların basınç dayanımının ve süneklik kapasitesinin artması dolayısıyla deprem etkileri altındaki performasının iyileştirilmesi/artırılması hedeflenmektedir. Performanstaki artış, temel olarak, kullanılan LP'yi oluşturan liflerin özelliklerine (elastisite modülü, çekme dayanımı, kopma birim uzaması ve etkili kalınlık), kolonun en kesit geometrisine (dairesel, kare, dikdörtgen vb.), LP'nin uygulama kalitesine ve hacimsel oranına bağlı olarak değişmektedir.

Son yıllarda karbon, cam, aramid ve basalt gibi geleneksel liflere ek olarak Polietilen Tereftalat (PET) ve polyethylene naphthalate (PEN) gibi yeni lifleri içeren LP kompozit malzemeler üretilmiştir. Bu yeni liflerin belirgin mekanik özelliği, geleneksel liflere göre daha çekme etkileri altında daha yüksek kopma uzamasına sahip olmalarıdır. Ayrıca, bu liflerin elastisite modülü ve çekme dayanımı daha düşük olup lif kalınlığı geleneksel liflere göre daha fazladır.

Sunulan tez çalışması, günümüzde tek tip lif kullanılarak yapılan LP uygulamalarından farklı olarak karbon ve PET LP kumaşların bir arada kullanılarak standart altı beton kolonların sargılanmasını ve monotonik eksenel basınç yüklemesi altında bu hibrit LP kompozit sargının performansını deneysel olarak belirlemeyi hedeflemektedir. Çalışma, farklı mekanik özelliklere sahip iki farklı LP lifin aynı sargılama uygulamasında kullanımı ile bu liflerin avantajlarından en üst düzeyde faydalanmayı amaçlamaktadır. Karbon ve PET lifin avantajları, sırasıyla, elastisite modülünün ve uzama kapasitesinin yüksek olmasıdır.

Bu liflerin birlikte kullanılmasıyla elde edilen kompozit malzemenin, daha iyi performans gösterebileceği ve aynı zamanda maliyet açısından da daha avantajlı olabileceği düşünülmektedir.

Hibrit LP sargılamanın etkinliğini deneysel olarak araştırmak üzere 18 adet numune düşük dayanımlı betonla üretilmiştir. Numuneler kare kesitli olup en kesit boyutları

275x275 mm ve yüksekliği 550 mm'dir. Numunelerin köşe yarıçapları 30 mm olacak şekilde üretim yapılmıştır. Test değişkenleri, LP sargılama konfigürasyonu ve LP sargı tabaka sayısı olarak planlanmıştır. Numuneler, kullanılan LP katmanlarının türüne göre sınıflandırılmıştır: (a) LP içermeyen yani sargılanmamış numunelerin bulunduğu kontrol grubu, (b) geleneksel olarak yani tek tip lif içeren LP ile sargılanan numuneler ve (c) her iki lif türünü birleştiren hibrit-LP ile sargılanmış numuneler olmak üzere 3 grup numune üzerinde testler gerçekleştirilmiştir.

Bu araştırmanın temel amaçları aşağıda sıralanmaktadır:

(a) Basınç dayanımı ve eksenel süneklik açısından hibrit LP kompozitlerin etkinliğini deneysel olarak araştırmak.

(b) Hibrit LP kompozit numunelerin basınç yüklemeleri altındaki davranışını gösteren deneysel veri elde etmek.

(c) Hibrit ve tek tip LP kompozitler ile sargılı kare kesitli beton numunelerin performansını karşılaştırmalı olarak ele almak.

(d) LP kompozit sargılı numunelerin davranışını tahmin etmek üzere literatürde mevcut olan modellerin hibrit ve tek tip LP kompozit ile sargılanan numune davranışını tahmin etmek üzere değerlendirilmesi.

Bu çalışmanın amaçlarına ulaşmak için numune konfigürasyonu planlandıktan sonra eski betonarme binaların düşük dayanımlı beton karakteristiğini temsil etmek için düşük dayanımlı beton elde etmek üzere farklı beton karışımları denenmiş ve en uygun karışım oranı belirlenmiştir.

Tez çalışmasının ikinci aşamasında ise karbon ve PET LP'nin çekme etkileri altındaki davranışını belirlemek üzere ASTM D3039 [1] standardı esas alınarak kupon numuneler hazırlanmıştır. Kupon numuneler, ASTM D3039 [1] standardında belirtildiği şekilde çekme etkileri altında test edilmiş ve test sonuçlarından elastisite modülü, çekme dayanımı, kopma birim uzaması ve göçme modları elde edilmiştir. Ayrıca, her bir kupon numunesinin çekme gerilmesi-birim uzama ilişkilerini gösteren grafikleri çizilmiştir.

LP sargı malzemelerinin çekme etkileri altındaki davranışı belirlendikten sonra numune sargılama konfigürasyonu tekrar gözden geçirilmiş ve uygun olduğuna karar verilmiştir. Kare numuneler, LP malzemelerle sargılanarak epoksi reçinenin kuruması için dış ortamda bekletilmiştir. Numunelerin basınç etkileri altındaki davranışlarını anlamak için test öncesi, her bir numunenin her bir yüzeyinin orta bölgesine yerdeğiştirme ölçerler yerleştirilmiştir. Ayrıca, LP malzemenin birim uzamalarını tespit etmek üzere numune orta bölgesine yatayda farklı konumlarda olmak üzere LP üzerine şekildeğiştirmeölçerler yapıştırılmıştır. Kare numunelerin basınç testleri, İTÜ, Yapı Malzemesi Laboratuvarı'nda bulunan 5000 kN kapasiteli Instron test cihazı kullanılarak gerçekleştirilmiştir. Test sonuçları kullanılarak her bir numunenin basınç dayanımı, bu dayanıma karşı gelen birim kısalması ve kopma birim uzaması hesaplanmıştır. Ayrıca, numuneler test boyunca gözlemlenerek hasar gelişimi ve göçme modu anlaşılmıştır. Testlerden elde edilen veri kullanılarak her bir

numunenin basınç gerilmesi-birim kısalma ve basınç gerilmesi-birim uzama ilişkileri elde edilmiştir.

Hibrit LP kompozitlerle ile sargılanmış düşük dayanımlı kare numunelerin basınç yüklemeleri altındaki test sonuçları, hibrit LP sargılamanın betonun hem basınç dayanımını hem de eksenel şekildeğiştirme sünekliğini önemli oranda artırttığını göstermektedir. Hibrit LP kompozitlerle sargılanan numunelerin basınç gerilmesi-birim uzama ilişkisini, üç bölgeyle tarif etmek mümkündür. Birinci bölgede, sargılanmamış betonun özellikleri etkili olup bu bölgedeki eğrinin başlangıç eğimi, sargılanmamış betonun elastisite modülüne eşdeğerdir. İkinci bölgede, betonda çatlakların oluşmasıyla eğrinin eğimi azalmakta ve hibrit sargının devreye girmesiyle basınç dayanımı artarken eksenel deformasyonlar da artmaktadır. Bu eğilim karbon liflerin uzama kapasitesine erişip kopmasıyla son bulmaktadır. Üçüncü bölgede ise karbonun devredışı kalması nedeniyle sargılama basıncının sadece PET lifler tarafından sağlandığı düşünülmektedir. PET LP sargı miktarına bağlı olarak üçüncü bölgenin eğimi; azalma, sabit veya yükselme eğiliminde olabilmektedir. PET liflerin kopma uzama kapasitesine ulaşmasıyla numune taşıma gücüne erişmektedir. Sonuçlar, hibrit LP kompozit sargılı numunelerin dayanım artışını daha çok karbon liflerin; uzama kapasitesi artışını da PET liflerin sağladığını göstermektedir. Test verileri kullanılarak hesap edilen eksenel şekildeğiştirme artışı, uygulanan sargılama tekniğinin düşük dayanımlı betonun sünekliğini artırmada başarılı olduğunu göstermektedir. Her iki malzemenin avantajlarını birleştiren hibrit LP kompozit sistemi ile, güçlendirilecek bir binanın dayanım ve süneklik ihtiyaçları dikkate alınarak, optimal tasarımlar yapmanın mümkün olduğu düşünülmektedir.

Karbon LP kompozit ile sargılanan kare numunelerin dayanımının büyük oranda arttığı görülmüştür. LP katman sayısının ikiye çıkarılması durumunda, beklendiği üzere, tek katlılara göre dayanım ve eksenel şekildeğiştirme artışları daha büyük olmuştur. PET LP ile sargılanan numuneler büyük deformasyon artışları göstererek taşıma gücüne erişmişlerdir. Sargı katman sayısının artması dayanım ve süneklikte daha büyük artış oranları sağlamıştır. Tek katman PET LP ile sargılanmış numuneler (1P) basınç dayanımı artışı açısından %1.23 ve birim kısalma artışı açısından %15.51'lik bir değişim göstermiştir. İkinci bir katman eklenerek oluşturulan 2P numuneleri için dayanım ve birim kısalma artış miktarları, sırasıyla, %1.29 ve %27.47 olarak hesaplanmıştır. Üç katman PET LP ile sargılanan numunelerin ortalama dayanım ve birim kısalma artış oranları, sırasıyla, %1.44 ve %30.54 olarak bulunmuştur. Bu artış miktarları, PET LP kompozit ile sargılı düşük dayanımlı betonun taşıma kapasitesine büyük deformasyonlarla ulaştığını göstermektedir. Bu nedenle bu tür kompozitlerle yapılacak sargılamanın, özellikle enerji yutma ve süneklik açısından iyileştirmeler sağlayacağı düşünülmektedir.

Ayrıca, tez çalışmasında, literatürdeki mevcut analitik modeller incelenmiş ve bu modeller kullanılarak test edilen kare numunelerin basınç dayanımı ve eksenel şekildeğiştirme kapasiteleri tahmin edilmiştir. Test sonuçları ile model tahminleri karşılaştırılarak modellerin bu çalışmadaki LP sargılama konfigürasyonları için uygun olup olmadığı araştırılmıştır. Karşılaştırmalar, özellikle, hibrit LP kompozitlerle sargılanmış düşük dayanımlı betonun gerilme-şekildeğiştirme ilişkisi için model önerme gerekliliğini ortaya koymuştur.

Sunulan tez çalışması kapsamında elde edilen deneysel ve analitik çalışma verisi ve sonuçlarının hibrit LP sargılama tekniğinin geliştirilmesi için katkı sunacağı düşünülmektedir.

Hibrit LP sargılama sisteminin farklı enkesitli beton/betonarme elemanlar için farklı tip liflerle oluşturulması ve farklı yüklemeler altında test edilerek etkinliğinin ortaya çıkarılması, çevresel koşullar açısından durabilite çalışmalarıyla incelenmesi vb. konularda araştırmalara ihtiyaç duyulduğunu düşünülmektedir.

1. INTRODUCTION

1.1 Background

Concrete is a fundamental material widely used in modern construction due to its notable benefits, including its strength, durability, and adaptability [2]. Within the context of Turkey, an overwhelming majority, namely 80% or more [3], of the current building infrastructure is built utilizing reinforced concrete materials. The increase in migration, namely from rural regions to urban centers, has led to the rapid and uncontrolled growth of concrete structures. Unfortunately, a significant proportion of these buildings were built without obeying to the seismic design codes that were in place at the time of their construction. Moreover, there are problems with buildings that are built to meet seismic design criteria due to specific conceptual flaws that are present in outdated guidelines. Reinforced concrete structures built in Turkey before the early 2000s lacked sufficient seismic resistance [3]. Furthermore, the strengthening process is significantly influenced by several factors, including structural deterioration, exposure to corrosive substances, and changes in usage patterns [4].

Hence, research on the enhancement of structural integrity in buildings has gained significant attention in recent years. The primary objective of structural strengthening It is to reduce the risk of serious damage or collapse during overloads such as earthquakes by increasing the load-carrying capacity and ductility of the elements [5].

Mechanical attached steel plates, near surface mounted reinforcing, energy dissipation device, shear walls are among conventional strengthening techniques. In addition, fiber reinforced polymers (FRP) have recently been used due to their high mechanical performance, ability to be produced in any shape and ease of installation. [6].

FRP composites involve a polymer matrix reinforced with fibers, and they are extensively utilized in several industries, including aerospace, automotive, marine etc., due to their exceptional strength-to-weight ratios [2,3]. Notably, considerable focus

have been directed towards the capacity of this material to enhance the strength of damaged concrete elements, involving beams, slabs, columns, and walls [7]–[10].

Reinforced columns sometimes need to be strengthened due to aging, damage, increased floor loads, or the addition of one or more stories to an existing multistory building. A lot of reinforced concrete columns that were built before 1970 are also considered non-ductile or have limited ductility. This is mostly because they don't have enough transverse steel strips [11]. In places prone to earthquakes, these columns can be in serious danger of collapsing and may need to be strengthened to increase their strength and ductility.

One application method of FRP to a structural element is to confine the RC column with fiber sheets arranged perpendicular to the longitudinal axis of the column. In this state, FRP jackets provide passive confinement to the column when the column is exposed to an additional axial load, causing expansion.

Multiple factors, such as the modulus of elasticity, thickness, and rupture strain of the fibers used, as well as the size and shape (circular, square, or rectangular) of the columns, affect the degree of confinement, and so do the strength and ductility enhancement ratios. For confinement purposes, circular column cross sections are considered to be extremely advantageous. This is primarily due to the circumferentially consistent radial expansion of the concrete, which results in uniform confinement pressure and tension within the FRP jacket. Scientific research has demonstrated that the confinement of square and rectangular cross sections reduces the effective confinement area and significantly decreases confinement pressure [12].

FRP composite structures mainly rely on carbon, aramid, basalt and glass fibers as the main form of reinforcement. However, the growing demands of the building industry have been accelerated by the introduction of new fibers like PET and PEN. These materials have brought out a new generation of construction materials that are not only essential for retrofitting construction but also have positive environmental implications. In contrast to conventional fibers, these novel alternatives demonstrate unique mechanical properties, including a high rupture strain and lower strength values [4,5,7,8].

The idea of hybrid FRP includes the incorporation of at least two different types of fibers into a composite material. Each constituent fiber possesses its own unique set of benefits and drawbacks in terms of mechanical characteristics. By combining these fibers, the resulting composite can exhibit enhanced mechanical properties and potentially achieve cost efficiency [9]. Our research focuses mainly on Hybrid fiber-reinforced polymers (FRP) that incorporate both Carbon and Polyethylene Terephthalate (PET) fibers.

1.2 Research Objective

The main goal of this study is to improve the compressive strength and axial strain ductility of low strength concrete by using PET-FRP sheets that are wrapped around a carbon FRP layer. When conventional FRP sheets fail it serves as an indicator, for the failure of the element. The whole system is expected to exhibit ductility compared to the brittle behavior seen in traditional fiber reinforced polymer (FRP) materials. The purpose of this research is to achieve objectives:

(a) Investigate the efficiency of hybrid FRP composites for concrete confinement, focusing on their strength, elasticity, and compatibility with low-strength concrete.

(b) Conduct comparative studies to evaluate the performance of FRP reinforced specimens when compared to reinforced and unreinforced samples.

(c) Analyze failure patterns

(d) Contribute new insights to the existing knowledge on FRP confinement.

(e) Perform theoretical analyses to predict axial behavior of confined specimens and compare these predictions, with empirical results.

1.3 Thesis Organization

This thesis consists of a total of eight chapters. The first chapter serves as an introduction, which has already been provided above. Chapter 2 presents an overview of the literature review on strengthening columns with FRP jackets. The methodology is introduced in Chapter 3. Chapter 4 discusses the coupon test, while Chapter 5

covers low-strength concrete. In Chapter 6, the compression tests of square specimens wrapped with conventional or hybrid FRP were presented. The test results were explained to describe the compression behaviors of the specimens produced with LSC, and in Chapter 7, the axial stress-strain response of the tested specimens was predicted using several models. Finally, in Chapter 8, the outcomes obtained from the thesis study are presented briefly.

2. LITERATURE REVIEW

2.1 General Introduction

This chapter presents previous research directly related to the strengthening of concrete columns. To facilitate understanding, the chapter is divided into three parts. The first part is to examine the concrete columns that have been strengthened with CFRP. The subsequent part presents a concise overview of the studies carried out on concrete columns that were wrapped with PET-FRP. The study's third part focuses on the experiments performed on concrete columns strengthened with hybrid FRP.

2.2 Concrete Columns Strengthened With CFRP

A research study conducted by Jiang et al. (2019) [13] introduced a modified approach to analyze how FRP-confined square concrete sections behave under stress and strain by calculating the local stresses at certain places of the numerically simulated sections. They built upon the existing concept of the "arching effect," which is commonly used to evaluate confinement in steel and FRP-confined sections.In addition, they utilized the concept of the "arching effect" to categorize confinement into three levels:ineffectively-, moderately- and highly-confined zones. This provides an understanding of how confinement impacts behavior.

Liu Jin et al. [14] examined how the size of columns wrapped with CFRP (carbon fiber reinforced polymer) affects their failure under axial compression. The study used a 3D mesoscale simulation approach. Included 30 columns with a maximum width of 600mm. The findings revealed that larger columns exhibited failure characteristics leading to a decrease in displacement ductility coefficient and hoop strain. Importantly, the study validated an updated size effect law that correlated well with both the data and simulation results. These results indicate that the performance of CFRP confinement is influenced by the size of the specimen.

Wang *et al.* [15] examined how the size of CFRP-confined columns affects the axial stress strain behavior. Their findings indicate that there is no impact on the small and medium-sized concrete columns when it comes to FRP confinement. However, for larger-scale columns, there were differences in the stress-strain response as the specimen size increased. The researchers stated that with larger specimen sizes, the rupture strain of FRP at corner regions decrease. Finally, a modified model has been introduced that accounts for the FRP strain factor.

Al Rousan *et al.* [16] performed research to investigate the impact of various surface preparation procedures on the bonding of CFRP sheets. The researchers conducted experiments utilizing eight prisms that had different surface preparations, drilling procedures, sizes, and shapes. Through the implementation of double shear tests, the researchers examined the many ways in which bond slip occurs and studied its behavior after failure. The results indicated that the drilling method employed had an important impact on the bond's strength, as greater drilling amplitudes and surface areas led to stronger bonds. Furthermore, it was found that the dimensions of CFRP sheets adhered to concrete had a significant impact on both the adhesive strength and slippage. Remarkably, it was discovered that the compressive strength of concrete had an impact on these characteristics. The researchers documented two distinct forms of failure: failure at the boundary between concrete and CFRP sheets, and concrete layers that separated from the CFRP following failure, occurring at different thicknesses. Bond slip behavior may be divided into two stages: first, it increases linearly as the bond strength increases, but then slippage occurs, resulting in either full debonding or the separation of the concrete layer interface. This study highlights the need to take surface preparation into account when developing and executing CFRP applications in order to enhance the bonding process.

Gambarelli *et al.* [17] concentrated on examining the compression behavior of columns under CFRP constraints. Based on the datasets consisting of stress-strain correlations and failure modes, they incorporated a microplane-based model to account for the effects of axial stress conditions on concrete. The findings of the study revealed that when applying CFRP confinement, it is less effective for square-shaped columns compared to cylindrical ones. Additionally, the study examined how the corner radius

influences stress distribution. By testing both confined and unconfined specimens, they calibrated a finite element model using a specialized microplane constitutive law designed specifically for concrete materials. The results indicated that column failures often occurred due to failure in fibers located at corner zones, which were either explosive or highly brittle in nature.

Nisticò *et al.* [18] used expressions to determine the peak strength and ultimate strain in sections of FRP-confined concrete. The researchers carefully analyzed a dataset of over 655 tests carried out on both square and circular specimens. Their findings revealed that the accuracy in predicting peak strength was generally better compared to predicting strain, indicating dependable strength estimations. However, it was noted that predicting strain presented challenges due to the significant variability in strain data. Notably, recent models for peak strength exhibited suitability for sections with a high level of accuracy demonstrated by recent advancements, resulting in an average absolute error rate of approximately 12%.

Diego *et al.* [19] examined how the corner curvature of specimens surrounded by FRP affects the confinement performance. The findings revealed that rounding the corners has an impact on the effectiveness of FRP confinement, resulting in improved strength and ductility. It was observed that as the unconfined compressive strength increases, the efficacy of FRP confinement decreases. The researchers also noted that increasing the corner curvature further enhanced the strength improvement. In medium-strength specimens, the strain efficiency factor remained consistently at 0.60; however, it exhibited some variability in low-strength specimens. These results suggest that existing design standards, like TR55 [20], may need revision as they do not completely align with these findings.

The research conducted by Benzaid *et al.* [21] investigated the behavior of columns with different shapes strengthened with CFRP sheets when subjected to axial loading. The experiments are conducted on sixty sets of specimens exposed to compression to analyze their responses. It has been observed that the FRP frequently experiences failure prior to reaching its maximum strain capacity. This discovery indicates an initial failure mechanism that deviates from the typical scenario, in which the

FRP would rupture when it reaches its maximum strain capacity. The existing models predict that the FRP will rupture at its maximum capacity, which is not how FRP-confined concrete actually behaves. These models fail to consider premature failure, necessitating the development of new models that account for the variations between anticipated outcomes and actual ones. The researchers proposed equations to predict the strength of FRP-confined concrete and the corresponding strain for cross-sectional geometries. These equations consider factors such as confining pressure and effective circumferential FRP failure strain. It is discovered that the effectiveness of confinement strongly depends on the column sectional shape, the number of CFRP sheet layers used, and the strength of unconfined concrete.

The purpose of the study conducted by Riad Benzaid *et al.* [22] was to examine how externally applied CFRP (Carbon Fiber Reinforced Polymer) affects reinforced columns. Tests are performed on 48 specimens, considering factors such as the number of CFRP layers, column slenderness, and section shape. The specimens were subjected to compression until they failed. The results showed that using a wrap significantly improved the performance of reinforced concrete columns by increasing their maximum strength and capacity. The study confirmed that CFRP reinforcement is effective for both circular and square column shapes. Similar to research, the CFRP-wrapped specimens exhibited failure accompanied by preceding cracking sounds. In columns, failure typically initiates at or near the corners due to stress concentrations in those areas. The CFRP-reinforced specimens displayed a two-stage response, where the initial stage was influenced by the stiffness of the concrete. Increasing the number of CFRP sheets enhanced the strength of confined columns although to an extent compared to deformation capacity improvement. In particular, CFRP confinement performed well in cylinder shapes compared to square shapes.

The research conducted by Alper Ilki *et al.* [23] in 2004 examined the axial stress-strain behaviour of concrete columns strengthened with different thicknesses of CFRP composite sheets under un-axial load. The study included 46 samples with square and rectangular shapes all having unconfined concrete compressive strengths ranging from 6 to 10 MPa. The objective was to evaluate external CFRP confinement in

terms of strength, deformability, and energy dissipation enhancements. The findings indicated that using CFRP sheets for confinement proved efficient when the unconfined concrete had lower compressive strength compared to normal or high strength concrete. Existing analytical formulas at the time of conducting the research for CFRP confined high strength concrete are not accurate enough in predicting the behavior of CFRP confined low strength concrete. Therefore the researchers proposed formulas to estimate the strength and ultimate axial strain of low strength concrete confined by CFRP. Applying a jacket made from CFRP sheets significantly improved the behavior of low strength components across various cross sections notably enhancing their ability to dissipate energy. It was essential to round the corners in specimens to achieve a better improvement in compressive strength. The positive effects of CFRP jackets on enhancing both strength and deformability were more effective in specimens, with lower unconfined concrete compressive strength.

In a research conducted by Scott T. Smith *et al.* [24] In 2010 the focus was, on examining the strength and behavior of 250 mm diameter cylinders that were confined using FRP wraps. The experiment aimed to understand the impact of factors such as the number of FRP layers overlap locations and wrapping configurations (versus continuous). To measure strain electrical resistance strain gauges and Electronic Speckle Pattern Interferometry (ESPI) were utilized. The results obtained from ESPI indicated that there was a concentration of strain at the ends of the overlap regions, which could potentially lead to failure in the wrap. Strain gauges were used to measure both the effectiveness of the FRP wrap and the distribution of hoop strain in areas with overlap and without overlap. By comparing wrapping configurations (versus continuous) researchers examined their influence, on how effectively confinement was achieved. Overall this study highlights how important it is to consider both wrap configuration and overlap regions when designing FRP confinement systems.

The studies in this section are summarized with a number of points:

- column size: no impact on the small and medium sized columns when it comes to FRP confinement. However, as specimen sizes get larger leading to a decrease in

displacement ductility coefficient and the rupture strain of FRP at corner regions decrease.

- shape: applying CFRP confinement is less effective for square shaped columns compared to cylindrical ones but it is better than rectangular one.
- corner: the corner radius influences stress distribution and with rounding the corners in specimens lead to achieve a better improvement in compressive strength.
- rupture of CFRP: column failures often occurred due to failure in fibers located at corner zones due to stress concentrations in those areas and as well some studies concluded that there is concentration of strain at the ends of the overlap regions . Moreover, FRP often experienced failure before the FRP reached its strain capacity with brittle failure accompanied with loudly sound. So, it raises the importance of planning and execution, in the design.
- strength of concrete: CFRP sheets for confinement proved efficient when the unconfined concrete had lower compressive strength compared to normal or high strength concrete.
- Prediction: the accuracy in predicting peak strength was generally better compared to predicting strain indicating dependable strength estimations. However it was noted that predicting strain presented challenges.
- thickness of FRP: . Increasing the number of CFRP sheets enhanced the strength of confined columns although to an extent compared to deformation capacity improvement.

2.3 Concrete Columns Reinforced With PET-FRP

In a study, by Isleem *et al.* [25] the aim was to develop a confinement model for LRS FRP confined concrete. To achieve this they used Artificial Neural Networks (ANN) to analyze data. The dataset used in the study consisted of 226 compression experiments conducted on samples of LRS FRP confined concrete. Various test parameters such as sectional form, corner radius and FRP material type were considered. The ANN models presented in the study predicted the strength and strain of LRS FRP confined concrete with good accuretly , as well as the stress strain relationship it exhibited. The parameter of the study relied mostly on factors like the number of layers of FRP wrapping jacket and the volumetric ratio of steel hoops. The researchers converted their ANN models into user equations making them practical for implementation. A comparison was made between existing models and the proposed models for LRS FRP confined concrete. The results showed that the suggested approaches demonstrated improved prediction accuracy. In summary Isleems research shows how advanced techniques, like Artificial Neural Networks (ANN) can be employed to simulate the behavior of LRS FRP confined concrete.This approach offers an practical method to predict the strength and structural changes of concrete wrapped FRP.

In a study, by Mohammadi [26] (2022) the focus was on investigating the behavior of circular concrete columns confined with Low LRS FRPs under axial monotonic compression. The research involved conducting tests on 23 samples and examining factors such as aspect ratio, number of LRS FRP layers and type of LRS FRPs used. To analyze the behavior accurately the Concrete Damage Plasticity Module (CDPM) was calibrated using pressure and confinement stiffness methodologies in Finite Element Analysis (FEA). Unlike conventional FRPs , LRS FRPs have bilinear material stiffness, which largely impacts the FEA of confined columns.The study revealed that concrete confined by LRS FRPs experienced a dilation angle increase at a rate three times faster compared to concrete confined by conventional FRPs. Additionally, when using LRS FRPs for confinement there were variations observed in the loading paths of concrete subjected to compression. Both aspect ratio and

confinement stiffness ratio affected both the stress strain curve and distribution within the confinement region. To improve the design process, for circular LRS FRP confined concrete columns, a unique model was proposed focusing on enhancing stiffness based considerations. This model build in the revised equations derived from the study, by Bai *et al.* [27].

A study by Bai *et al.* [28] (2023) concentrated on the seismic retrofitting of reinforced concrete square columns using LRS FRP. It compared a control column with 9 FRP-wrapped columns with different FRP layers and types. The performance of the structure during an earthquake was studied using both experimental analysis and numerical simulations with OpenSees. Failure modes, hysteretic behaviour, energy dissipation, and FRP strain evolution were all investigated. The study noticed that the ductility of the columns improved as the confinement pressure provided by the FRP increased, Enhanced FRP confinement leads to restricted and postponed the buckling of longitudinal reinforcement bars. LRS FRP strengthening notably enhanced the seismic behavior of the columns, although the enhancement of the lateral peak load was limited, Continuous FRP strengthening showed better performance compared to strip strengthening, preventing concrete spalling and maintaining the integrity of concrete. The results from numerical simulations based on the LRS FRP-strengthened concrete model and steel reinforcing bar buckling model, aligned well with experimental curves for columns with lower confinement.

The influence of internal steel bars on the axial compressive response of noncircular RC columns confined with PET FRP was examined in a study by Saleem *et al.* [29] (2020). In evaluating 32 specimens subjected to constant axial compression, variables such as the distance between stirrups, the number of PET FRP layers, and the cross-sectional aspect ratio were considered. An increase in PET FRP confinement significantly enhanced strength and deformation capacities, minimizing the effect of buckling length, according to the study. The deformation of longitudinal bars was weakly but constantly constrained by PET FRP confinement, which maintained stress concentrations at corners and contributed to a ductile response. In comparison to rectangular specimens, the peak and post-peak strengths of square cross-section specimens were greater. With the addition of more PET FRP layers, the impact of

stirrup spacing on strength diminished. Disparities resulting from stirrup spacing were reduced in specimens that were adequately confined, suggesting an improvement in the uniformity of stress distribution. The elevated axial deformations observed in all specimens were a result of the LRS property of PET FRP. Although the fracturing of internal steel bars was postponed, it remained uncontrolled in every aspect. The study conducted by Saleem *et al.* [29] offers light on the capacity of PET FRP to augment the seismic resistance of RC columns. This finding illustrates that the application of PET FRP confinement may improve the ductility and load-bearing capacity of columns, specifically in terms of regulating the deformation of internal steel bars.

An experimental investigation was done by Bai *et al.* [30] (2022) to analyze the axial compressive behavior of square RC columns with considerable scale that were confined with PEN/PET FRP composites. Axial compression was applied to 10 large-scale square RC columns, of which 8 were covered in LRS FRP and 2 served as control specimens. Vital parameters considered in the study which is the corner radius of the sections, the thickness of the FRP and the type of LRS FRP.The investigation introduced that the effective confinement stiffness ratio of the FRP jackets had a major impact on the axial compressive behavior of the columns. The average strain on the FRP hoop was found to be less at the rounded corners compared to the flat sides and transition points. This observation implies that the strain distribution at FRP rupture was more uniform in square columns. The current models utilized to analyze LRS FRP-confined concrete in noncircular columns exhibited a tendency to overestimate the specimens compressive response. With the help of reduction factors for axial strain and stress, the researchers suggested a new model that provides more accurate prediction to the compressive characteristics of large-scale square columns confined by LRS FRP.

The studies in this section are summarized with a number of points:

- Prediction: The current models utilized to analyze LRS FRP-confined concrete in noncircular columns exhibited a tendency to overestimate the specimens compressive response ,however , advanced techniques, like Artificial Neural

Networks (ANN) can be employed to simulate the behavior of LRS FRP confined concrete.

- LRS: Unlike conventional FRPs , LRS FRPs have bilinear material stiffness
- FRP confinement: increase the confinement of FRP leads to improvement in the ductility of the column , to enhance strength and to restricted and postponed the buckling of longitudinal reinforcement bars in additional to reduce the the impact of stirrup spacing on strength diminished
- Hoop strain : The average strain on the FRP hoop was found to be less at the rounded corners compared to the flat sides and transition points. This observation implies that the strain distribution at FRP rupture was more uniform in square columns.
- Shape: In comparison to rectangular specimens, the peak and post-peak strengths of square cross-section specimens were greater.

2.4 Concrete Columns Reinforced With Hybrid FRP

The study by Nain *et al.* [31] (2020) examined the behavior of high-strength concrete (HSC) filled with hybrid FRP tubes using different combinations of LRS-FRP (made from PEN and PET) and small rupture strain FRP (SRS-FRP). The researchers concluded that LRS-FRP significantly improved the ductility and ultimate strength of confined concrete compared to SRS-FRP confined concrete. The study also evaluated existing models in predicting the ultimate stress-strain behavior of hybrid LRS-FRP and suggested refinements for better accuracy. Hybrid FRP tubes (H-CFFTs) showed greater efficiency in terms of strength compared to both LRS and SRS FRP. Both LRS-CFFTs and H-CFFTs were efficient in energy dissipation, indicating their potential for seismic applications. The research underscores the potential of using hybrid FRP tubes for enhancing the strength and ductility of HSC columns.

Bai *et al.* [32] investigated the compressive behavior of concrete cylinders wrapped with LRS FRP and hybrid CFRP. 34 concrete cylinders were subjected to monotonic and cyclic axial compression for the investigation. The main goal was to find out how

different types and thicknesses of FRP affected a number of performance indicators, including energy loss, efficiency factors, failure modes and stress-strain responses. It was found that the hybrid confinement mechanism successfully combined the good things about CFRP and LRS FRP, making it better at dissipating energy and deforming while also making up for the bad things about each one. In order to simulate the monotonic stress-strain behavior, the researchers devised an analysis-oriented model that emphasized lateral stress-strain relationships and the localized CFRP fracture effect. Additionally, a cyclic stress-strain model was constructed utilizing this methodology. The fact that the ultimate axial stress and strain of hybrid-wrapped concrete went up by a lot shows that hybrid FRP confinement works. The increased axial rigidity of the composite FRP wrapping contributed to a rise in energy dissipation capacity. Researchers saw that the outer PET FRP and PEN FRP rupture strains got pretty high, which means that the FRP materials were used well. The study stresses how important it is to pick the right thickness and mix of CFRP and LRS FRP in order to get the most out of the benefits of hybrid confinement. This research adds a lot to what is known about using hybrid FRP materials to reinforce concrete, especially when it comes to making it better at releasing energy and making the best use of stress-strain relationships.

That study by Chaiyasarna *et al.* [33] (2021) looked into how well hybrid basalt/E-glass FRP composites work for recycled aggregate (RAC) with Clay bricks as aggregate (CBA) . 36 concrete cylinders (12 unconfined and 24 confined with basalt and glass-FRP (BE-FRP)) were subjected to pure axial compression in this investigation. CBA was produced using three varieties of bricks that exhibited different strengths and water absorption capacities. BE-FRP composites substantially improved the ductility, rigidity, and strength of RAC when combined with CBA, according to the findings. A significant enhancement in both strength and ductility was detected as the confinement level of the BE-FRP jackets was increased. It was discovered that the hybrid basalt/E-glass FRP composites significantly improved the efficacy of RAC with CBA. Significantly greater ultimate stresses were observed in low-strength and high-strength RAC-CBA specimens compared to unconfined control specimens. Experimental findings were typically overestimated in comparison to theoretical predictions derived

from established ultimate strength and strain models. This study makes a substantial contribution to the advancement of economically viable and environmentally friendly reinforcement strategies for recycled aggregate concrete.

Shen *et al.* [34] (2023) studied how interlayer hybrid FRP composites made of polypropylene (PP) and glass fabrics behaved when they were pulled apart. The main goal was to compare these composites to standard FRP composites in terms of their mechanical qualities, such as how stiff and flexible they are. Finite element (FE) analysis was used to find possible ways for the material to fail, especially delamination. They discovered that the glass/PP FRP composites were stiffer and more flexible than regular FRP composites. Failure modes were studied using the FE method, and it was found that delamination was the most common failure mode that could be used in civil engineering. To figure out how the glass/PP FRP composites behave when they are pulled apart, a structural model was created with the failure mode of delamination as its main focus. In the first linear stage, the stiffness of the composites was found to depend a lot on how stiff the glass layer was. There was a strong link between the glass layer volume fraction and the hybrid effect. The FE modeling method used could correctly predict how the composites would react to stress and pressure and how they would break.

Tang *et al.*'s study [35] from 2022 addressed the hybrid confinement mechanism in concrete cylinders by combining FRPs with high rupture strain (PET-FRP, PEN-FRP) and FRPs with low rupture strain (CFRP, GFRP, BFRP). Using hybrid layout sheets also helped us understand how the large-small rupture strain FRP mechanism works better. Under axial compression, a total of 39 FRP-confined concrete cylinders were evaluated. It was found that mixing FRP sheets with different elongation capacities led to pseudo-ductility behavior. This behavior increased strain capacity but depended on how stiff the FRPs were along their lengthways axes. In terms of elongation capacities, cylinders contained by hybrid FRP sheets behaved in a manner similar to that of cylinders contained by single FRP sheets. Three critical mechanical mechanisms in hybrid FRP sheets intended for confined concrete cylinders have been identified: Enhanced ultimate strength in comparison to its constituent parts; pseudo-ductile behavior; improvement in second strength contingent on the axial stiffness of the

FRP with greater elongation. Implementation of FRP sheets with reduced elongation, wherein the rupture timing fluctuates as a result of stress concentration, In order to quantify the ultimate strength of Type II mechanism specimens, a multi-linear model was constructed. In this study, Tang *et al.* [35] highlight the effectiveness of hybrid FRP sheets in reinforcing concrete cylinders, particularly in enhancing strength and ductility. The research paper presents predictive models for the strength of hybrid FRP-confined concrete and offers significant insights into its mechanical properties. Significant progress is made toward the creation of more effective and efficient confinement strategies for concrete structures employing hybrid FRP technologies as a result of these findings.

Determining the cyclic axial behavior of concrete confined with hybrid FRP, consisting of carbon or glass sheets (low tensile strain capacity) and polyethylene terephthalate (PET) sheets (high tensile strain capacity), was the objective of a study by Ispir *et al.* [36]. In order to examine the axial stress-strain relationship and dilation behavior of hybrid FRP-confined specimens subjected to axial compression loads, experimental data were gathered.The hybrid-confined specimens demonstrated distinct behavioral patterns, which were determined by the outer FRP jacket's tensile strain and lateral confinement stresses.While the lateral strain efficiencies of the hybrid configurations exhibited consistent improvement under monotonic loadings, no discernible superior compression response was detected in specimens subjected to cyclic testing.A stress-strain model was put forth to account for the envelope curve of the cyclic response, and the experimental and predicted stress-strain curves agreed well.General principles of FRP-confined concrete, such as greater confinement stress resulting in less concrete core dilatation, were validated by the study in hybrid FRP cases. This study enhances knowledge regarding the cyclic characteristics of hybrid FRP-confined concrete by shedding light on the intricate interplay among various FRP material types when arranged in a hybrid configuration. For designing resilient concrete structures in seismic regions, it is crucial to be able to predict the behavior of such confined concrete under cyclic loads. The proposed stress-strain model provides this capability.

The studies in this section are summarized with a number of points:

- Hybrid of LRS-FRP and SRS-FRP : hybrid confinement mechanism successfully combined the good things about CFRP and LRS FRP, making it better at dissipating energy and deforming while also making up for the bad things about each one. for high-strength concrete filled with hybrid FRP tubes, enhance the strength and ductility at the same time showed greater efficiency in terms of strength compared to both LRS and SRS FRP. It was efficient in energy dissipation, indicating their potential for seismic applications.
- The RAC-CBA specimens' strength and ductility were significantly improved by the BE-FRP jackets; low-strength and high-strength specimens exhibited considerably greater ultimate stresses than unconfined controls.
- under tensile stress, experimental observations revealed that glass/PP FRP composites exhibited superior stiffness and flexibility compared to traditional FRP composites, with the stiffness in the initial linear phase significantly influenced by the rigidity of the glass layer.
- When you combine FRP sheets with different elongation capacities, you get pseudo-ductility behavior, which raises the strain capacity. However, this raise depends on the difference in axial stiffness between the combined FRPs.
- While the hybrid configurations showed enhanced lateral strain efficiencies under monotonic loadings, they did not exhibit a superior compression response under cyclic loadings.

3. METHODOLOGY

To understand the behavior of square columns retrofitted by hybrid FRP under monotonic axial compression, an experimental program was conducted. For this, a total of 18 specimens was produced with low-strength concrete to represent existing buildings of low quality. In order to understand the behavior of hybrid-wrapped specimens, 2 specimens were left unconfined,and 10 specimens were wrapped with one type of FRP. This approach facilitated a deep exploration of the influence of the number of PET FRP layers and the inclusion of a carbon layer on the axial performance of the specimens.

The experiments on the square specimens were carried out at the Construction Materials Laboratory, Istanbul Technical University. All concrete was poured on the same day, and experienced workers prepared the specimens, ensuring the production of the specimens under the same conditions. FRP materials were sourced from a single provider, Kordsa Company.

This study has focused on the axial behavior of low-strength concrete wrapped with hybrid FRP. The test variables were chosen as the FRP type, the hybrid configuration, and the number of FRP layers. This allowed for a detailed comparison of various layer combinations under monotonic compression axial loads. During the tests, axial and lateral strains and vertical deformations were measured by strain gauges and LVDTs. Compression tests were conducted utilizing an Instron testing device with a maximum capacity of 5000 KN. This chapter provides a detailed overview of the study's goals, characteristics of the specimens, properties of the materials, and procedures employed.

3.1 Objective of Experimental Program

The experimental program was designed to achieve the following objectives:

- Investigate the behaviour of square columns strengthened by hybrid FRP under uniaxial compressive load, focusing specifically on the enhancement in ultimate strength and the enhancement in the axial strain ductility.

- Investigate the failure modes and examine the effect of hybrid FRP.
- Predict the compression behavior with several models and compare the predicitons with the test results.

3.2 Design of Test Specimens

To achieve the above-mentioned objectives, square columns with uniform dimensions were produced. In order to represent some characteristics of the substandard existing concrete buildings in Turkey, the square specimens with a crosssectional dimension of 275x275 mm were produced with low strength concrete.

Additionally, the exploration of wrapping with the used type of FRP in a hybrid form is a pivotal aspect of the design, as this is an underexplored area in current research, ensuring that the study contributes valuable insights in the field.

The dimensions of the specimens were maintained constant, with a length of 550 mm, a square section with dimensions of 275 mm, and a corner of 30 mm. The specimens were divided into different groups based on the type and number of FRP layers used for wrapping, as presented in Table 3.1.Two identical specimens were prepared for each group.

In Table 3.1, the details of the specimens are listed. Specimens were categorized based on the type and number of FRP layers used for wrapping, and each category contains details on whether the specimens are hybrid or not. This table illustrates the varied configurations used to investigate the behavior of the retrofitted square columns. In the results chapter, the findings of this experiment are primarily analyzed in terms of the type of FRP, the number of layers, and whether the configuration is hybrid. Figure **??** shows these FRP sheets wrapped with concrete.

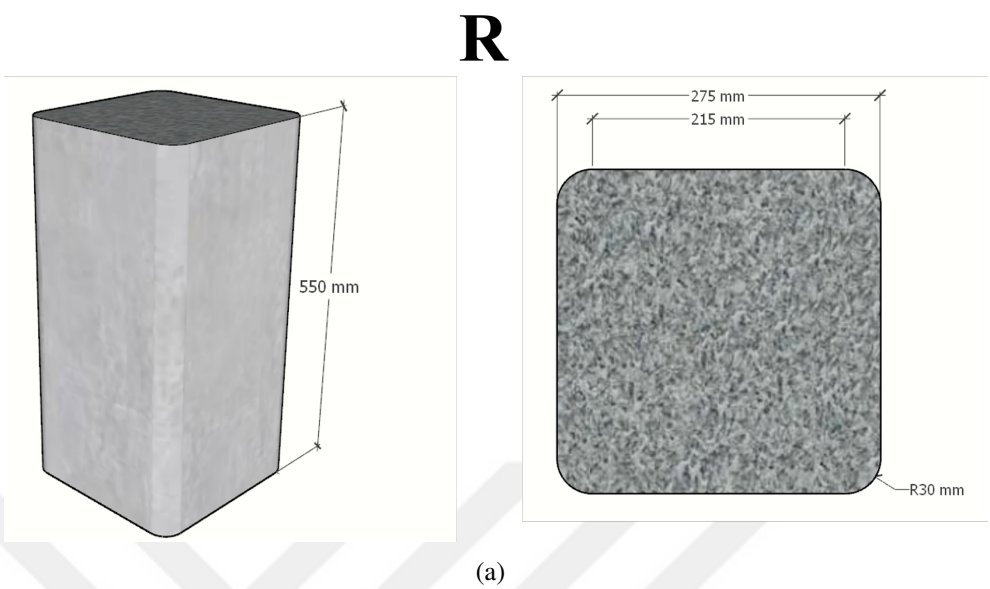

(a)

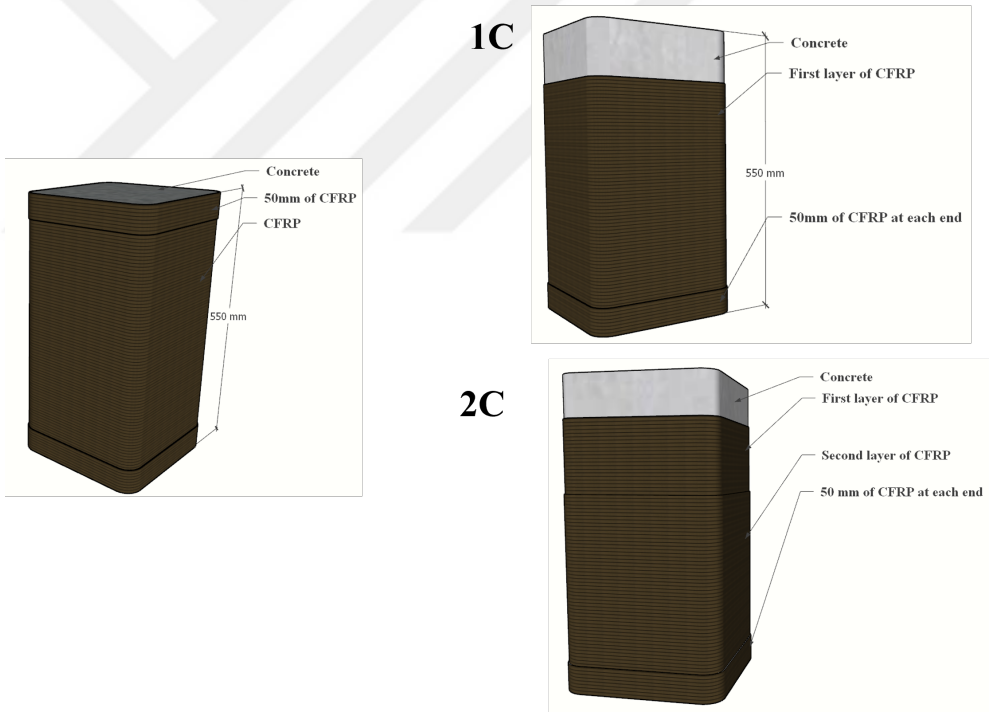

(b)

Figure 3.1 : Concrete columns wrapped with different configurations of FRP sheets where (a) is the reference: unwrapped concrete column, (b) CFRP confinement: columns wrapped with 1C and 2C FRP layers.

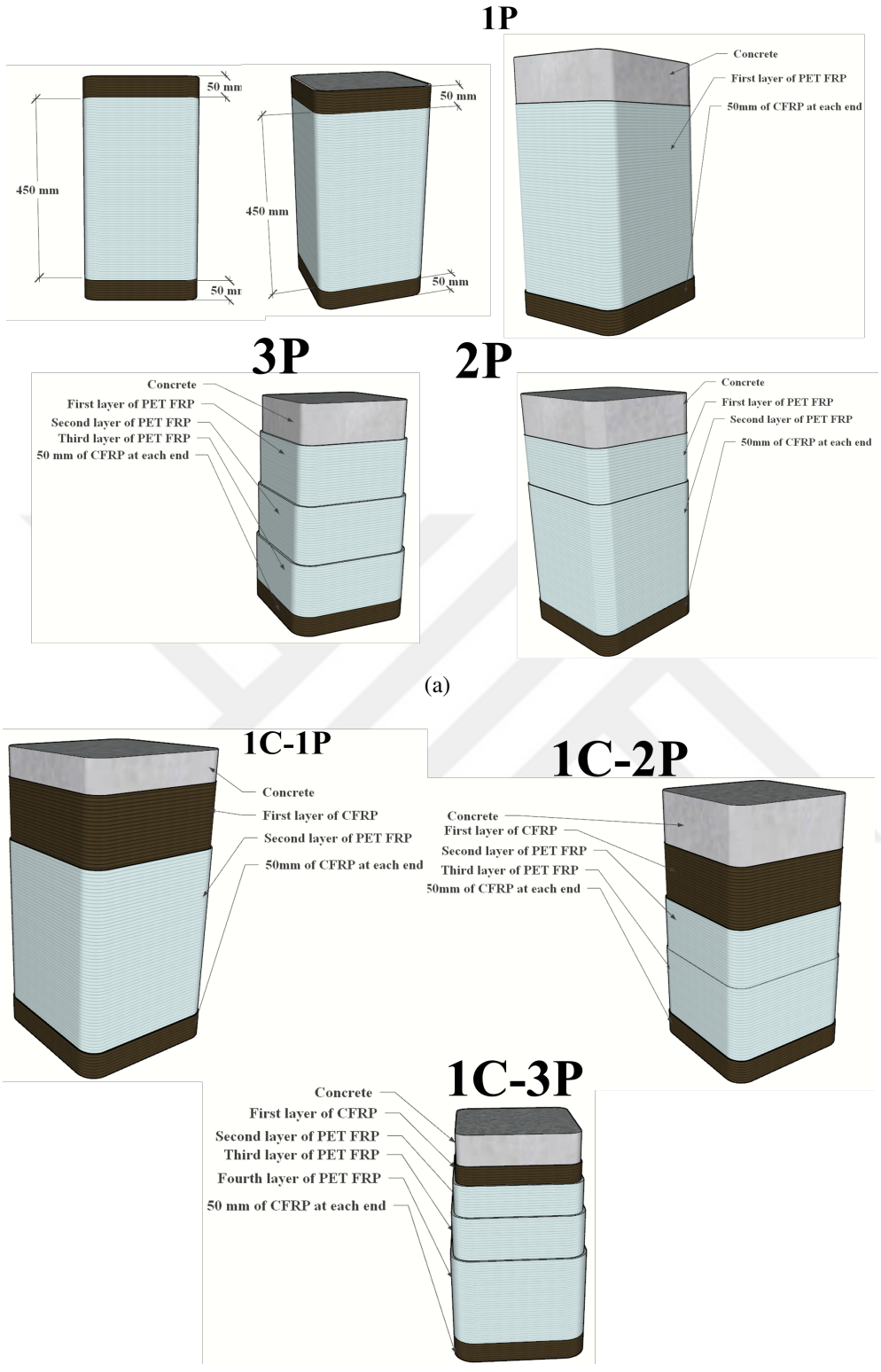

Figure 3.2 : Concrete columns wrapped with different configurations of FRP sheets : (a) columns wrapped with 1P, 2P, and 3P FRP layers, (b) the hybrid confinements: columns wrapped with 1C1P, 1C2P, and 1C3P FRP Layers.

Table 3.1 : The test matrix.

Group	Description	No. of Samples
R	References without wrapping FRP	2
1C	One layer of carbon FRP	2
2C	Two layers of carbon FRP	2
1P	One layer of PET FRP	2
2P	Two layers of PET FRP	2
3P	Three layers of PET FRP	2
1C-1P	One layer of carbon with one layer of PET FRP	2
1C-2P	One layer of carbon with two layers of PET FRP	2
1C-3P	One layer of carbon with three layers of PET FRP	2

3.3 Material Properties

3.3.1 Concrete

İSTON A.Ş. provided the concrete, which was pre-mixed to yield a low-strength concrete suitable for the study. Table 3.2 outlines the composition of the C10 concrete mix, crafted to simulate the substandard existing RC concrete structures. The table enumerates the components—cement, two varieties of aggregates, water, and a particular additive to enhance the concrete's properties—and their proportions, aimed at attaining a Ĩ4 MPa strength while preserving workability and other essential attributes.

Wooden molds were prepared for the production of the specimens, depicted in Figure 3.3a. These molds were meticulously cleaned to remove any dust, and their inner surfaces were oiled to ease the subsequent removal of the set concrete.

To ensure uniform compaction of the concrete within the molds, the mix was compressed manually with a steel rod, as shown in Figure 3.3b. Additionally, standard cyclinder concrete specimens were prepared specifically to assess the 28-day strength, as demonstrated in Figure 3.3e.

All molds were consistently filled with the same concrete mix. During the pouring process, The concrete temperature was monitored as 12.7°C. A flow test was also

carried out. The results of these tests are concisely presented in Table 3.3 and depicted in Figure 3.3c-d below.

Table 3.2 : The weight proportions of concrete mixes for low-strength concrete.

Material	Weight Proportion (%)
Cement (Bulk) PC	8.55
Aggregate No.1 (Unwashed)	27.91
Mountain Sand 0-4	29.26
Stone Dust (Unwashed)	24.76
Water	9.45
Chemical Additive Superplasticizer	0.07

Table 3.3 : Concrete temperatures and flow test results during casting.

Temperature (°C)	Flow diameter (cm)
15.7	40.5
15.6	38.0
15.5	39.0
15.6 (Average)	39.2 (Average)

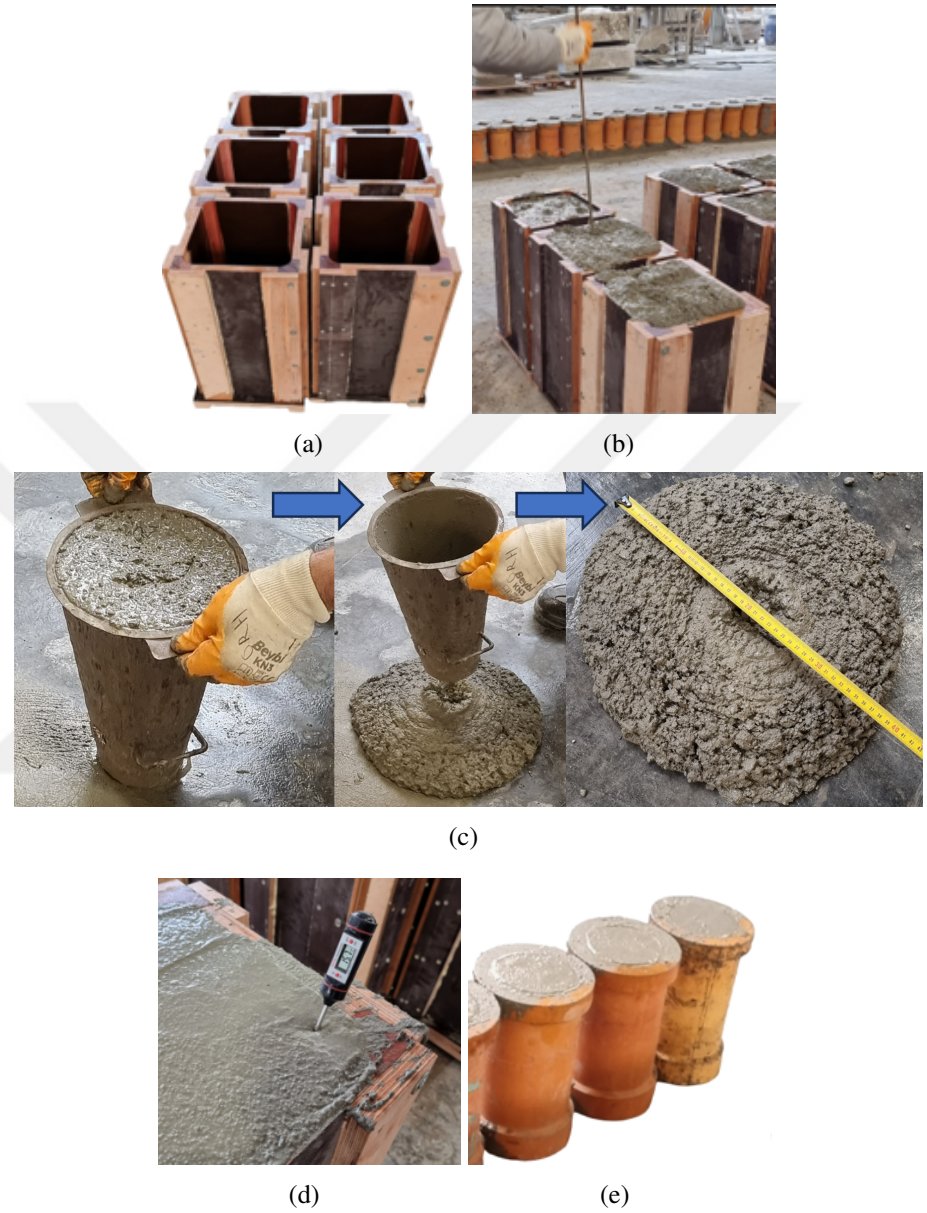

Figure 3.3 : Stages of concrete preparation (a) wooden molds, (b) manual compaction of concrete using a steel rod, (c-d) flow test and temperature measurements, (e) cylindrical concrete samples for 28-day strength assessment.

3.3.1.1 28-Day strength test for concrete

Cylindrical monotonic uniaxial test was performed in this study as it is a fundamental and universally accepted method for determining the compressive strength of concrete. This test, crucial in concrete analysis, is typically performed on standard cylindrical specimens at 28 days in line with ASTM C469 [37], three concrete cylinders, each with a diameter of 150 mm and a height of 300 mm, were tested. Additionally, another set of three samples was tested concurrently with the wrapped concrete, ensuring a comparative analysis of the specimens under identical conditions. The summarized outcomes of these tests are presented in Table 3.4, with detailed results to be discussed in the chapter 5. In this test, a concrete cylinder is placed in a compression testing machine, and an axial load is applied constant rate of displacement (0.6 mm /min) until the specimen fails. The load at the point of failure is recorded and used to calculate the concrete's compressive strength. This test method is direct and offers a reliable metric of the concrete's ability to withstand compressive forces. For a visual representation of this setup in Figure 3.4, which depicts the arrangement and execution of the monotonic uniaxial compression test.

Table 3.4 : Compressive strength of concrete cylinders.

Sample ID	Age (Days)	Compressive Strength (MPa)
Sample 1	28	8.60
Sample 2	28	9.24
Sample 3	28	9.23
Sample 1	312	12.96
Sample 2	312	15.57
Sample 3	312	14.84
Average	28	9.0
Average	312	14,5

Splitting tensile tests (indirect tensile test) were also done in this study as they are crucial for understanding the tensile strength of concrete. This test method provides valuable insights into the tensile characteristics of concrete, which are difficult to measure directly due to concrete's brittle nature. During the splitting tensile test, a concrete cylinder is placed horizontally between the loading surfaces of a compression testing machine and a load is applied along the diameter until failure occurs. The test is

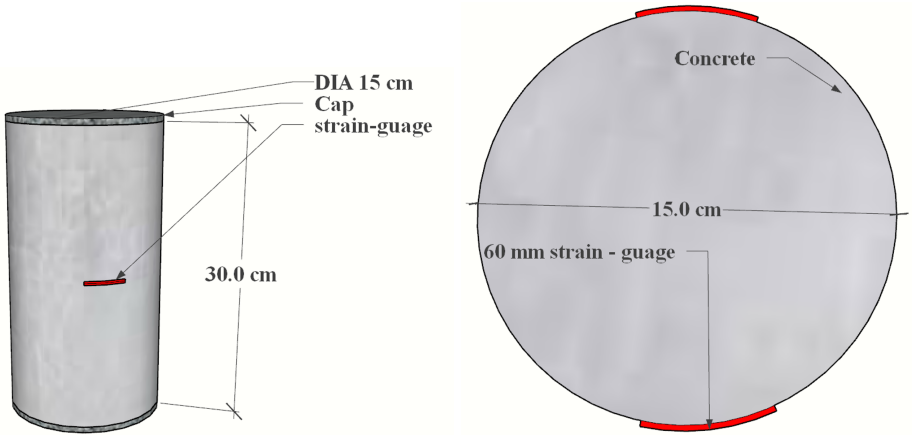

(a) (b)

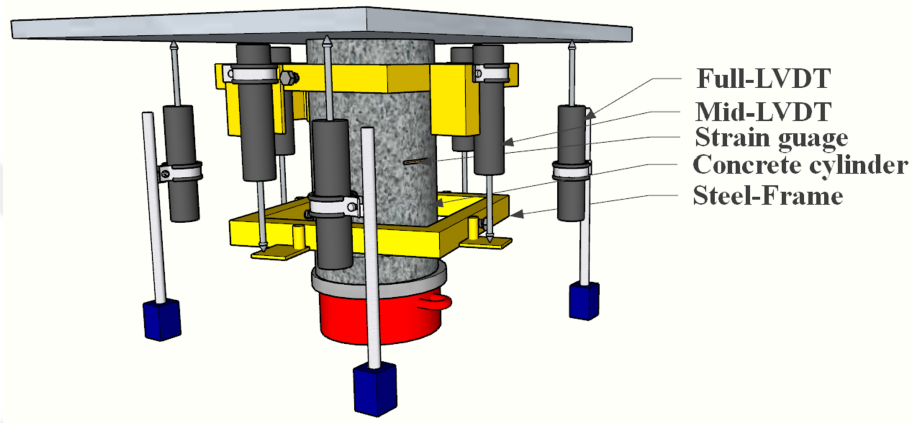

(c)

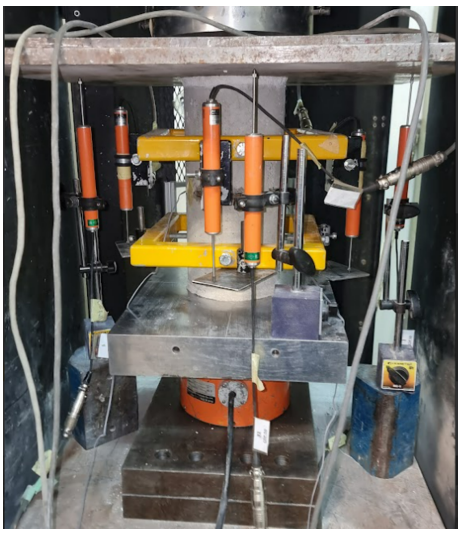

(d)

Figure 3.4 : Comprehensive Overview of the monotonic uniaxial compression test setup of the unconfined concrete cylinder: (a) dimensions of the cylinder specimen, (b) positioning of the strain gauge, (c) 3D view of the setup and instrumented cylinder, (d) the set-up.

based on generating a uniform tensile stress along the vertical diameter of the cylinder, eventually causing the specimen to split along the vertical plane. The resulting tension failure provides an estimate of the concrete's tensile strength, which is typically a fraction of its compressive strength. The formula to calculate the splitting tensile strength from a cylindrical test specimen is:

$$\text{Splitting tensile strength} = \frac{2P}{\pi DL} \tag{3.1}$$

Where:

- P is the maximum load applied to the specimen (in Newtons).
- D is the diameter of the cylinder (in meters).
- L is the length of the cylinder (in meters).

The 28-day tensile strength test is a vital component of this study because it shows that the specially made low-strength concrete mix meets certain performance standards. This test is very important for finding out if the concrete has the natural ability to get stronger through confinement. It is done after the normal curing period. Before any reinforcing techniques are used, it is essential to have a basic understanding of the concrete's tensile resistance.The result of test shown in Table 3.5 and the set-up illustrated in Figure 3.5.

Table 3.5 : Splitting tensile strength of concrete cylinders.

Sample ID	Max. Load (KN)	Splitting Tensile Strength (MPa)
1	75.6	1.07
2	87.6	1.24
3	93.7	1.33
Average	85.6	1.2

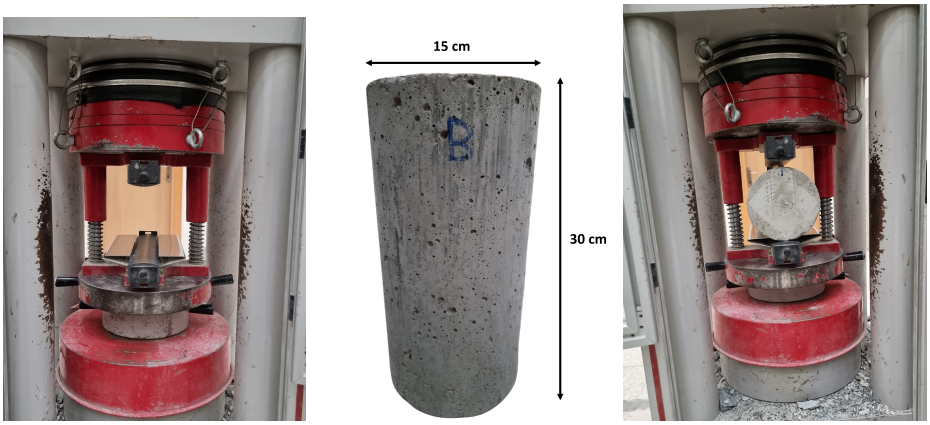

(a) (b) (c)

Figure 3.5 : Splitting tensile test process: (A) splitting test machine, (B) concrete cylinder specimen (15 cm x 30 cm), (C) image capturing the test in progress.

3.3.2 FRP materials

This study sourced carbon and PET sheets, and epoxy from Kordsa Inc., a prominent Turkish manufacturer renowned for their specialized composite materials. The CFRP fabric stands out due to its remarkable unidirectional tensile strength, achieving levels up to $\tilde{2}777$ MPa. Despite its significant tensile strength, the strain capacity is limited, yet the fabric retains its elasticity until breaking. In contrast, PET FRP is especially recognized for its superior rupture strain. Table 3.6 presents the standard properties provided by the manufacturer, highlighting key metrics such as the elastic modulus, material thickness, tensile strength, and tensile strain capacity. These details offer deep insights, becoming indispensable for professionals, including composite designers, engineers, and technicians. Such data forms a foundational reference for informed decisions when employing FRP composites in structural designs. Figure 3.6 provides visual references for the materials, where (a) shows the carbon fiber and (b) shows the PET fiber. The coupon test of the FRP materials, which provides additional data on their performance, will be detailed further in Chapter 4.

3.4 Applying External FRP Confinement to the Specimen

The specimens were categorized into several groups to represent different confinement levels for concrete columns. Group R specimens were left unconfined. The 1C and

Table 3.6 : Standard properties of CFRP and PET FRP materials provided by the manufacturer.

Material	Tensile Strength (MPa)	Modulus of Elasticity (MPa)	Elongation at Break (%)	Thickness (mm)
Carbon	3430	230000	1.49	0.165
PET	500	6900	15	0.65



(a) (b)

Figure 3.6 : Types of Fiber-Reinforced Polymers (FRP) used in the study:(a) Carbon Fiber Reinforced Polymer (CFRP), (b) Polyethylene Terephthalate (PET) Fiber Reinforced Polymer

2C groups were externally wrapped with one and two layers of CFRP respectively, while groups 1P, 2P, and 3P were confined with one, two, and three layers of PET FRP respectively. Additionally, groups 1C1P, 1C2P, and 1C3P featured a combination of one layer of CFRP and one, two, and three layers of PET FRP respectively. All wrappings were applied in the transverse direction with a 200 mm overlap to prevent failure caused by the separation of the FRP layer in the overlap region. Figure 3.7 illustrates the cross-sections of FRP confined columns, showcasing the overlap. Before confinement, the specimens were removed from the water, their surfaces cleaned and left to dry. Once the surfaces were thoroughly dried, the wrapping process began. The wet-layup method was used for confinement. FRP sheets were cut and prepared in advance. Following the manufacturer's guidelines, epoxy resin and hardener were mixed at a 3:1 weight ratio at room temperature and stirred for about two and a half minutes. The epoxy was then brushed onto both the specimens and the FRP sheets. To prevent premature failure at the both ends due to non-uniform confinement and concentration of stress in this regions, different numbers of CFRP layers, each 50 mm

wide (CFRP rings), were applied to the top and bottom of each column, as detailed in Table 3.7. The process of preparing the specimens is depicted in Figure 3.8.

Table 3.7 : Number of CFRP ring layers.

Group	Number
R	0
1C	3
2C	4
1P	3
2P	4
3P	5
1C-1P	3
1C-2P	4
1C-3P	5

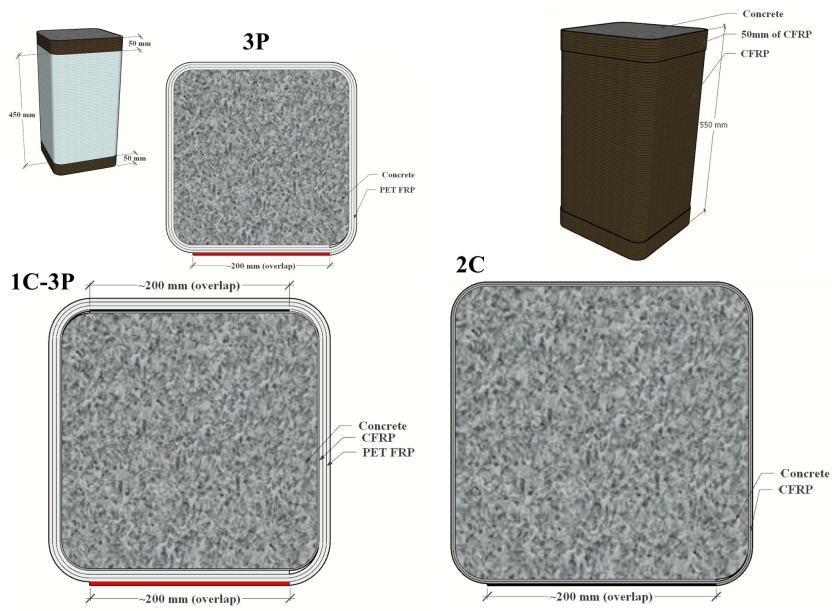

Figure 3.7 : Cross-sections of FRP confined columns showing overlap.

3.5 Cap

For axial compression tests on columns, the capping process is critical to ensure even load distribution and test accuracy [38]. The procedure begins by placing the columns on a flat surface. Next, their surfaces are roughened with an angle grinder, which helps the mortar adhere better. After this, any dust from the roughening process is cleaned off. The columns are then dampened with water, a step that enhances the bonding of the mortar. For the capping, Sika MonoTop®-2400 mortar is used because of its



(a) (b) (c)



(d) (e) (f)



(g) (h)

Figure 3.8 : Preparation process of the concrete specimens for confinement: (a) cutting the FRP material to size, (b) epoxy resin and hardener cans, (c) homogenizing epoxy components, (d) surface cleaning of columns, (e) application of epoxy to column surface, (f) adhering FRP wrap for confinement, (g) installation of CFRP rings, (h) final appearance of the confined column.

ease of use, effective workability, and strong bond strength due to its high polymer content. This mortar is mixed thoroughly by combining it with clean, cold water and stirring with an electric mixer for three minutes to ensure a uniform mixture before application. The entire capping process is illustrated in Figure 3.9, which provides a visual representation of each step.



Figure 3.9 : Steps in capping process of concrete column specimens: (a) preparing surface with angle grinder, (b) Surface post-roughening, (c) bag of Sika MonoTop-2400 mortar, (d) mixing mortar with electric hand mixer, (e) Oiling glass plate for leveling, (f) applying mortar to column top, (g) leveling mortar with glass plate, (h) Ensuring level surface with bubble level.

3.6 Test Setup

An Instron Satec 1000 RD universal testing machine was used to perform the compression tests on the square specimens.Each specimen was equipped with various strain gauges (PL-60, PFL-20) and TML transducers integrated into the Instron's load cell. Data from these instruments was channeled to the TML TDS 303 data logger via a TML ASW-50B switch box., enabling systematic strain measurement recording. This setup allowed for the automated capture of strain, deformation, and load measurements at two-second intervals during sustained loading tests, ensuring a continuous and detailed record of each specimen's behavior under load.

3.6.1 Strain gauges

Wire strain gauges, specifically the PL-60-11-3LJC-F and PFL-20-11-3LJC-F models were used to measure surface strain of the specimens during tests. These gauges, equipped with a fine electric resistance wire on a polyester resin backing, are adept at converting mechanical deformation into an electrical signal. This capability stems from their design to register changes in electrical resistance, which directly correlates to the strain experienced by the specimen. Aligning with methodologies prevalent in structural engineering research, the selection of the strain gauges mirrors that in studies like [39], who also used this particular model. In this study, the strain gauges with a 60-mm gage length were affixed horizontally to three faces of each square specimen at midheight, excluding the overlap face, to ensure comprehensive strain measurement. To further enhance the data collection, the strain gauges with a 20 mm gauge length (models PFL-20-11-3LJC-F) were strategically positioned at three corners on some columns. This arrangement allowed for a more thorough capture of lateral strain distribution through the circumference of the specimen. . Figure 3.10 provides a clear visual representation of both the types and locations of the strain gauges used.

The preparation of the column surfaces for strain gauge installation setup was executed through a methodically staged process. Initially, a thin layer of epoxy resin was applied to the surfaces of the columns. This layer was left to set for a period of two

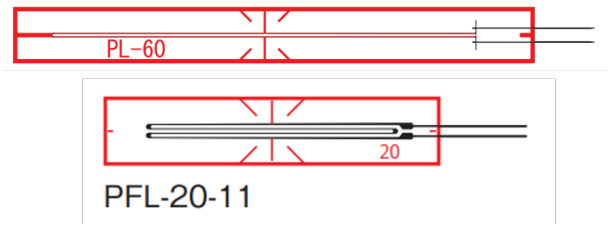

(a)

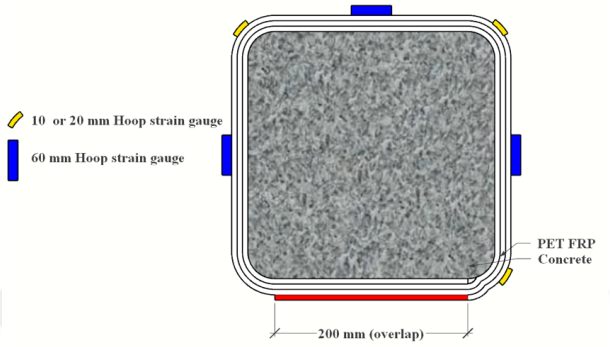

(b)



(c)

Figure 3.10 : Comprehensive visualization of strain gauge implementation: (a) the strain gauges utilized, (b) placement of strain gauges on column, (c) 3D view of a column with attached strain gauges.

weeks, allowing it to achieve the required hardness and adherence quality crucial for strain gauge installation. Following this curing period, the epoxy layer was carefully smoothed down with a sander machine to create an even thinner and more uniform epoxy coating. This meticulous preparation of the surface is pivotal for the effective attachment and performance of the strain gauges. After the surface was ready, the strain gauges were attached using Evobond 502 Super Japanese Adhesive, selected for its strong bonding properties. To ensure the formation of a robust and durable bond, these gauges were left undisturbed for a minimum of 24 hours, allowing the adhesive to fully cure. The detailed process of preparing the surfaces and placing the strain gauges on the FRP-wrapped columns is illustrated in Figure 3.11, which provides a step-by-step visual representation of the entire procedure, from surface preparation to the final placement of the strain gauges.

3.6.2 LVDTs

Linear Variable Differential Transformers (LVDTs) were crucial in monitoring the displacement of the columns during testing. LVDTs, renowned for their precision in displacement measurement, have been consistently used in engineering for their reliability in displacement measurement. four TML CDP50 type LVDTs, each with a gauge length of 50 mm, were strategically positioned at the midpoint of the specimens using a steel frame specifically designed to complement the specimens. To fully capture the strain distribution along the full length of the columns, additional four LVDTs of the same type were arranged around each specimen. This comprehensive array of LVDTs, connected through the TML ASW-50B/C switch box, facilitated the systematic collection of displacement data. The precise placement of these LVDTs is depicted in Figure 3.12, which illustrates their positioning on the specimens, offering a visual understanding of the measurement setup adopted.

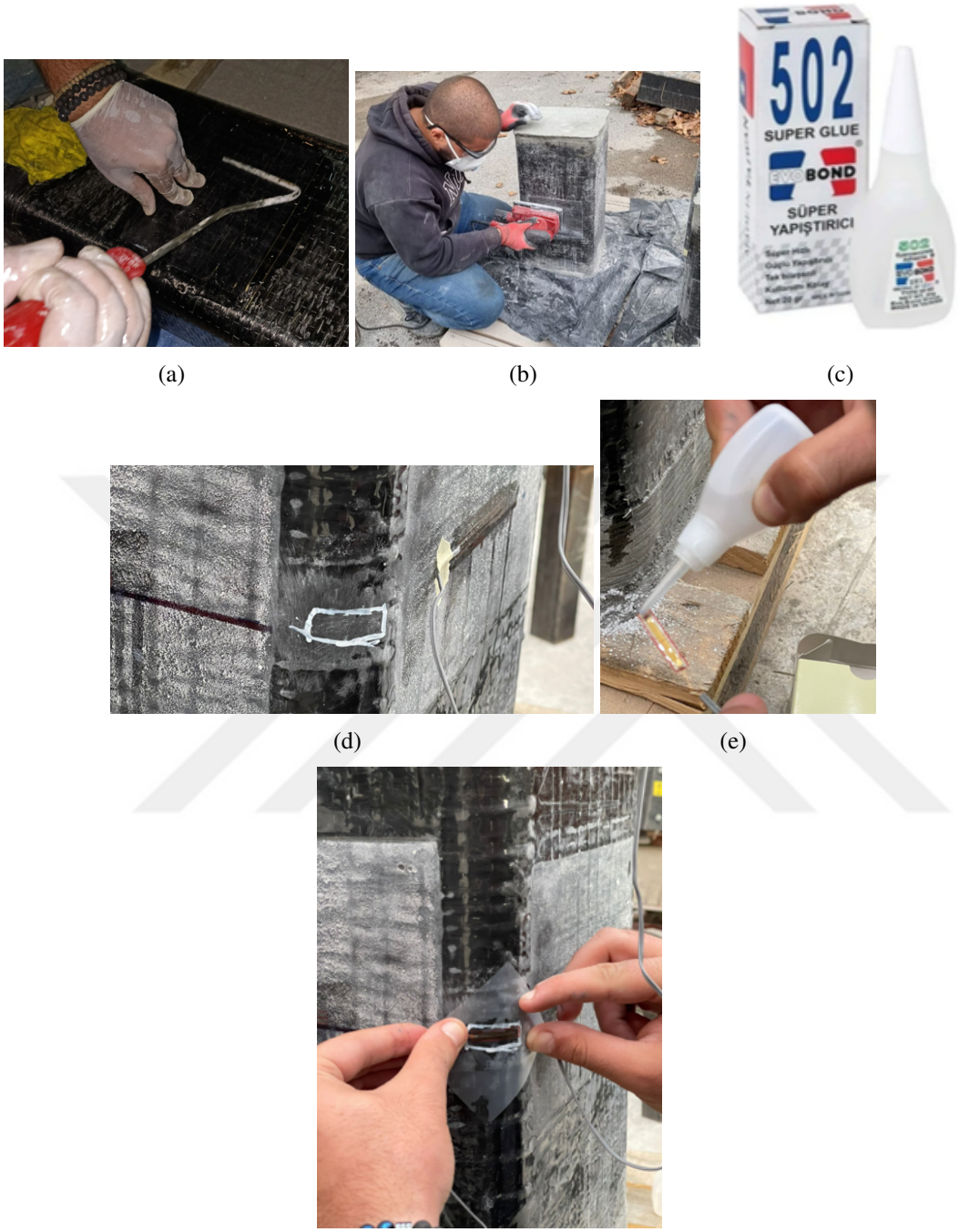

Figure 3.11 : Detailed stages of strain gauge installation on FRP-wrapped columns: (a) applying epoxy to FRP surface, (b) thinning epoxy layer with sander machine, (c) Evobond 502 super Japanese adhesive, (d) marking strain gauge locations, (e) applying adhesive on strain gauges, (f) securing strain gauges with pressing for one minute.

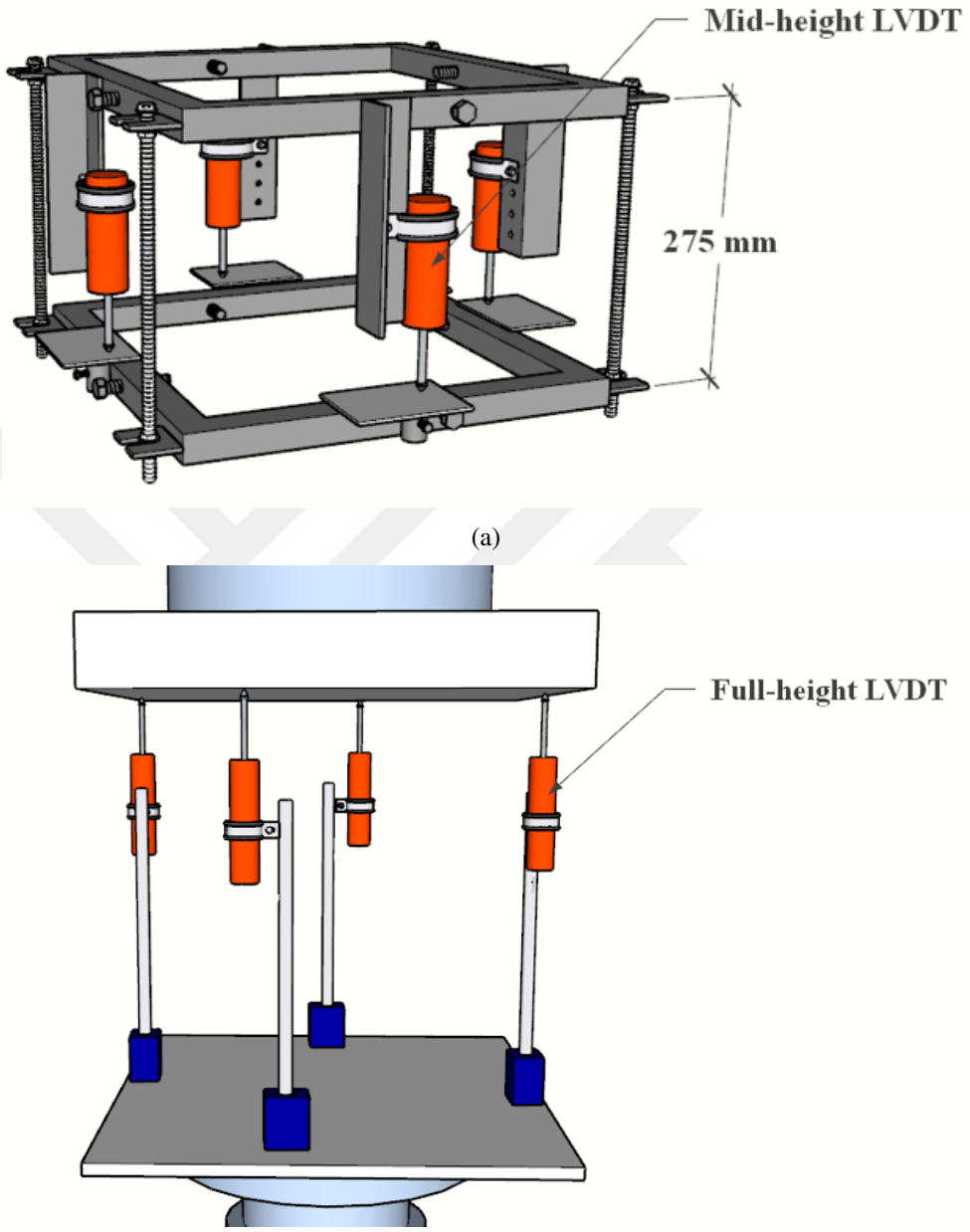

Figure 3.12 : Illustration of LVDT setup in axial displacement measurement: (a) 3D view of steel frame with mid-positioned LVDTs, (b) placement of full-length LVDTs.

3.6.3 Setup and calibration of specimens in the testing machine

An Instron Satec 1000 RD universal testing machine (with a compression capacity of 5000 kN) available at Istanbul Technical University, Civil Engineering Faculty, Construction Materials Laboratory, was utilized for monotonic compressive loading of the specimens. A pre-load of 14 kN was applied to each specimen prior to testing. The test was performed under displacement control with a constant rate of 0.6 mm/min. Data acquisition was maintained via a 50-channel TML ASW650C switch box and a TML TDS6303 data logger and stored on a computer. During the tests, displacement, strain, and load data were collected every two seconds automatically until the specimen completely lost its integrity. All the steps are shown in Figure 3.13 and Figure 3.14.

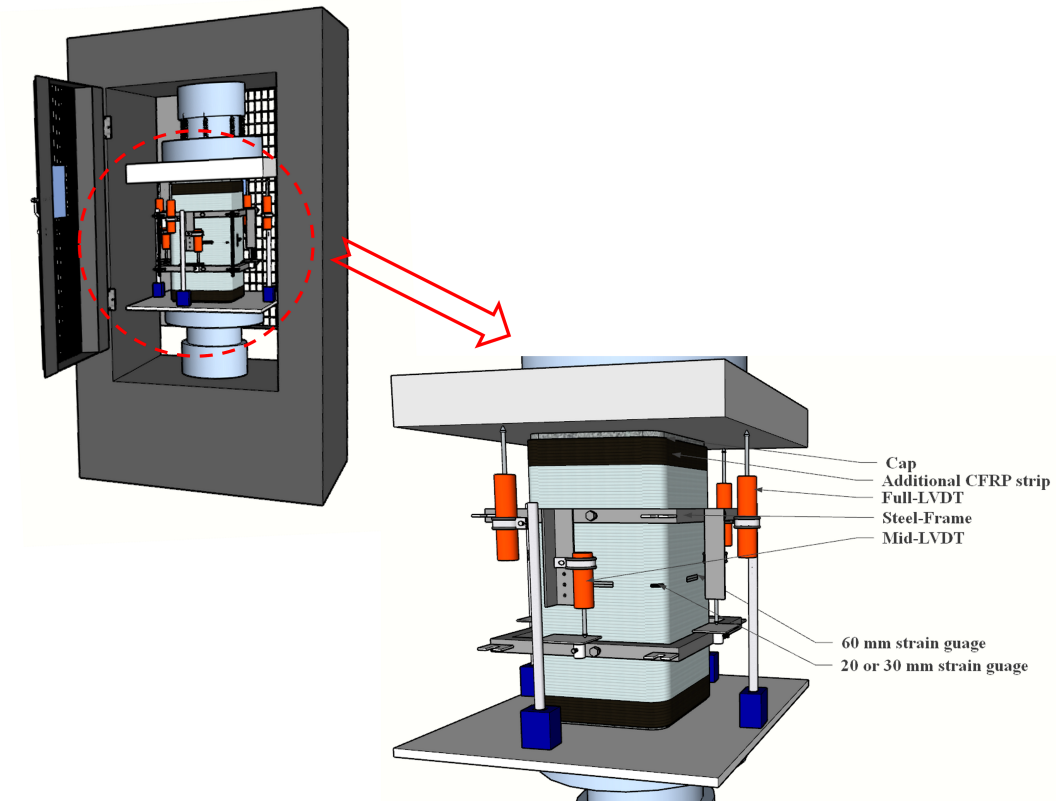

Figure 3.13 : 3D View of the instrumented specimen in testing setup.



(a) (b) (c) (d)



(e) (f)

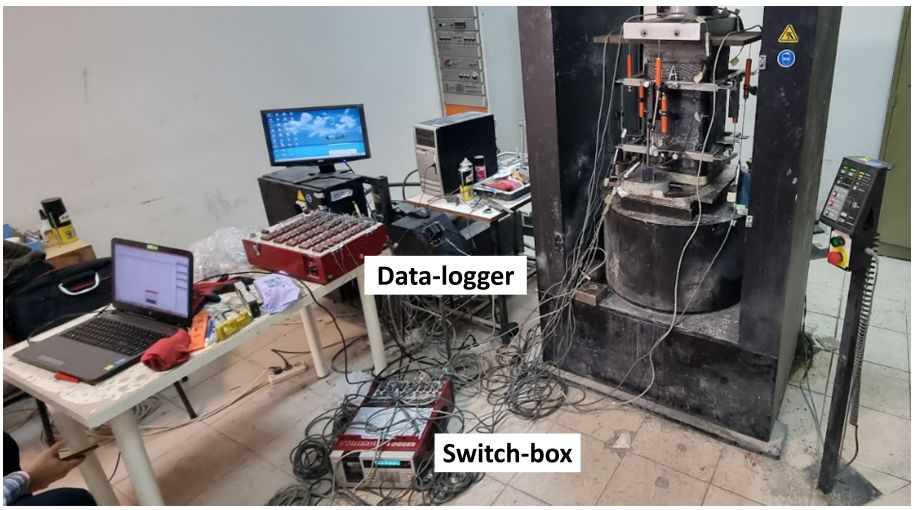

(g)

Figure 3.14 : Sequential stages in setting up the testing apparatus: (a) verifying base level of testing machine, (b) Marking specimen tops for centering guidance, (c, d) leveling steel frame and LVDTs, (e) connecting strain gauges to data logger, (f) connecting LVDTs to switch box, (g) overall view of the experimental setup.

4. COUPON TEST

4.1 Test Background

FRP composites are a diverse category of materials that involve a polymer matrix reinforced with fibers. FRPs are extensively utilized in several industries, including aerospace, automotive, marine, and construction, due to their exceptional strength-to-weight ratios [40,41]. Previously, composite structures mainly relied on carbon, aramid, basalt, and glass fibers as the main form of reinforcement. However, the growing demands of the building industry have been accelerated by the introduction of new fibers like PET and PEN. These materials have brought out a new generation of construction materials that are not only essential for retrofitting construction but also have positive environmental implications. In contrast to conventional fibers, these novel alternatives demonstrate unique mechanical properties, including a high rupture strain and lower tensile strength [27,42].

The idea of hybrid FRP includes the incorporation of two different types of fibers into a composite material. Each constituent fiber possesses its own unique set of benefits and drawbacks in terms of mechanical characteristics. By combining these fibers, the resulting composite can exhibit enhanced mechanical properties and potentially achieve cost efficiency [43]. The research presented here focuses mainly on hybrid fiber-reinforced polymers (FRP) that incorporate both carbon and polyethylene terephthalate (PET) fibers.

The investigation of the mechanical characteristics of hybrid composites yields valuable data that may inform composite designers, engineers, and technicians in their decision-making process about the use of hybrid composites for structural parts or components.

Tensile properties refer to the response of materials when subjected to tensile forces, demonstrating their ability to resist deformation. The determination of tensile

characteristics is of utmost importance as it yields valuable insights into many parameters such as the modulus of elasticity, elastic limit, elongation, tensile strength, yield point, yield strength, and other relevant tensile properties [44].

The primary objective of this work is to evaluate and clarify the mechanical characteristics of FRP material when subjected to tensile stress.

4.2 Experimental Details

4.2.1 Materials and specimens

The fiber sheets of carbon and PET, and epoxy resin were provided by Kordsa Inc., Turkey.

The carbon and PET fibers were cut into rectangular shapes of 50 cm by 61 cm, as shown in Figure 4.1. A total of six sheets of carbon and twelve sheets of PET fiber were utilized in the fabrication of the eight FRP plates, as indicated in Figure 4.1. As per the guidelines provided by the manufacturer, the epoxy resin and hardener were combined at room temperature with a weight ratio of 3:1. Subsequently, the resulting mixture was properly mixed for a duration of two and a half minutes. The choice of an acetate sheet as the foundational layer was based on its convenient removal properties, which may be attributed to its smooth surface and lack of adhesiveness.

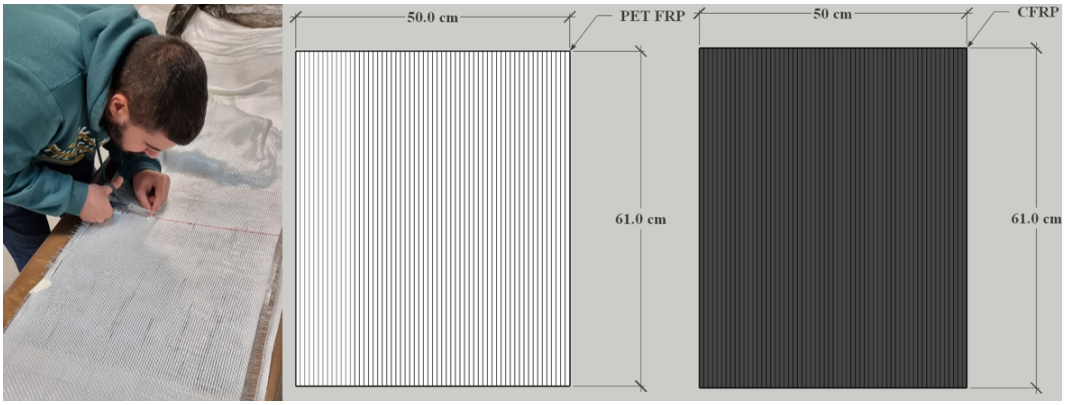

Figure 4.1 : Carbon and PET Fiber rectangular cut for FRP plate preparation.

The wet layup materials for flat tensile testing in the laboratory were prepared according to the standards outlined in Section L.2 of ACI 440.3R [45], as illustrated in Figure 4.3. The procedure involved the placement of an acetate sheet onto a level

surface, followed by the application of resin via a paint roller. Afterwards, the FRP fabric or sheet was placed into the resin, followed by applying the resin. The previously described procedure was repeated for several layers. An additional acetate sheet was laid out above the surface, and any extra resin and air were eliminated by employing the flat edge of a floor wiper, moving in alignment with the fibers. The composite material was allowed to undergo a 24-hour curing process at room temperature prior to the removal of the acetate sheets.

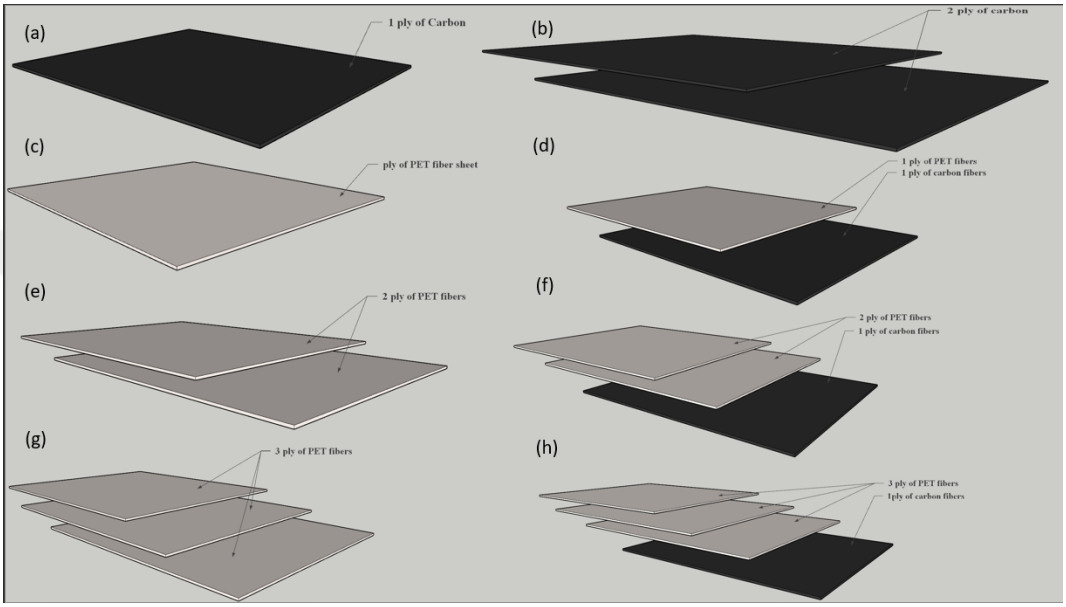

Figure 4.2 : Fiber layup arrangement for producing composite plates: (a) one-layer carbon, (b) two-layer carbon, (c) one-layer PET, (d) one-layer carbon and one-layer PET, (e) two-layer PET, (f) one-layer carbon and two-layer PET, (g) three-layer PET, (h) one-layer carbon and three-layer PET.

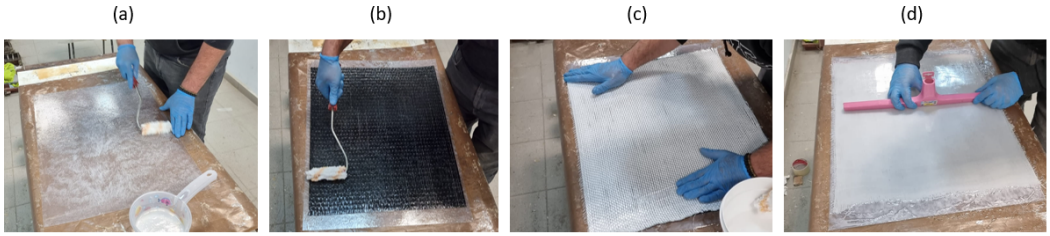

Figure 4.3 : The procedure to prepare the wet layup materials for flat tensile testing : (a) the application of resin via a paint roller to the foundational layer of acetate . (b) the carbon FRP sheet was placed into the resin, followed by applying the resin (c) placement of the second layer of PET sheet. (d) eliminating the extra resin and air using a floor wiper.

After two weeks, test coupons were prepared for mechanical tests by cutting from cured composite laminates in the 25 mm * 250 mm geometry suggested by ASTM

D3039 [1] for the uniaxial tensile test standard using the Kuka KR16 Ultra-F robot equipped with a high-performance water jet pump, as shown in Figure 4.4.

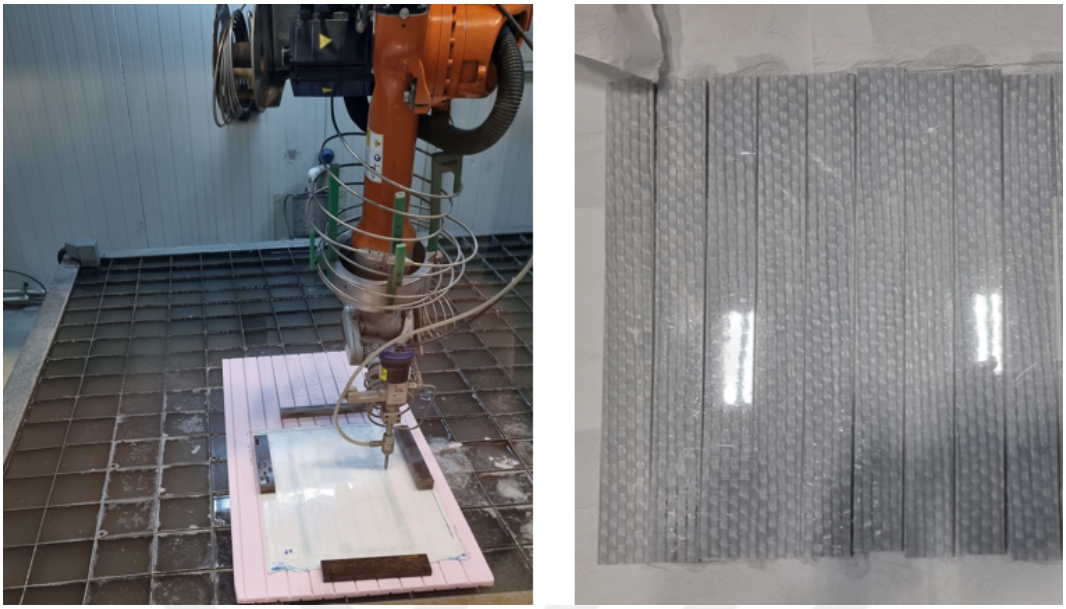

Figure 4.4 : Demonstrates the process of cutting FRP plates with the Kuka KR16 Ultra-F Robot equipped with a water jet pump on the left side, while the resulting cut coupons are displayed on the right side.

The grip locations of the specimens are ground with 800-grit sandpaper to remove any foreign particles, smooth the surface, and achieve better bonding with tab material. Sandpaper tabs, measuring 25x50 mm, are then adhered onto polished areas of test samples using (name of the glue), serving a dual purpose of bonding and stress reduction [46]. The gage length for the specimens was maintained at 15 cm, following ASTM D3039-D3039M-14 [1] standards, as depicted in the Figure 4.5 which shows a drawing to show the measurements of the test coupons and the placement of the tabs.

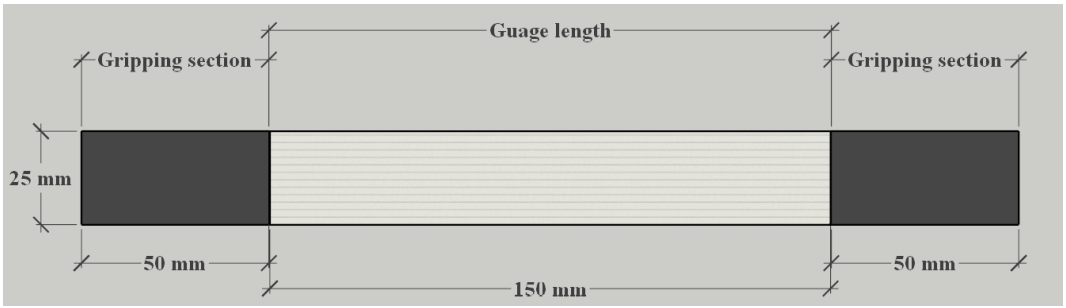

Figure 4.5 : the measurements of the test coupons and the placement.

4.2.2 Tensile test on composite

The experiments were performed using an Instron 5982 universal testing machine (UTM) at Sabancı University with a test speed of 2 mm/min, as seen in Figure 4.6. The specimens in Table 4.1 are incrementally loaded until they reach failure under uniaxial tensile. The integrated Bluehill software system provides the load measured by the load cell built into the Instron testing machine. The tensile strain is determined using a pair of linear strain gauges that are affixed to the gauge portion of the specimen.

Table 4.1 : Nominal thicknesses of the coupon specimens.

Configuration	Nominal Thickness (mm)	Sketch up
C-1C	0.165	
C-2C	0.33	
C-1P	0.65	
C-2P	1.3	
C-3P	1.95	
C-1C1P	0.815	
C-1C2P	1.456	
C-1C3P	2.115	



Figure 4.6 : Setting up of tensile test of coupon/specimen.

4.3 Coupon Test - Result

The coupon test results of 1C, 2C, 1P, 2P, and 3P are given in this part of the thesis. The coupon tests of the hybrid specimens will be given in another future study.

Using tensile test results, tensile stress-tensile strain curves are obtained. These curves are given in Figure **??**-Figure 4.17. It is seen that while CFRP exhibits a linear behavior under tension load, PET FRP exhibits a nonlinear behaviour characterized by two lines.

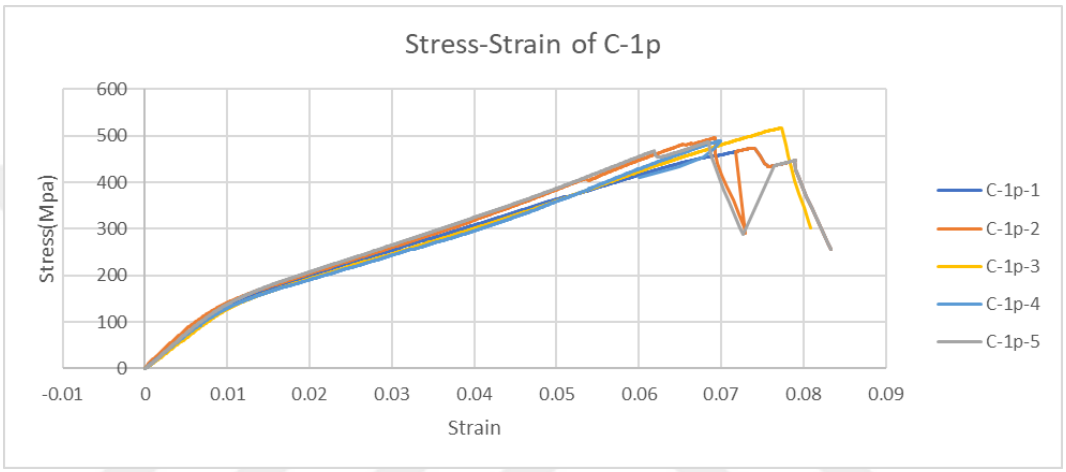

Figure 4.7 : Stress-strain curve of the coupon test results of C-1P.

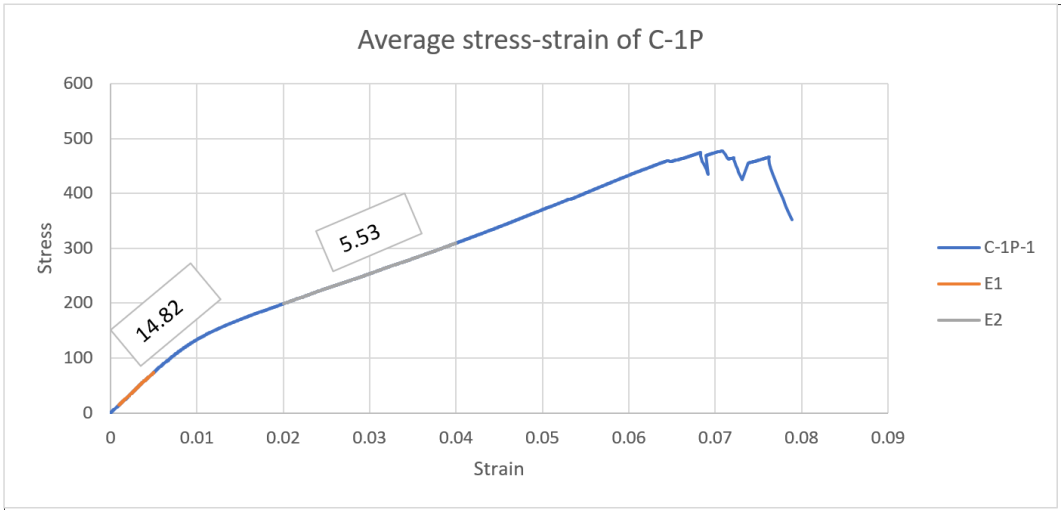

Figure 4.8 : Average stress-strain curve of the coupon test results of C-1P.

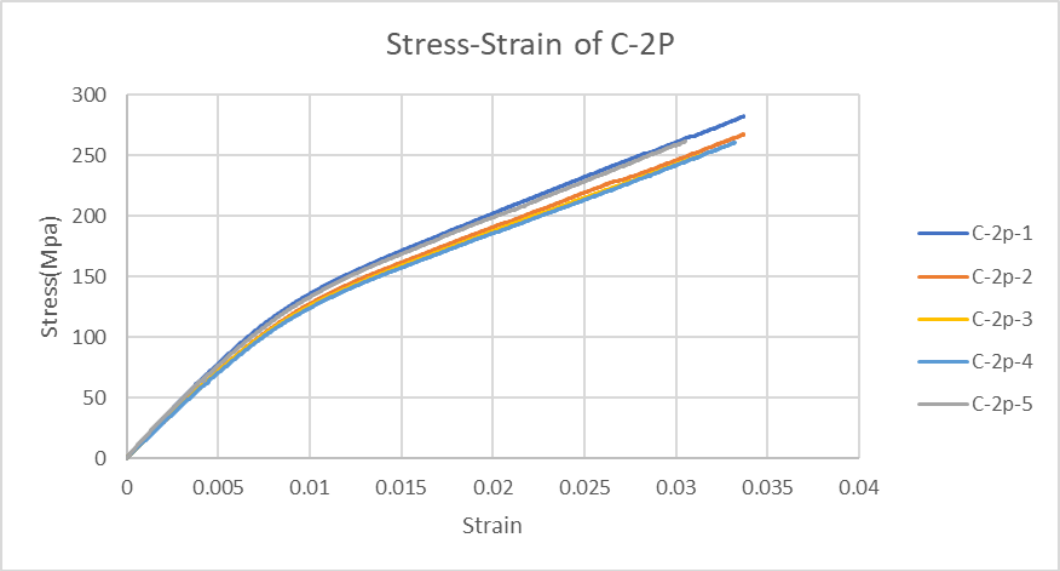

Figure 4.9 : Stress-strain curve of the coupon test results of C-2P.

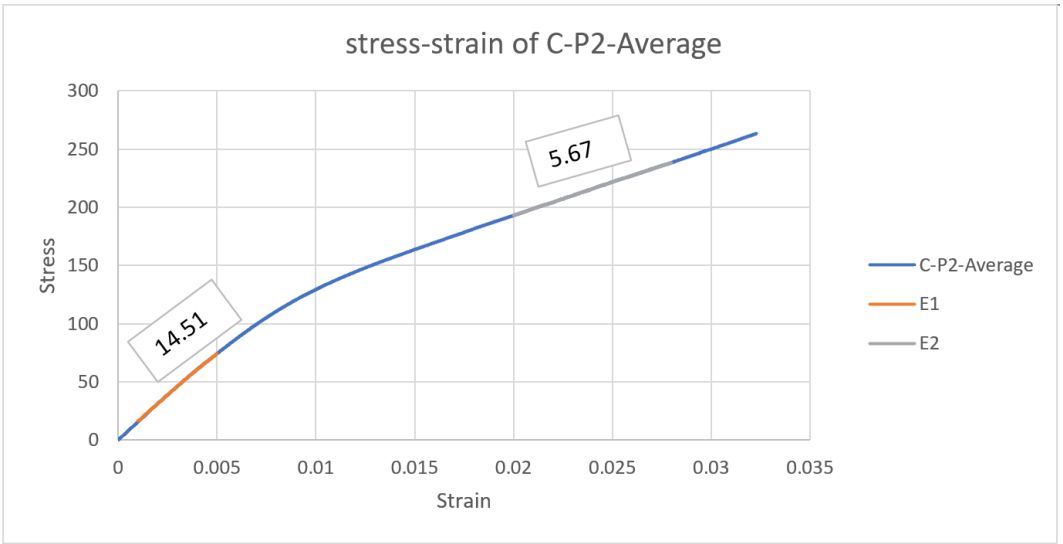

Figure 4.10 : Average stress-strain curve of the coupon test results of C-2P.

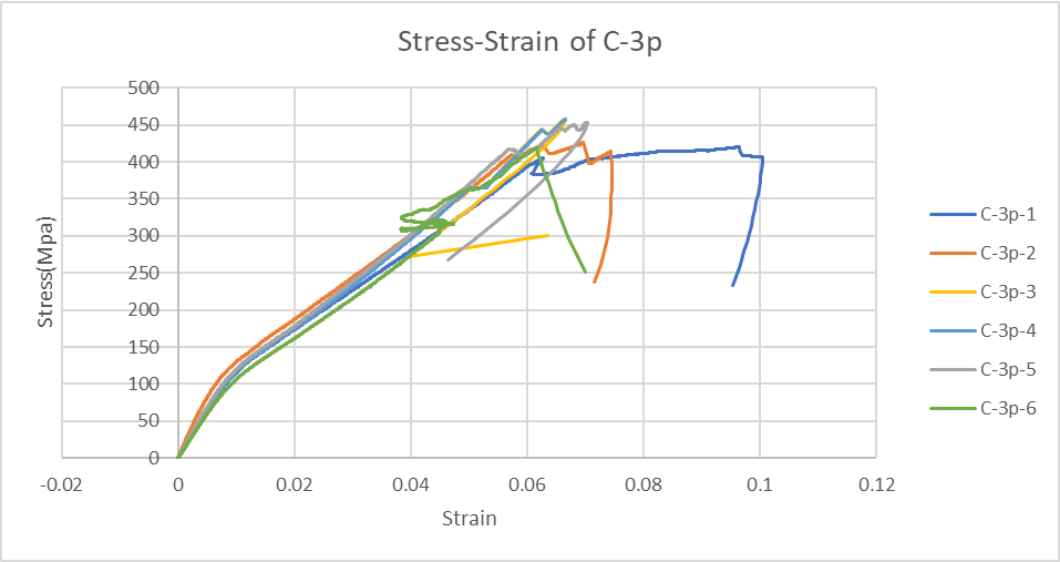

Figure 4.11 : :Stress-strain curve of the coupon test results of C-3P.

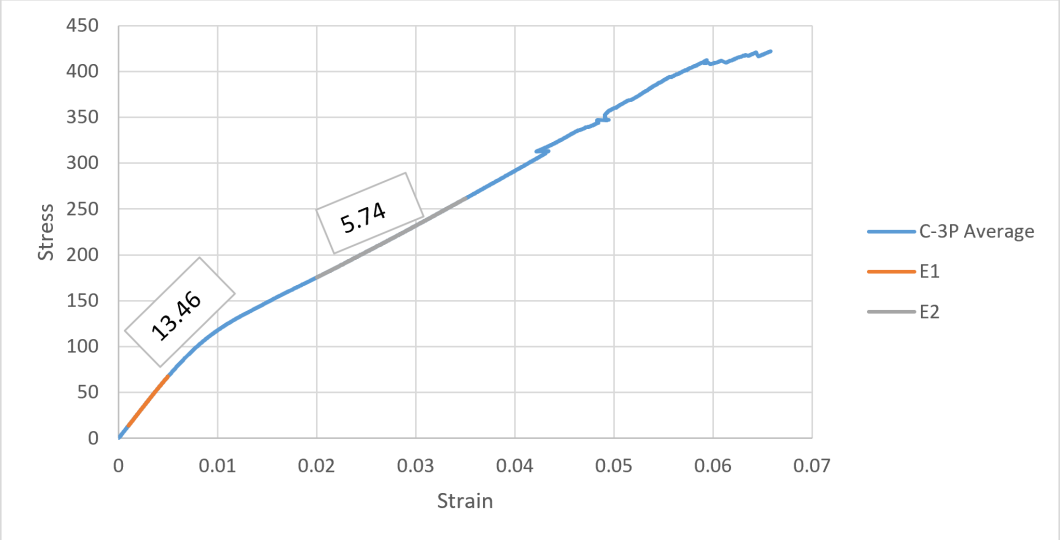

Figure 4.12 : Average stress-strain curve of the coupon test results of C-3P.

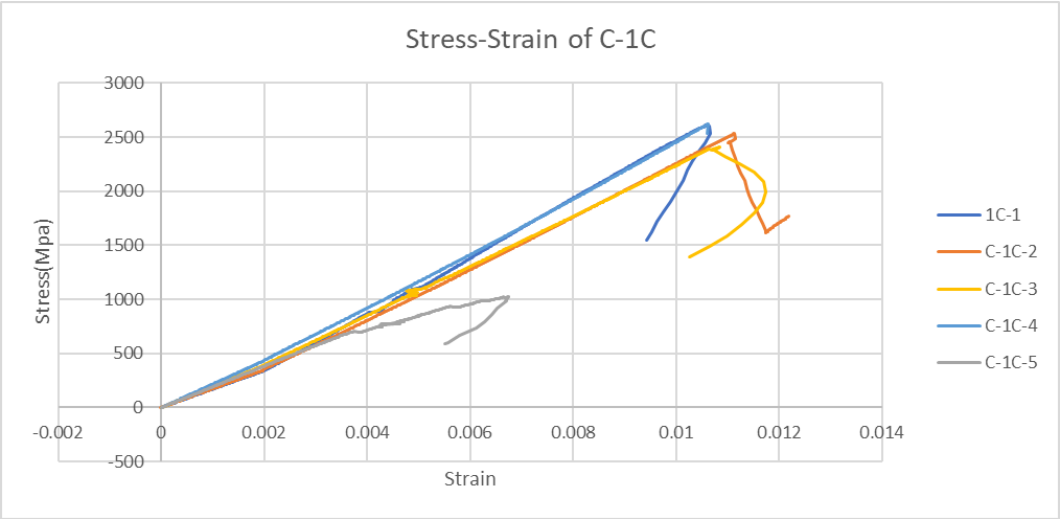

Figure 4.13 : Stress-strain curve of the coupon test results of C-1C.

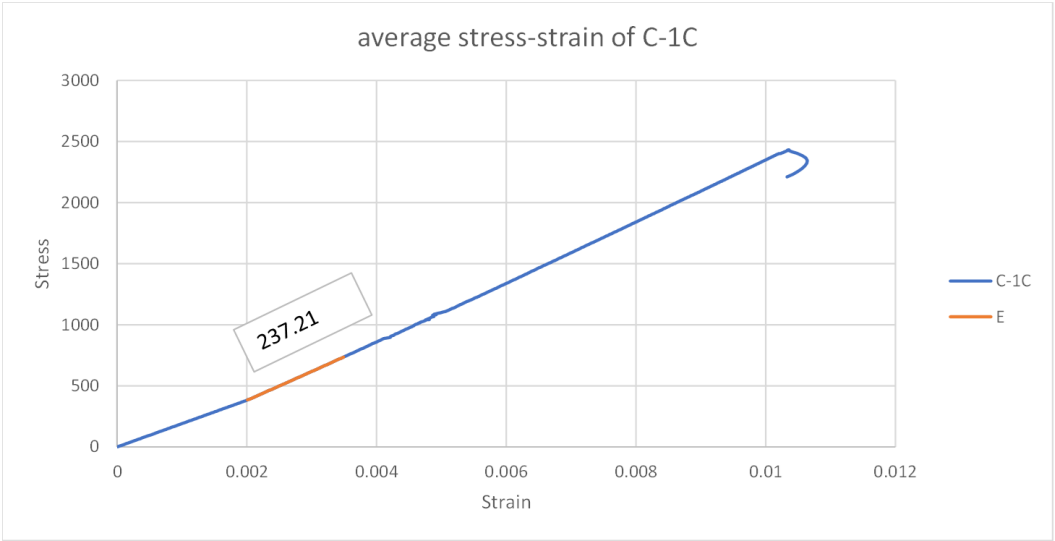

Figure 4.14 : Average stress-strain curve of the coupon test results of C-1C.

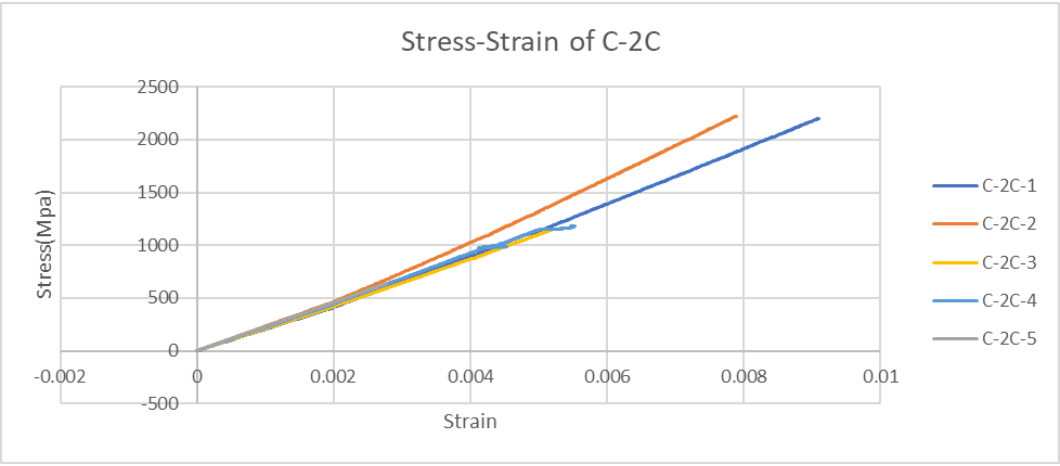

Figure 4.15 : Stress-strain curve of the coupon test results of C-2C.

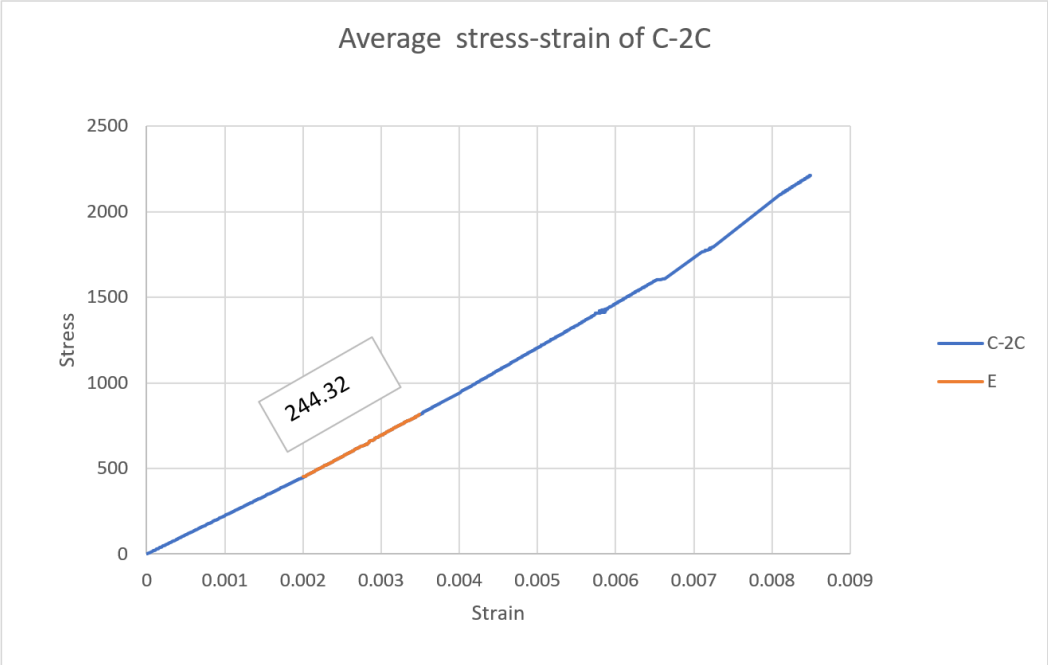

Figure 4.16 : Average stress-strain curve of the coupon test results of C-2C.

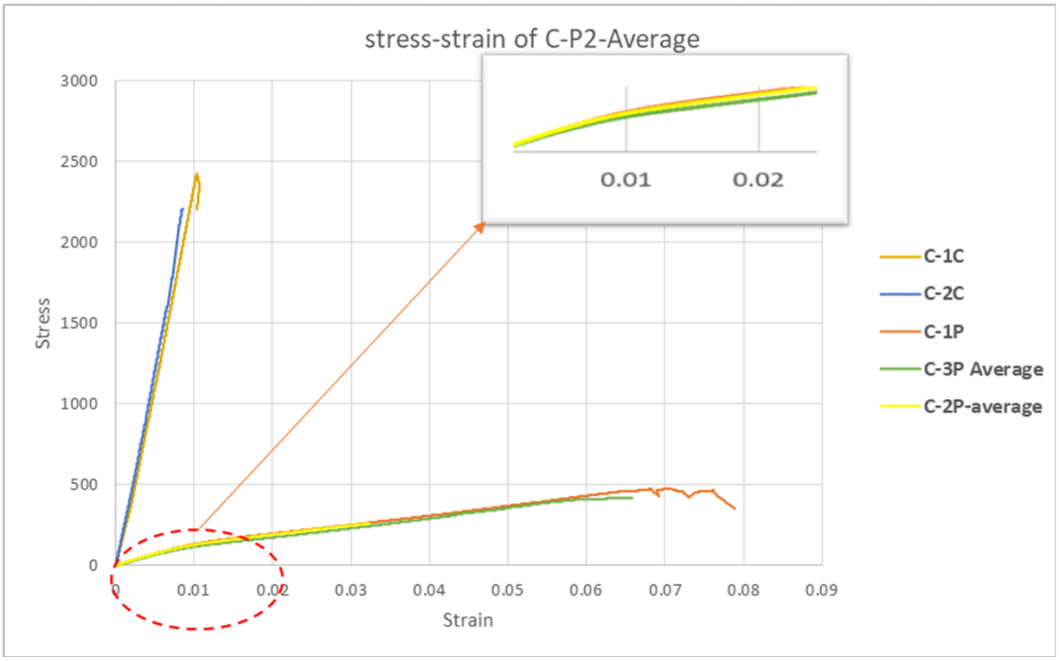

Figure 4.17 : Stress-strain curve of the coupon test.

4.3.1 Mechanical properties of FRP laminates

The average results in terms of elastic modulus (E_1), transition strain (εo), elastic modulus (E_2) which is after the transition strain, tensile strength, rupture strain are calculated.

Transition strain (εo): the strain at which the stiffness changed in PET-FRP and it is calculated as shown and indicated with red star in Figure 4.18

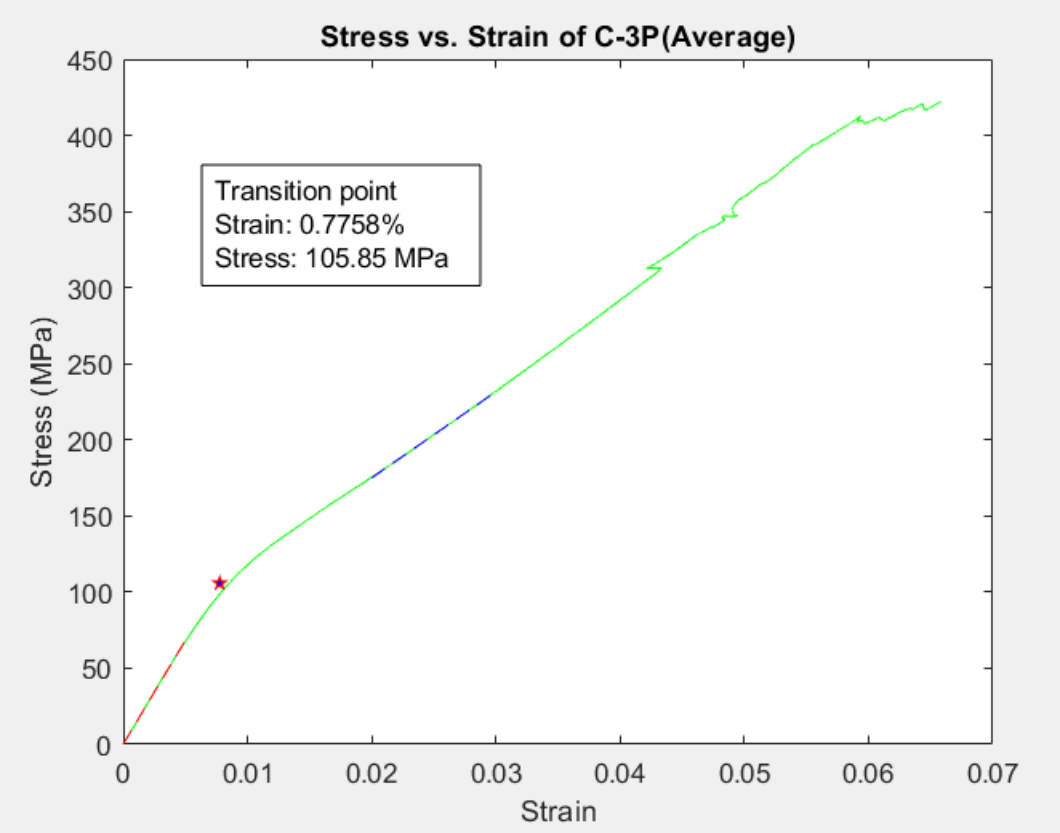

Figure 4.18 : Average stress-strain curve of the coupon test results of C-3P showing the transition strain.

In the stress-strain graph (Figure 4.18) , it is noticed a key point where two straight lines intersect, marking a significant change in how the material behaves when stress is applied. This specific point is accurately found by a mathematical approach utilizing the equations derived from the linear regression analysis of two separate regions of the stress-strain curve.

The values of strain and stress at this point 0.7758% strain and 105.85 MPa stress. This point is typically where the material starts to deform in a way that cannot be reversed fully. Table 4.2 presents the results obtained from the coupon tests.

Table 4.2 : Mechanical properties of FRP from the coupon test.

	C-1C	C-2C	C-1P	C-2P	C-3P
Max. tensile stress (MPa)	2541.75	2777.15	492.14	494.66	439.18
SD of stress	98.5	381.5	16.3	43.0	19.1
εo (%)	-	-	0.965	0.854	0.776
rupture strain (%)	1.136	1.133	7.178	6.82	7.182
SD of strain	0.088	0.178	0.378	0.751	1.242
E1 (GPa)	239.5	244.4	14.8	14.5	13.4
SD of E1	18.0	20.8	1.1	0.6	1.3
E2 (GPa)	-	-	5.5	5.8	5.8
SD of E2	-	-	0.25	0.21	0.33

the stress-strain relationship for PET (Polyethylene Terephthalate) samples is characterized by two distinct phases of stiffness, which are represented by two different elastic moduli Figure 4.7 - 4.12. These two phases are clearly delineated in the figures and in Table 4.2, with E_1 representing the initial, more rigid phase of the material's response, and E_2 corresponding to a second, less stiff phase of elasticity.

The apparent non-linear progression of the PET-FRP stress-strain curve is attributed to the behavior of the material's amorphous regions, which begin to shift under the applied load, subsequently causing an increase in strain as the material's molecular structure is engaged. The eventual failure of the PET-FRP is caused by the slippage or breakdown of these molecular chains, as detailed in reference [47].

From the experimental data presented, it is evident that the second-stage modulus E2 is significantly lower—between 37% to 43%—than the first-stage modulus E1. This observation aligns with the findings from another study referenced as [48], which approximates E2 to be nearly 42% of E1. The initial modulus, E1, is recognized from previous research by the authors [49] as the defining elastic modulus for PET-FRP, capturing its initial and most responsive elastic behavior.

5. UNCONFINED CONCRETE PROPERTIES

5.1 Overview

Understanding the properties of low-strength concrete (LSC) is crucial for evaluating the structural and seismic resilience of buildings made with lesser-quality materials. This chapter's primary goal is to define the compressive attributes of the LSC examined in this research. To achieve this,the experimental outcomes are introduced and displayed through graphs that show the relationship between compressive stress and axial strain. Additionally, compressive strength, corresponding strain, and modulus of elasticity are calculated. Next, the accuracy of the existing theoretical model is evaluated, which is used to predict the growth in strength after 28 days.

5.2 Test Result & Stress-Strain Curves

The behavior of LSC when subjected to compression is showcased through the examination of test results from six standard cylindrical specimens. These specimens are categorized into two sets, each containing three samples, differentiated by the age at which the tests were conducted, as detailed in Table 5.1. The graphical representation of how each group compresses under stress is displayed in Figure 5.1. To calculate the stress, the force applied to the specimens is divided by their initial cross-sectional area. The axial strain is determined by comparing the average change in length, as measured by linear variable differential transducers (LVDTs) attached to the steel frame, to the specified gauge length of 150 mm. Each stress-strain curve is comprised of two segments: the initial segment, which continues until peak stress is reached, and the subsequent post-peak segment, which extends from the peak stress to the point of ultimate strain.

Table 5.1 introduces specific terms related to the compressive strength of concrete. Here, f_c signifies the compressive strength of concrete, εco represents the axial strain

Table 5.1 : Compression test results of LSC.

				E (MPa)		
	fc (Mpa)	εco	$\varepsilon cu85$	TS 500	EN 12390-13	ASTM C469/C469M
cyl-1-1	8.62	0.0027	0.0056	11336	11754	11115
cyl-1-2	9.25	0.0022	0.0057	14555	14614	14966
cyl-1-3	9.23	0.0026	0.0064	12842	11130	11111
avg. of group-1	9.02	0.0025	0.0059	11917	11473	11302
cyl-2-1	12.97	0.0018	0.0034	16380	14728	14543
cyl-2-2	15.57	0.0023	0.0041	16250	16243	16291
cyl-2-3	14.84	0.0022	0.0047	16568	16138	16256
avg. of group-2	14.46	0.0022	0.004	16791	15493	15538

at the peak stress, and $\varepsilon cu85$ denotes the axial strain at 85% of the peak stress during the descending portion of the stress-strain curve. The data reveals that as the concrete's compressive strength increases, both εco and $\varepsilon cu85$ values tend to decrease. The term E refers to the modulus of elasticity, a measure of the concrete's stiffness.

In this investigation, the modulus of elasticity for each concrete sample is calculated following the procedures outlined in various technical standards, each offering a different methodology for its determination. ASTM C469/C469M [50] calculates the chord modulus using the stress at an axial strain of 0.00005 and 40% of the peak compressive strength ($0.4fc$). TS 500 [51] outlines the calculation of the secant modulus of elasticity (Ecs) at a stress equivalent to 40% of fc. EN 12390-13 [52] defines the chord modulus (Ecc) using the stress between 10% and 33% of the fc. Consistently observed from Table 5.1, the modulus of elasticity (E) increases with an increase in the compressive strength of the concrete samples.

5.3 Compressive Strength Prediction

The aim of this section to check the accurately of prediction of compressive strength by using the model preposed by [53], based on the compressive strength at 28-day er going to use the model to predict the compressive strength at 312-day by using two simple equation:

$$B = 0.005(fc28)^2.20 \tag{5.1}$$

$$A = 1.4035ln(B) + 2.9956 \tag{5.2}$$

$$fct = A\ln(t) + B \tag{5.3}$$

where $fc28$ is the compressive strength at 28-day, and t is the day at which you would like to predict the compressive strength , and fct is the compressive strength at the desired day.

Using this model, the 312-day strength is predicted to be 14.13 MPa, and the percentage error is 2.28%. Although there is a limited specimen number, it may be concluded that the prediction capability of the model is good.

5.4 Test Outcome

It is observed that the modulus of elasticity (E), a measure of the stiffness of concrete, exhibits an increasing trend in line with the rise in the compressive strength of the concrete samples. This suggests a correlation where stronger concrete samples tend to be stiffer.

As the compressive strength of the concrete increases, the data suggests that both εco (axial strain at peak stress) and $\varepsilon cu85$ (axial strain at 85% of peak stress in the post-peak phase) exhibit a decline. The mentioned pattern suggests that LSC exhibits enhanced resistance to axial deformation in comparison to normal-strength concrete (NSC), thereby signifying a more ductile response when subjected to stress [54].

The average moduli of elasticity, calculated as per ASTM C469/C469M [50], TS 500 [51], and EN 12390-13 [52], show relatively similar values across these standards. However, the modulus of elasticity values obtained following ASTM

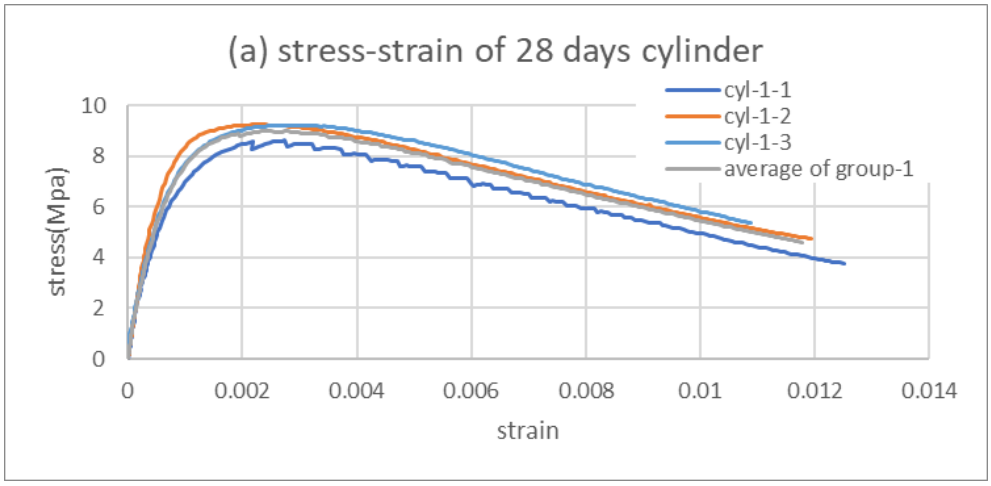

(a)

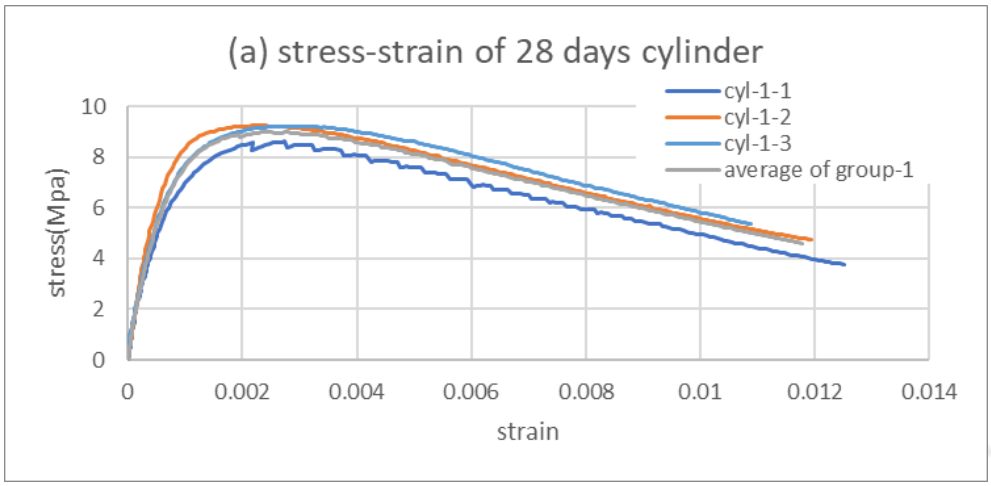

(b)

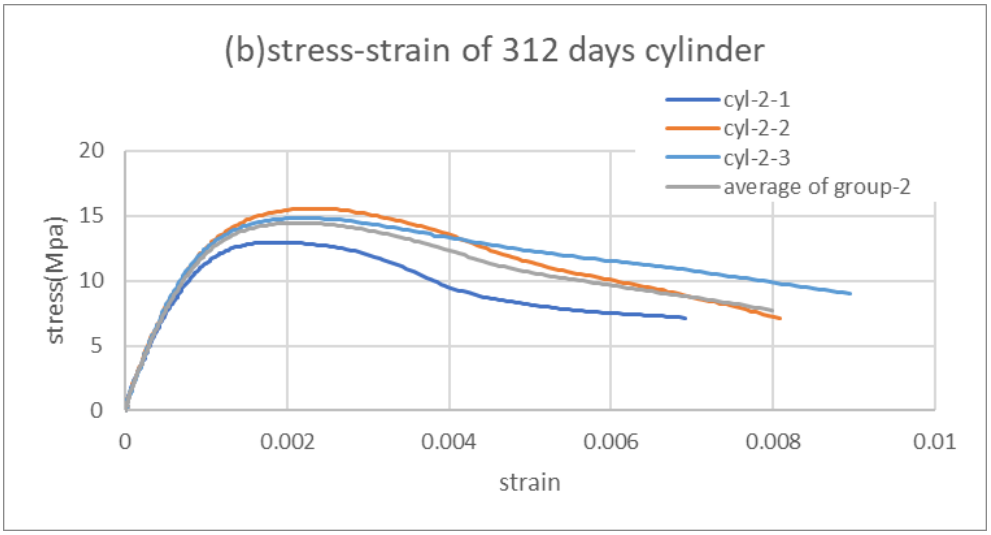

(c)

Figure 5.1 : (a) 28-Day concrete cylinders: stress-strain response,(b) 312-Day concrete cylinders: stress-strain characteristics, (c) comparative stress-strain curves for 28-Day vs. 312-Day cured concrete cylinders.

C469/C469M [50] and EN 12390-13 [52] are more closely aligned compared to those calculated using TS 500 [51]. This highlight slight variations in the modulus of elasticity as derived from different technical documents, though the differences are not substantial.

6. COMPRESSION TESTS OF FRP-WRAPPED SQUARE SPECIMENS

6.1 Overview of Experimental Findings

This section focus on the axial behavior of hybrid-FRP wrapped LSC. In order to understand this behavior, it is needed to know the behavior of LSC-wrapped with conventional FRP.

Hybrid FRP means using more than one type of FRP material, like carbon and PET, taking advantage of the positive aspects of each. In this study, the effectiveness of this type of hybrid FRP on LSC confinement was experimentally examined. Conventionally wrapped specimens were also tested to clearly understand the effect of each type of FRP.

The section will present axial stress-strain curves and hoop strain profiles, which are essential in assessing the mechanical response and deformation characteristics under stress.

Moreover, this section will cover the ultimate limit states observed during the experiments, particularly focusing on the ultimate axial strength and strain capacity. These metrics are crucial in determining the enhancements in columns due to FRP confinement. The presentation of these results will incorporate both graphical and tabular formats for a clear and concise representation of the findings.

6.2 Stress-Strain Response

Here, the stress-strain curves for all specimens that were exposed to monotonic axial loading are provided. The analysis of these curves is essential for comprehending the mechanical response of the concrete columns, especially when subjected to the effects of FRP wrapping. The strain distribution and appearance of the sample will be exhibited at particular points.

Measurement Techniques:

- The axial strain values were determined using an average of the readings from four mid-linear variable differential transformers (LVDTs). These values were recorded up to the point of unconfined concrete strength (fco). Beyond this point, axial strain was measured using four full-LVDTs until the failure of the specimens.
- Axial stress values were calculated based on the load applied per unit area of the specimens. This method provides a direct measurement of the stress experienced by the columns under load.
- The hoop strain by taking the average reading of the four strain gauges.

Assessing Confinement Effectiveness:

- The effectiveness of the applied FRP confinement is evaluated based on the behavior of the stress-strain curve, particularly in its second portion, which occurs after the strength level of unconfined concrete.
- According to [55], confinement is considered sufficient if providing axial strain and strength enhancements with respect to an unconfined state.
- The threshold confinement is identified at the point where the slope of the second portion of the curve becomes horizontal (zero slope). This is a critical transition point that defines the effectiveness of the confinement.

6.2.1 R Group

The stress-strain curves of unconfined concrete specimens are presented in Figure 6.3. Initially, the curve rises steeply, indicating elastic behavior where the concrete deforms proportionally to the applied load. This part of the curve is linear, reflecting the material's modulus of elasticity. However, once it reaches its peak, representing the maximum compressive strength, the curve abruptly descends, indicating a loss of capacity to withstand further stress.

In the presented research, unconfined concrete columns labeled R-1 and R-2 which is a baseline for measuring enhancements from various confinement methods. Tthe average compressive strength of the unconfined is 13.11 MPa. This figure is lower by 9.28% compared to the 14.45 MPa obtained from testing three cylindrical columns under similar conditions. This observation, recognized by both [56,57], reflects a common phenomenon where larger concrete specimens tend to have lower strength. This is due to the mix's natural inconsistency, as concrete cannot be 100% homogeneous, resulting in an uneven distribution of properties within the material.

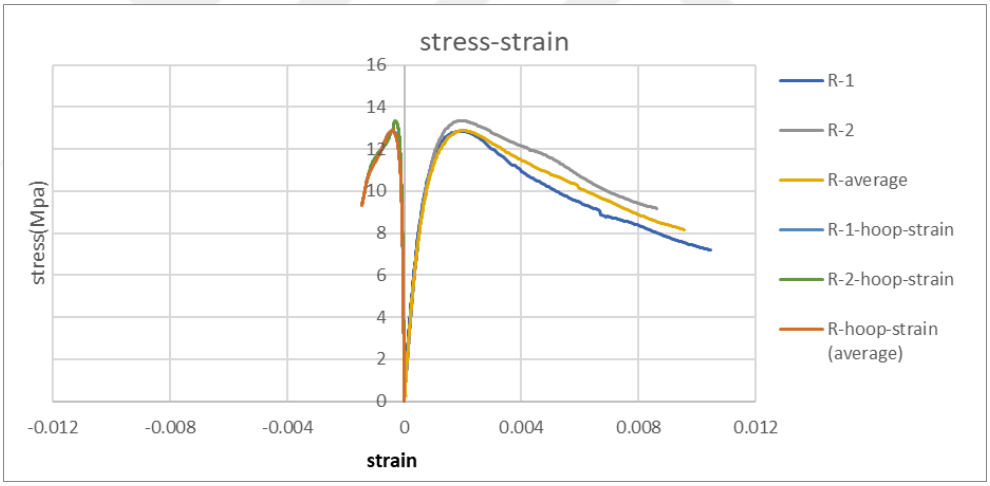

Figure 6.1 : Stress-strain behavior of unconfined concrete specimens (R1 & R2).

6.2.2 Group 1C & 2C

This section is started with analyzing Figure 6.2, which depicts stress-strain curves for concrete specimens enhanced with a single layer of CFRP, identified as 1C-1 and 1C-2. These samples demonstrate comparable ultimate stress levels, pointing to the consistent effect of the CFRP wrapping. The average stress response and hoop strain data are also presented, emphasizing the enhancement benefit provided by the CFRP.

Shifting the attention to Figure 6.3, it is observed that the augmented load-bearing and deformation capabilities of specimens 2C-1 and 2C-2, each fortified with two CFRP layers, illustrating the incremental reinforcement advantage of an additional CFRP layer. Furthermore, Figure 6.4 offers a comprehensive view of the stress-strain relationships for unconfined and CFRP-wrapped specimens, with average stress responses denoted for the unconfined (R-average), single-layer CFRP (1C-average), and double-layer CFRP (2C-average) specimens. The data clearly shows that CFRP wrapping, particularly with two layers, significantly enhances the structural capacity of concrete specimens, as evidenced by the elevated and sustained stress levels at higher strains for the 2C samples.

To summarize, the analysis of stress-strain behavior in Figures 6.2 to 6.4 shows a clear difference in performance between unconfined concrete specimens and those wrapped with CFRP layers. Unwrapped samples generally exhibit a rapid rise in stress as strain increases, followed by a fast decrease, suggesting a brittle failure. On the other hand, when comparing 1C specimens that are covered with a single layer of CFRP, there is a significant increase of 26% in strength and a large gain of 527% in strain capacity. In comparison to their unconfined counterparts, the 2C specimens, which are comprised of two layers of CFRP, exhibit even greater performance, with a strain capacity increase of 987% and a strength increase of 56.5%. This demonstrates the critical significance of CFRP in the strengthening of the concrete columns.

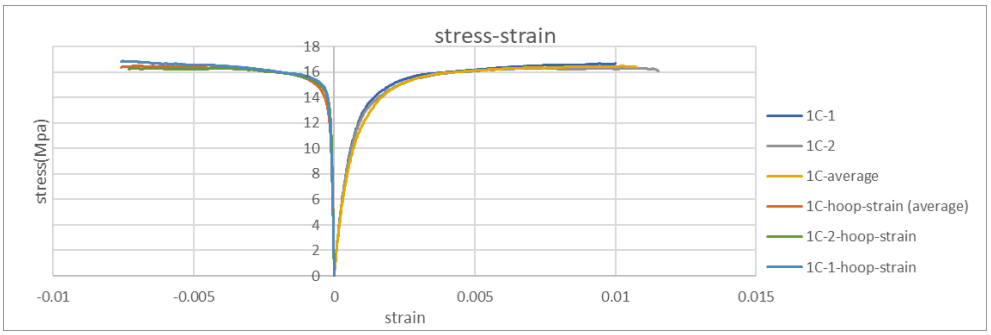

Figure 6.2 : Stress-strain behavior of confined concrete specimens (1C-1 & 1C-2).

6.2.3 Group 1P & 2P & 3P

The stress-strain graphs represented in Figures 6.5-6.7 illustrate the impact of PET-FRP wrapping on concrete specimens. Figure 6.5 (1P) displays the enhancement

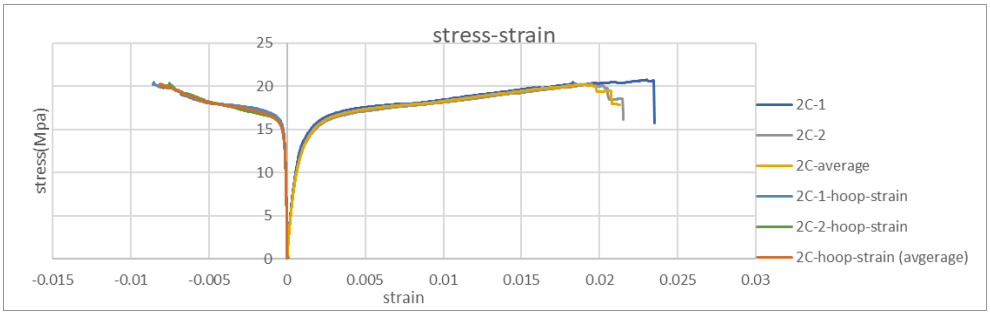

Figure 6.3 : Stress-strain behavior of confined concrete specimens (2C-1 & 2C-2).

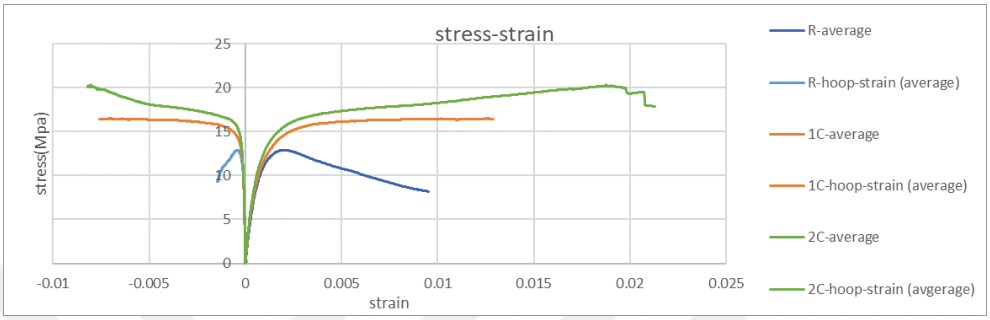

Figure 6.4 : Comparative stress-strain curves and hoop strain analysis for unconfined and CFRP-wrapped concrete specimens.

in structural capacity with a single layer of PET-FRP, where an improvement in both the strength and ductility of the specimen is observed. In Figure 6.6 (2P), the addition of a second PET-FRP layer leads to further increases in these mechanical properties. Figure 6.7 (3P) confirms this trend, showing that a third layer of PET-FRP confers even greater strength and deformation capability to the concrete. In concrete wrapped with a single layer of LRS FRP, the transition zone is more extended than in concrete wrapped with conventional FRP, as indicated by the concrete's curve as shown in figure 6.8. This difference is due to the LRS FRP's almost bilinear material properties [27,32] depicted this transition zone in their simulation using a straightforward linear segment.

Figure 6.8 depicts a thorough comparison of Stress-Strain curves for several specimens, including the unconfined specimen, specimens wrapped with CFRP (1 and 2 layers), and specimens wrapped with PET-FRP (1, 2, and 3 layers). The graph enables a comprehensive examination of how various types and amounts of FRP wrapping impact the mechanical characteristics of the columns. The starting slopes of the curves indicate the elastic modulus which is controled by the concrete as the FRP system is not working yet at this region. The inflection points where the curves diverge

from linearity, known as transition point, and the maximum stress values, referred to as ultimate strength, provide valuable information on the increase or modification of these characteristics using FRP wrappings. Furthermore, the magnitude of the curves and their response under increased stresses offer insights into the ductility and probable failure mechanisms of the specimens. This image is an essential tool for comprehending the mechanical consequences of using CFRP and PET-FRP wrappings with different layers on column.

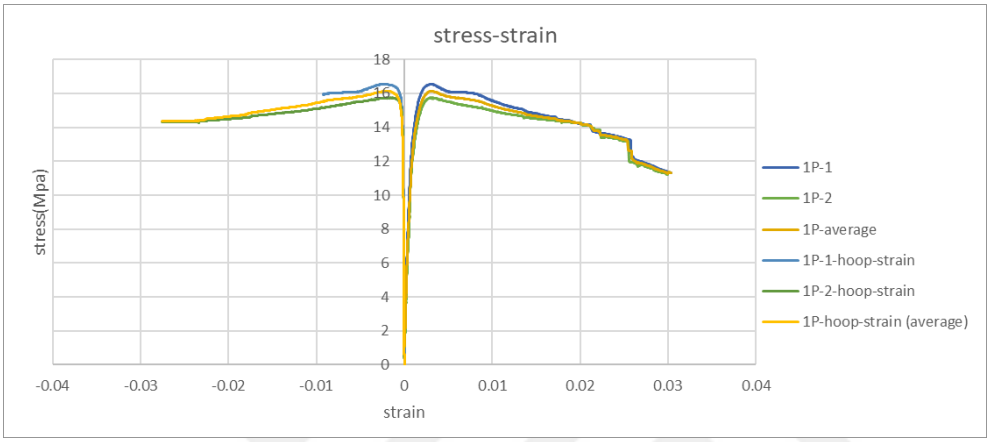

Figure 6.5 : Stress-strain behavior of confined concrete specimens (1P-1 & 1P-2).

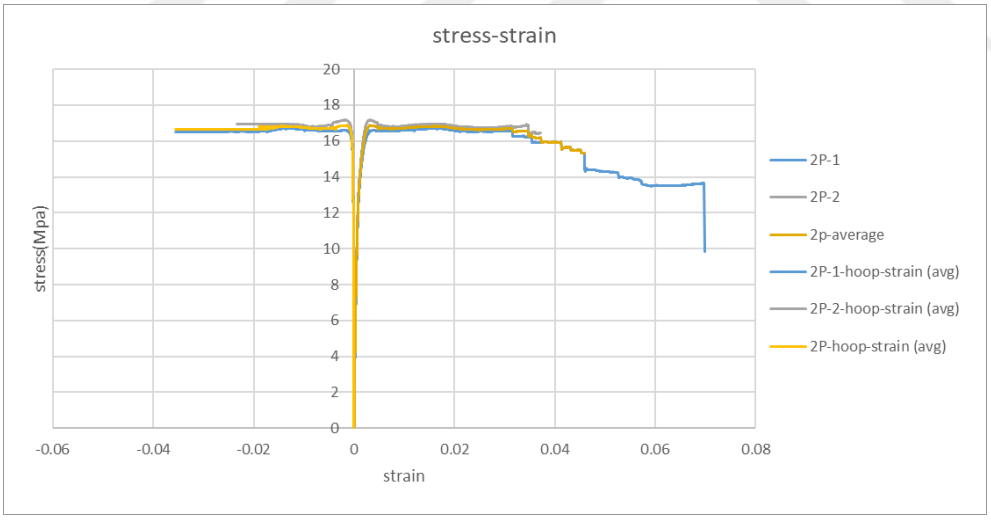

Figure 6.6 : 4.6: Stress-strain behavior of confined concrete specimens (2P-1 & 2P-2).

6.2.4 Group 1C1P & 1C2P & 1C3P

Regardless of the kind of FRP, the core concrete determines the initial rising phase of the stress-strain curve for concrete covered with FRP. After the transition zone,

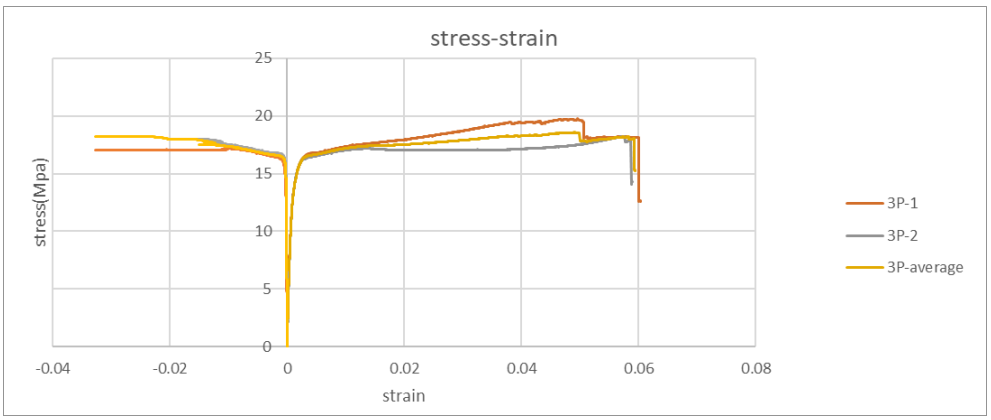

Figure 6.7 : Stress-strain behavior of confined concrete specimens (3P-1 & 3P-2).

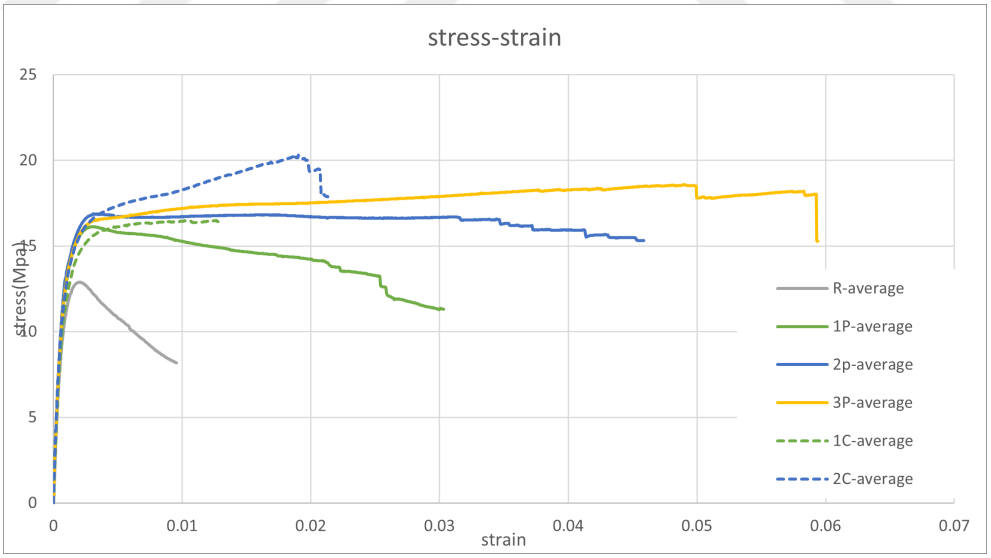

Figure 6.8 : Comparative stress-strain curves for unconfined and CFRP-wrapped concrete and PET-FRP-wrapped concrete specimens.

the steepness of the following upward curve is determined by the tensile rigidity of the FRP, increasing until the FRP fractures. Hybrid FRP-wrapped concrete displays identical characteristics to CFRP-wrapped concrete until the inner CFRP layer fractures, as a result of the combined effect of the inner CFRP and outside PET-FRP during this phase. The stress-strain curves might exhibit ascending, descending, or stabilizing patterns in response to increasing stress variations as strain develops. CFRP fractures often begin in the central region adjacent to the curved corner of the column. Upon occurrence of this event, the external PET-FRP promptly activates to counterbalance the decrease in containment pressure resulting from the partial rupture of the internal CFRP. During the loading process, the inner CFRP gradually breaks as the concrete expands. At the same time, the outside PET-FRP consistently counteracts the decrease in confinement stress caused by the CFRP rupture. These changes in tension along the axis were detected by Ispir *et al.* [58] and Bai *et al.* [32]. Figure 6.12 illustrates that hybrid-wrapped concrete exhibits superior axial stiffness compared to PET FRP-wrapped concrete and larger axial strain than CFRP-wrapped concrete. After a CFRP fracture occurs, the stress-strain curves can either decrease, remain stable, or increase, depending on the ratio of PET FRP to CFRP. The hybrid-wrapped concrete column experiences gradual failure following the fracture of the inner CFRP, caused by the presence of the outer PET FRP. When analyzing the stress-strain behavior of concrete columns after the rupture of the inner CFRP layer, as observed in the series of Figures 6.9 to 6.14, distinct patterns emerge based on the relative confinement pressures of the CFRP and PET FRP layers. Specifically, if the external confinement pressure provided by the outer PET FRP is substantially higher than the pressure resulting from the inner CFRP, the stress-strain curves generally exhibit an increasing trend, as demonstrated in Figures 6.11 and 6.14. Conversely, when the confinement pressures exerted by the inner CFRP layer and the outer PET FRP layer are similar, the curves tend to stabilize, as shown in Figures 6.10 and 6.13. In cases where the pressure generated by the CFRP layer exceeds that of the PET-FRP, a decreasing pattern in the curves is observed, illustrated in Figures 6.9 and 6.12. This variation in behavior highlights the impact of the relative pressures exerted by the different FRP layers on the CFRP-post-rupture stress-strain characteristics of the columns. In summary,

the external PET-FRP plays a vital role in preventing the sudden failure of concrete columns wrapped with CFRP at the location where the CFRP material breaks. This significantly improves the efficiency of CFRP in situations when there is a requirement for early detection of column collapse.Figure 6.9-6.15 shows the axial stress vs strain for 1C1P,1C2P and 1C3P.

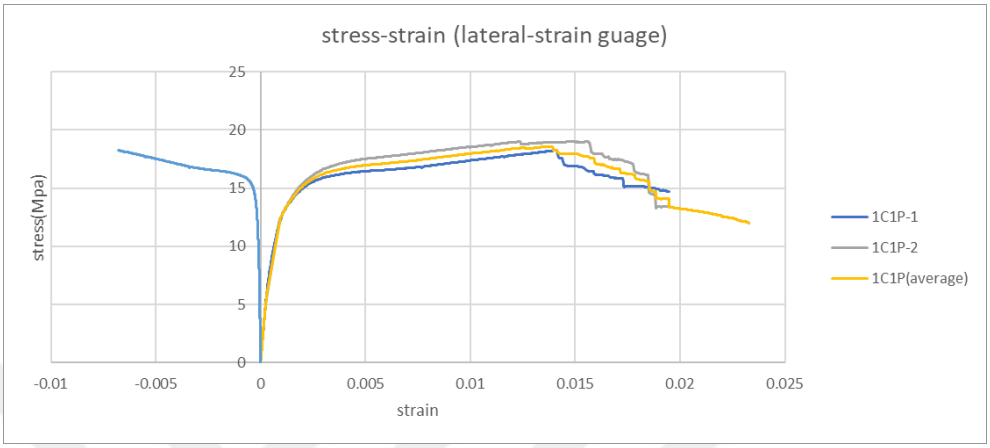

Figure 6.9 : Stress-strain behavior of confined concrete specimens (1C1P-1 & 1C1P-2).

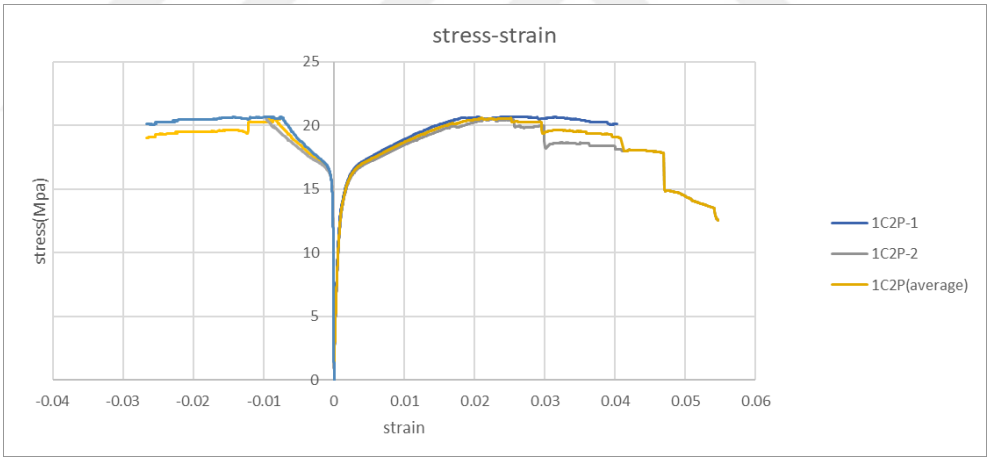

Figure 6.10 : Stress-strain behavior of confined concrete specimens (1C1P-1 & 1C1P-2).

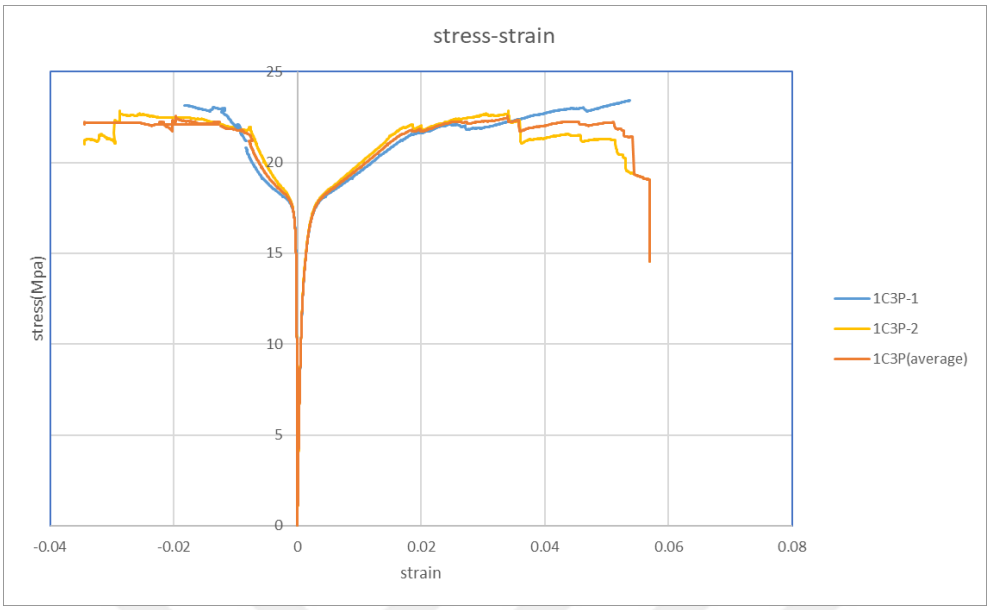

Figure 6.11 : Stress-strain behavior of confined concrete specimens (1C3P-1 & 1C3P-2).

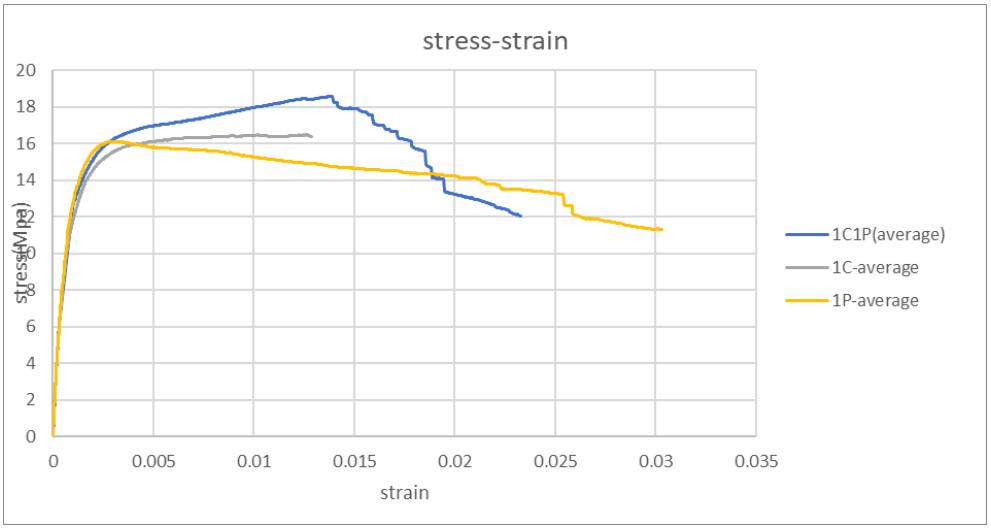

Figure 6.12 : Stress-strain behavior of confined concrete specimens (1C1P & 1C & 1P).

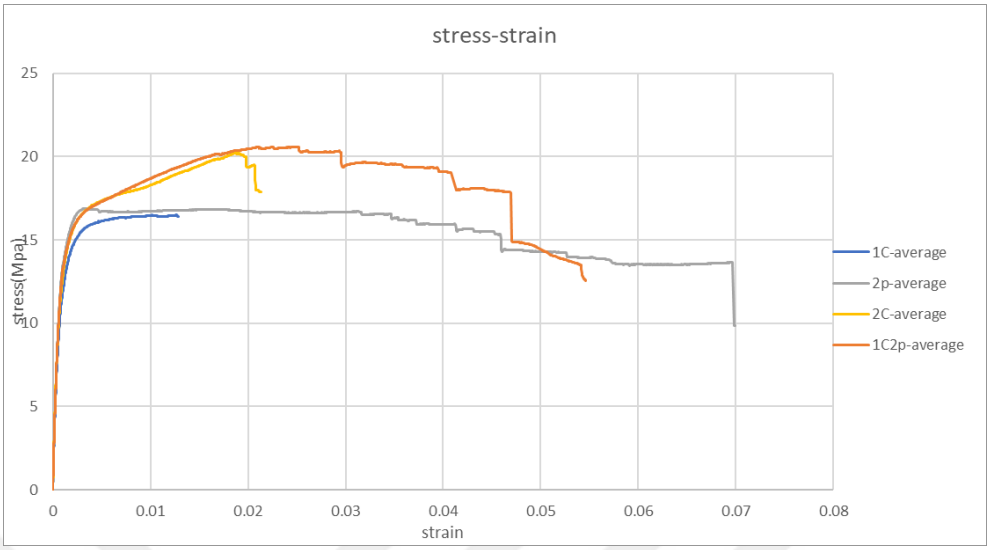

Figure 6.13 : Stress-strain behavior of confined concrete specimens (1C2P & 1C & 2C & 2P).

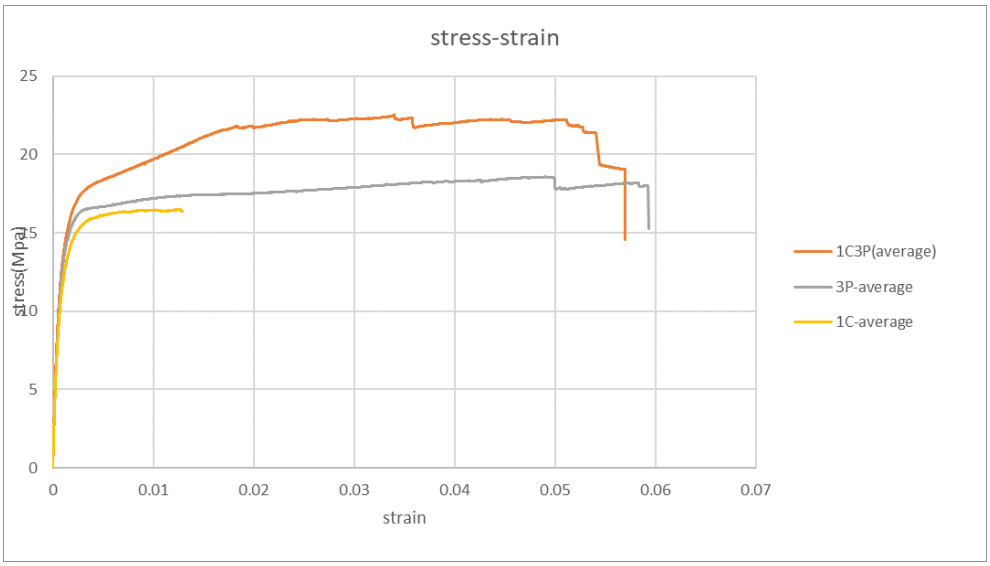

Figure 6.14 : Stress-strain behavior of confined concrete specimens (1C3P & 1C & 3P).

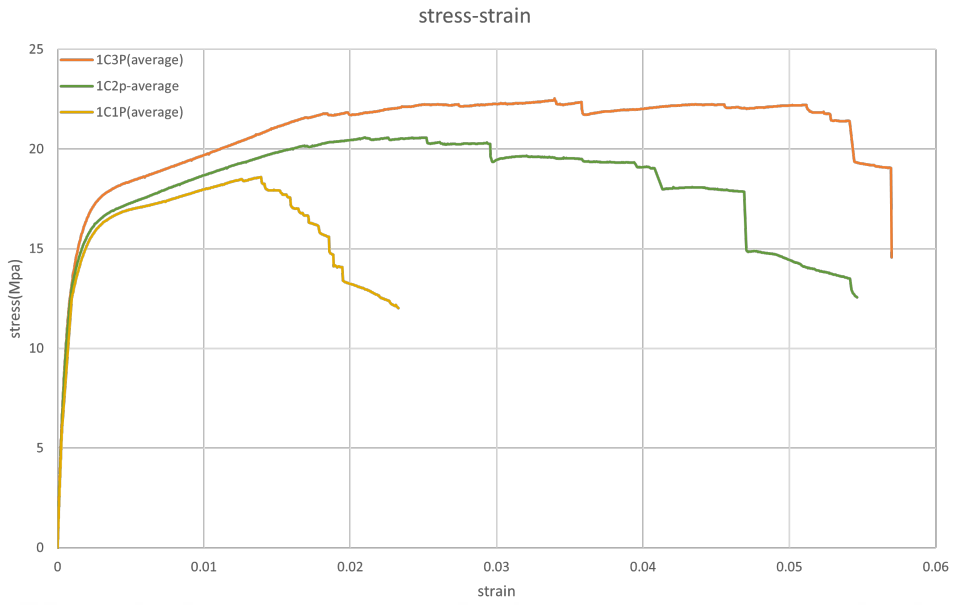

Figure 6.15 : Stress-strain behavior of confined concrete specimens (1C1P & 1C2P & 1C3P).

6.3 Insights Into Failure Mechanisms and Strain Distribution

6.3.1 Group R

As stress and strain values increase, Young's modulus value decreases and approaches zero at the strength point. At this point, there is a noticeable increase in the amount and size of cracks in the concrete, including several long cracks. As these cracks grow, a softening and decrease in the curve's steepness is seen, as shown in Figure 6.16. This kind of failure happens quickly and is severe, as shown by the crushing of the concrete on its sides, which is displayed in Figure 6.17 [59,60].

Figure 6.18 illustrates the critical points of stress and corresponding strain in unconfined concrete specimens, identified as R-1 and R-2. On the right, the stress-strain curves for both specimens are displayed, with red crosses marking the specific stress points under investigation.

To the left, the figure presents separate plots of hoop strain measurements, taken from different locations on the specimens. These measurements, such as 'strain-A' from face A and 'strain-AB' at the corner between faces A and B, help to map

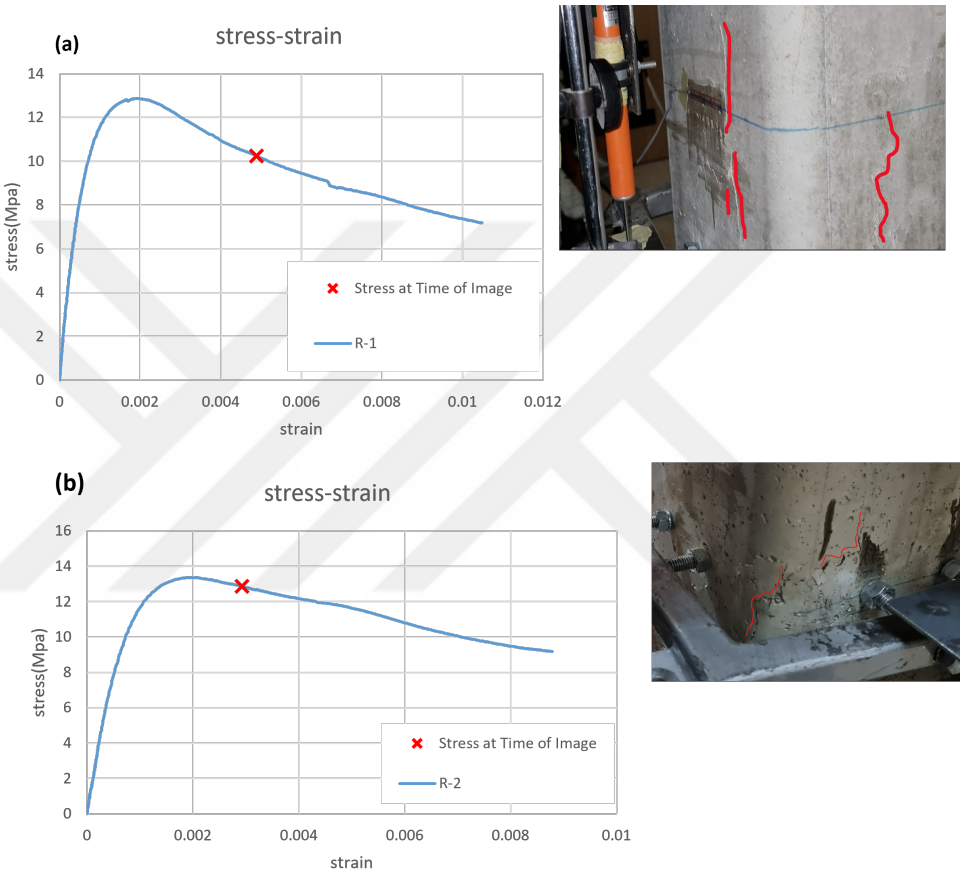

Figure 6.16 : A comparative display of stress-strain curves and corresponding failure states for specimens R-1 and R-2.



(a)



(b)

Figure 6.17 : Unconfined specimens: (a) R-1 ; (b) R-2 before and after testing.

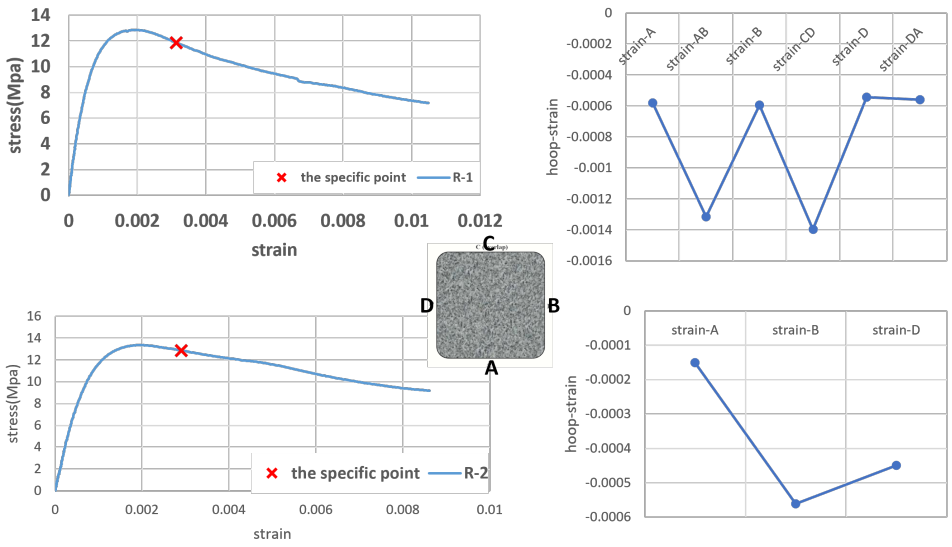

Figure 6.18 : Stress-strain characteristics and localized strain distribution in unconfined concrete specimens R-1 and R-2.

out how strain is distributed across the specimens' surfaces. The variation in these measurements indicates how the specimens deformed under stress, providing insight into where cracks might start and how the specimens may ultimately fail. Figure 6.18 is thus essential for understanding the deformation and failure processes of the concrete specimens tested. In the R-1 sample, the reason we see more strain at the corners, like AB and CD, is because of the way the shape of the column affects how stress is spread around. When a force pushes down on the column, it doesn't just compress; it also tries to spread outward, which is known as Poisson's effect. At the corners, this effect is stronger because the shape of the corner doesn't let the stress spread out evenly. So, the corners end up stretching more, which is why we see higher strain measurements there compared to the flatter sides. This happens because the material at the corners is 'squeezed' more due to the way the shape changes, making the corners a hotspot for more intense stretching under the same pushing force.

6.3.2 Group 1C & 2C

According to [61], CFRP-wrapped specimens usually fail in one of three ways: (i) the CFRP jacket tearing, often near a corner; (ii) the layers of the CFRP jacket separating from each other; or (iii) a mix of both tearing and layer separation. The point where the CFRP tears is considered the failure point, as the strength of the specimen drops sharply.

In the experiments, similar to other studies, we heard clicking noises during loading, and failure was sudden and loud. The failure was always due to CFRP tearing around the corners in the middle of the specimens, happening at higher strain levels compared to specimens without CFRP [23,62,63]. The internal concrete exhibited extensive damage, characterized by thorough crushing. We didn't see any separation of CFRP layers in our columns, suggesting that the overlapping of CFRP layers was enough. Also, we didn't have failures at the ends of the columns because we used an extra layer of CFRP there to prevent early failure. This is visually represented in Figure 6.19 and Figure 6.20, which shows the specimens before and after the test, highlighting the dramatic change and the specific areas of failure.

Figure 6.21 demonstrates the distribution of hoop strains around the circumference at the midpoint of CFRP-wrapped specimens. When the load is low, the hoop strains are quite small and even. As the load gets larger, the hoop strains increase a lot, showing that the CFRP is starting to work because of cracks and widening in the concrete. Notably, the strains at the corners are smaller than at the sides' centers, supporting findings by [15,24,64], suggesting that the FRP doesn't hold back the expansion of the concrete as strongly at the sides. Additionally, strain distributions at symmetric points vary, likely due to the concrete's inconsistency, causing non-uniform deformation and cracking, as explained by [65]. This suggests that the FRP doesn't provide the same amount of confinement all around the column, with more activity at the corners as seen in the plots.



(a)



(b)

Figure 6.19 : Visual comparison of CFRP-wrapped specimens 1C-1 (a) and 1C-2 (b) before and after axial load testing, highlighting failure modes.



(a)



(b)

Figure 6.20 : Visual comparison of CFRP-wrapped specimens 2C-1 (a) and 2C-2 (b) before and after axial load testing, highlighting failure modes.

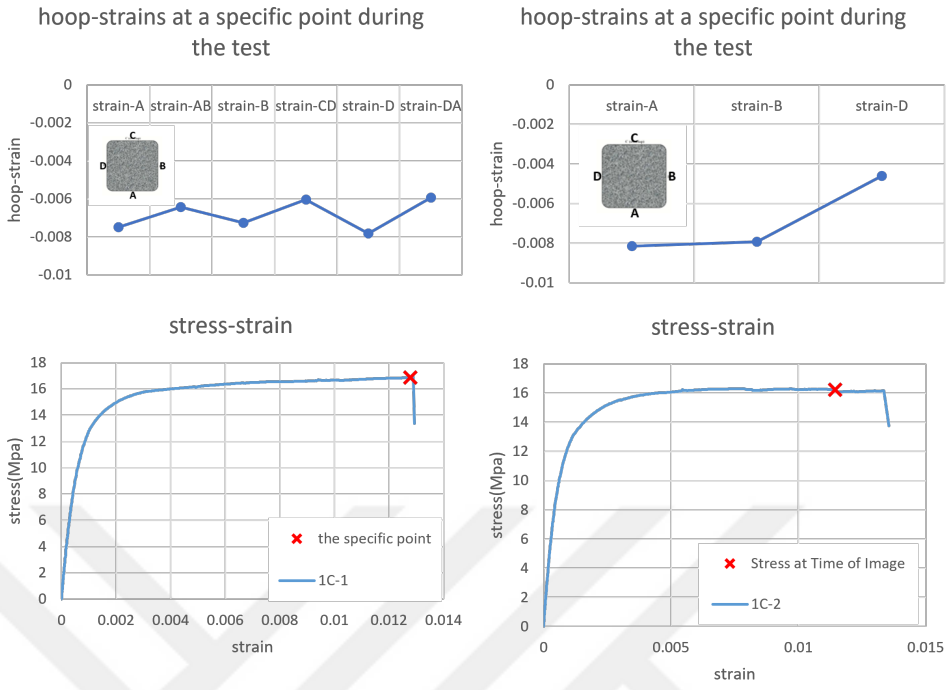

(a)

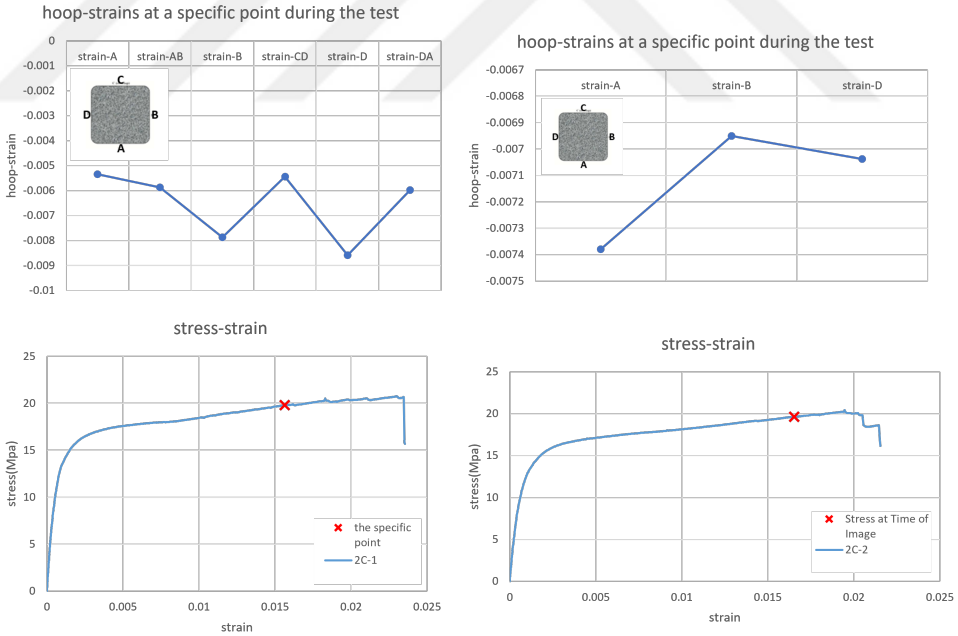

(b)

Figure 6.21 : Hoop strain analysis for (a) 1C and (b) 2C specimens with CFRP wrapping under axial stress conditions.

6.3.3 Group 1P & 2P & 3P

The failure modes of square PET FRP-confined specimens are detailed in Figures 6.22 to 6.24. For these specimens, a notable finding was the loss of hoop strain measurement due to the epoxy layer applied for strain gauges, which resulted in missing data on hoop strain rupture and because as well the local debonding of FRP in the hoop direction.

In specimen 1P-1, loud noises, typically associated with CFRP sample failures, was not observed. The failure initiated on face C's lower side, where the FRP application begins, leading to stress concentration caused by a change in fiber thickness—a geometric factor also noted by [24,66]. This could be due to the sudden bending of overlying layers, a view supported by further research by [29] on PET FRP-confined concrete. The fracture in this specimen grew toward the middle of face D, which initially experienced the most strain.

For specimen 1P-2, failure commenced in the middle and spread to faces A and B. In specimens with two layers of PET-FRP, there was no failure near the overlap. For 2P-1, the rupture was on face D, near the corner with face A, aligning with the observation of high strain at corner DA. A similar pattern was observed in specimen 2P-2, but with a smaller rupture on face A extending to face D.

The 3P-1 specimen exhibited local rupture on face A, followed by a significant rupture between faces C and B. The highest hoop strain and rupture occurred near the end of the overlap, consistent with [66] that high fiber strains are concentrated in a small zone, challenging to measure with standard techniques. For 3P-2, the rupture was between faces D and A, with the early measurement showing that hoop strain on side A was higher than other sides.

In the testing of PET-FRP wrapped columns, two main observations were made. First, local debonding of FRP along the hoop direction was a common occurrence, probably due to secondary axial stresses that led to the failure of the bond between the FRP and concrete. Second, as the modulus of elasticity decreased and passive confinement took effect, subtle cracking noises from the epoxy were initially heard and gradually intensified. Contrasting with CFRP-wrapped specimens, PET FRP-wrapped

specimens did not emit explosive sounds upon failure. Furthermore, the inner concrete of PET-wrapped specimens showed significantly more damage than that in CFRP-wrapped columns.



(a)

(b)

Figure 6.22 : Visual comparison of PET-FRP-wrapped specimens 1P-1 (a) and 1P-2 (b) before and after axial load testing, highlighting failure modes.



(a)

(b)

Figure 6.23 : Visual comparison of PET-FRP-wrapped specimens 2P-1 (a) and 2P-2 (b) before and after axial load testing, highlighting failure modes.



(a)



(b)

Figure 6.24 : Visual comparison of PET-FRP-wrapped specimens 3P-1 (a) and 3P-2 (b) before and after axial load testing, highlighting failure modes.

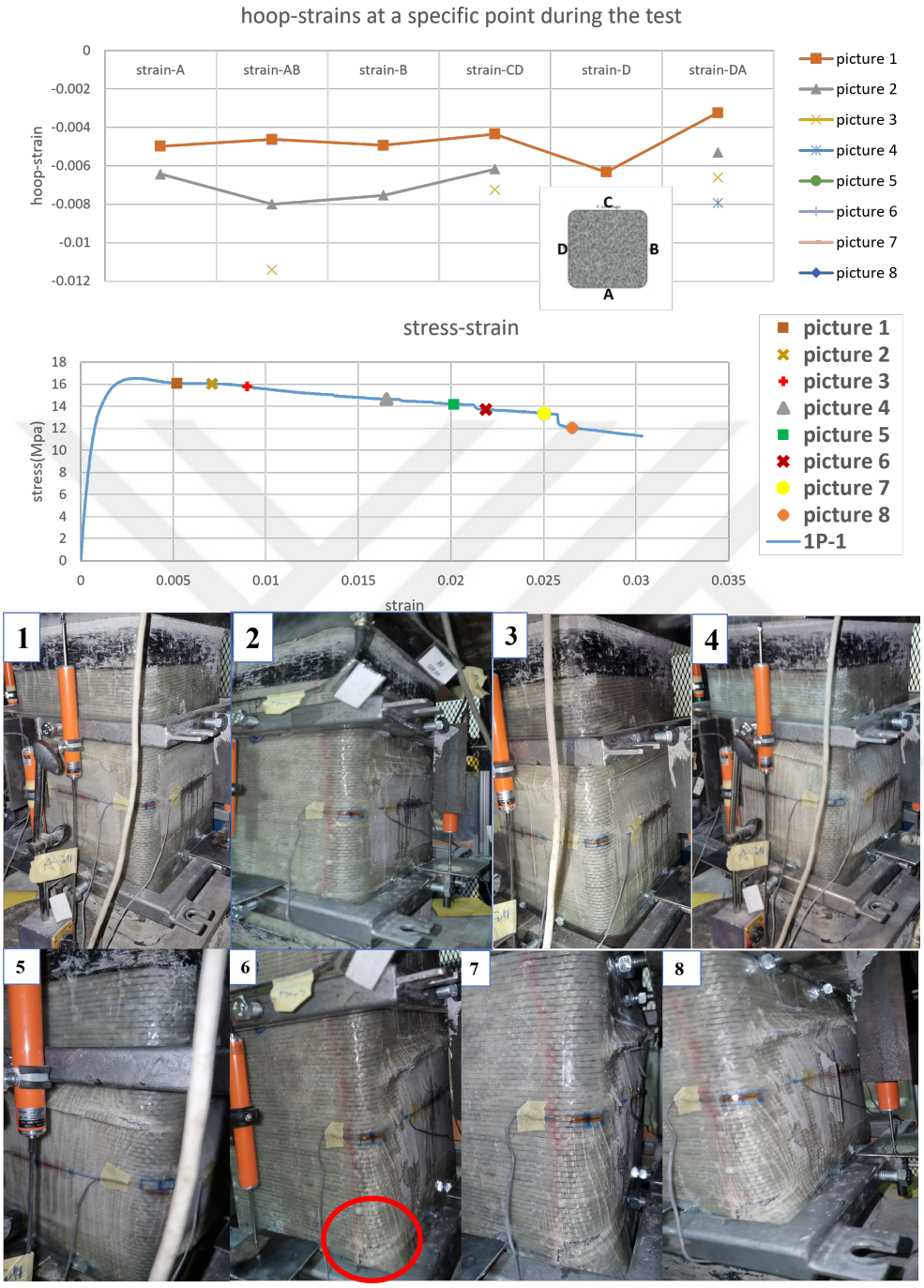

Figure 6.25 : Hoop strain response, stress-strain values, and in-test visuals for PET-wrapped specimens (1P-1) under axial loading.

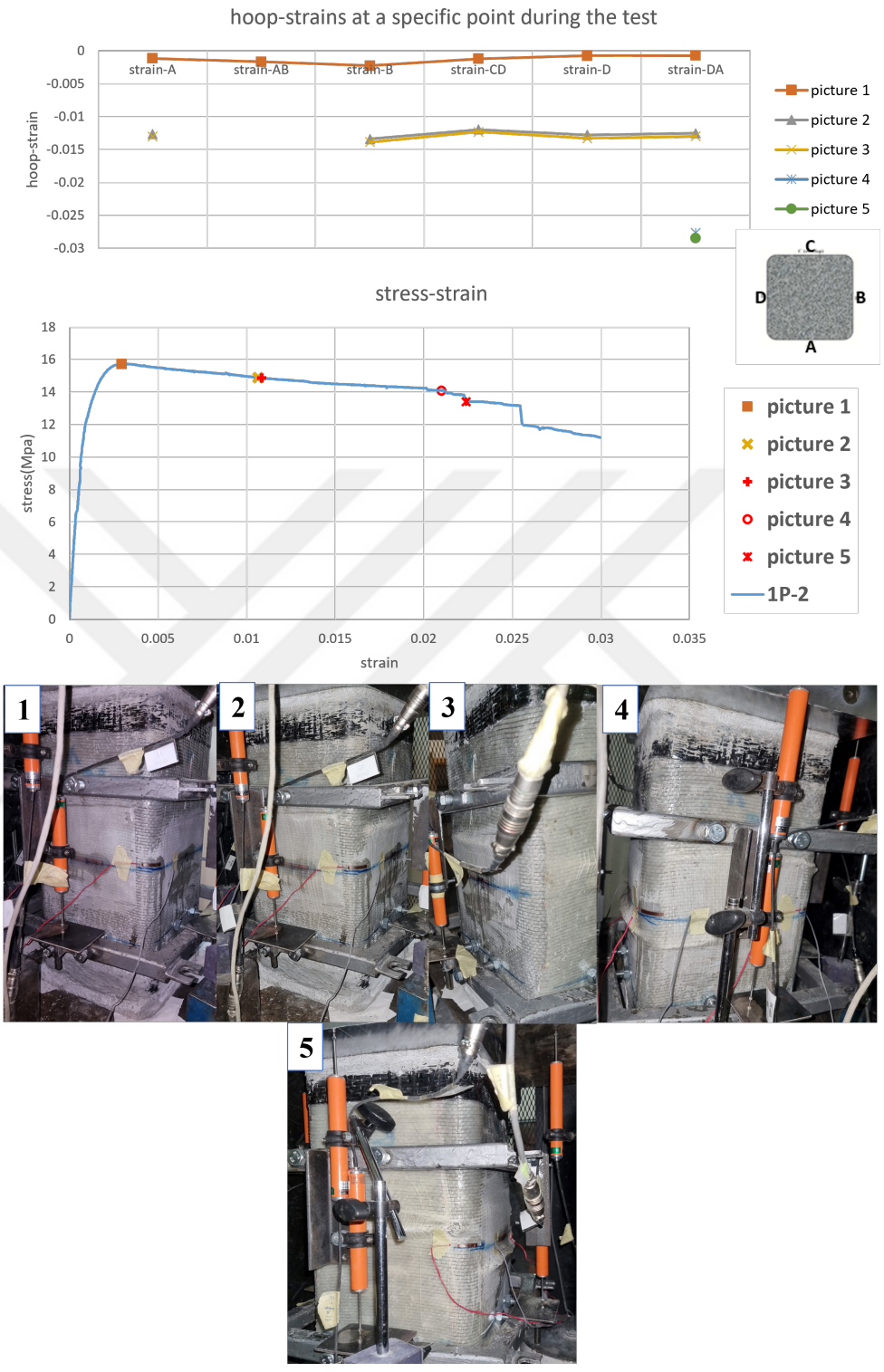

Figure 6.26 : Hoop strain response, stress-strain values, and in-test visuals for PET-wrapped specimens (1P-2) under axial loading.

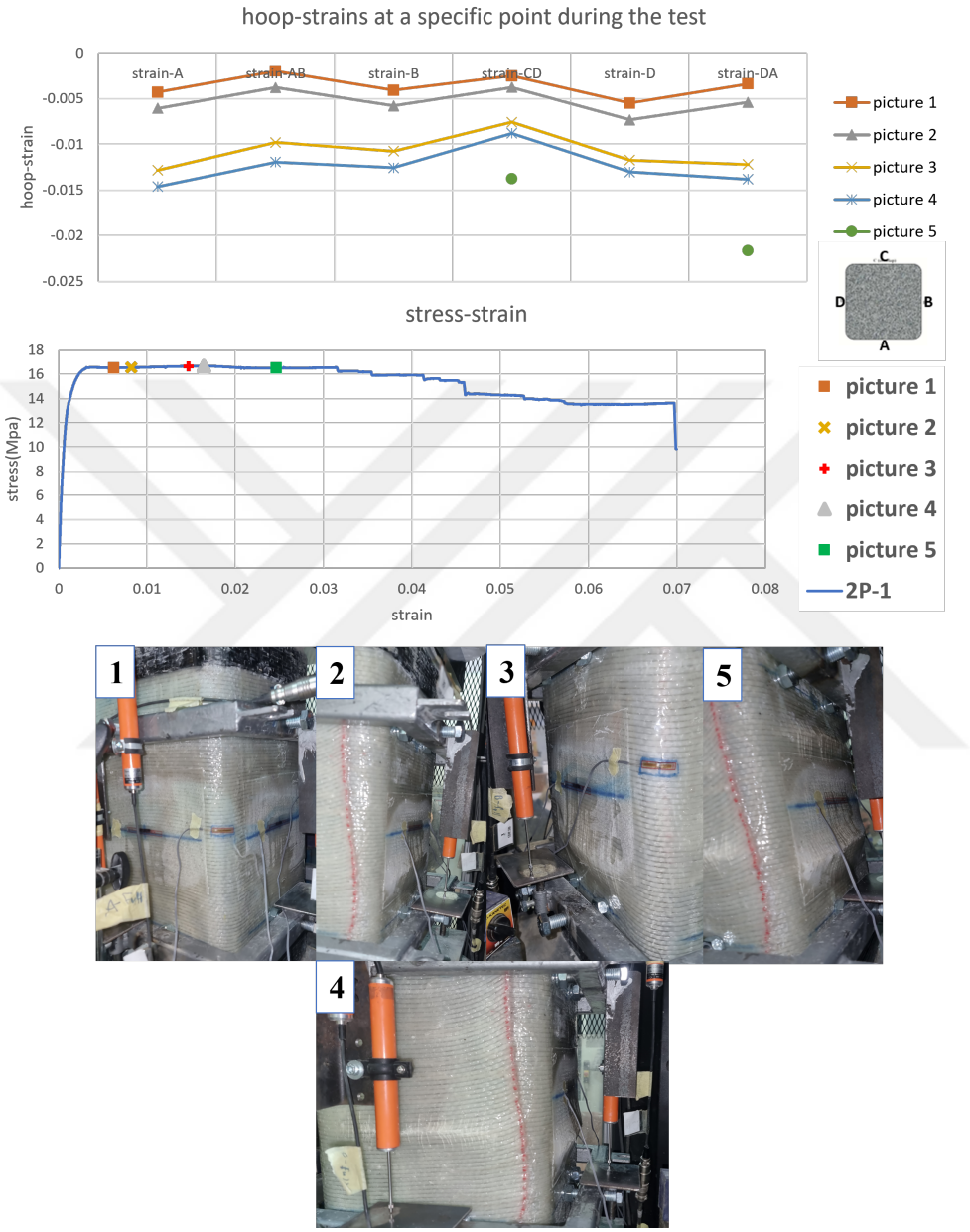

Figure 6.27 : Hoop strain response, stress-strain values, and in-test visuals for PET-wrapped specimens (2P-1) under axial loading.

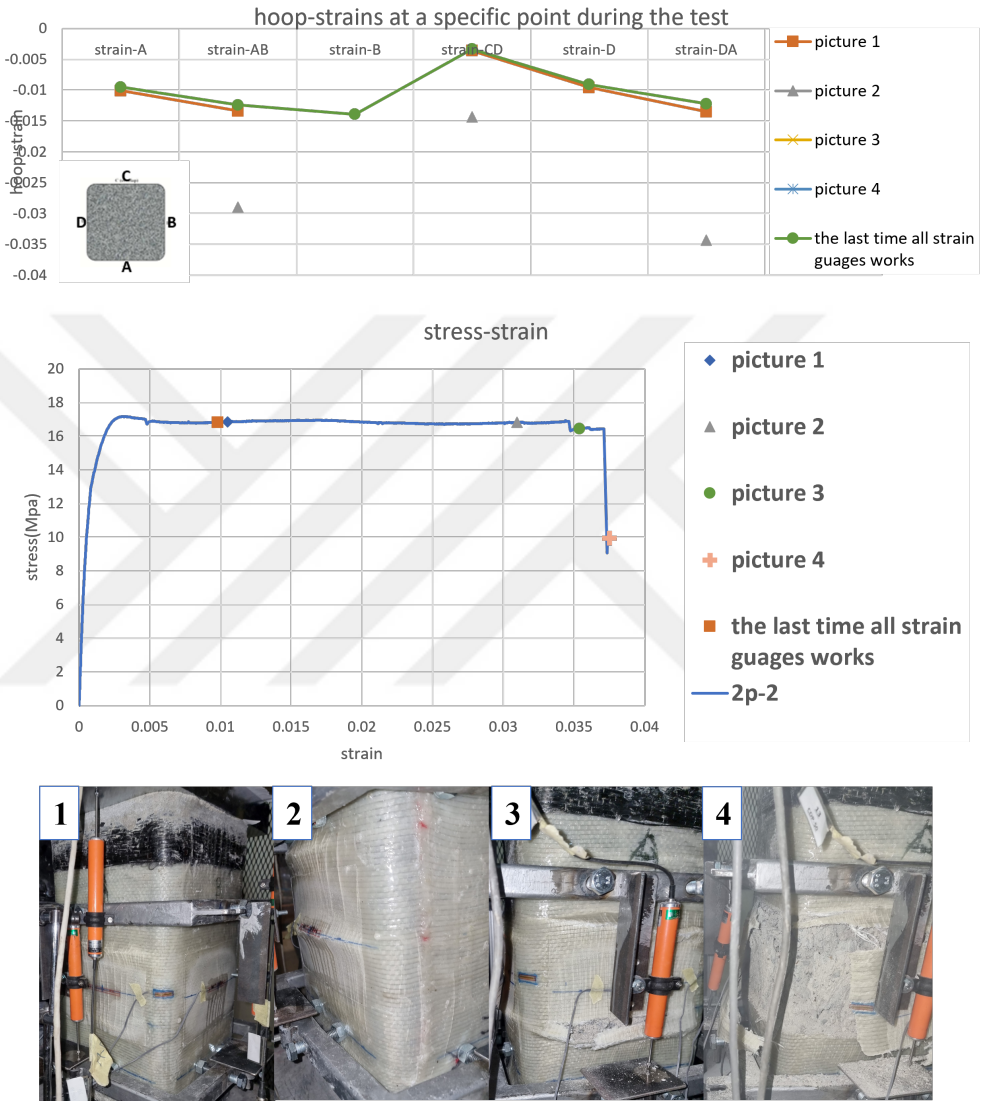

Figure 6.28 : Hoop strain response, stress-strain values, and in-test visuals for PET-wrapped specimens (2P-2) under axial loading.

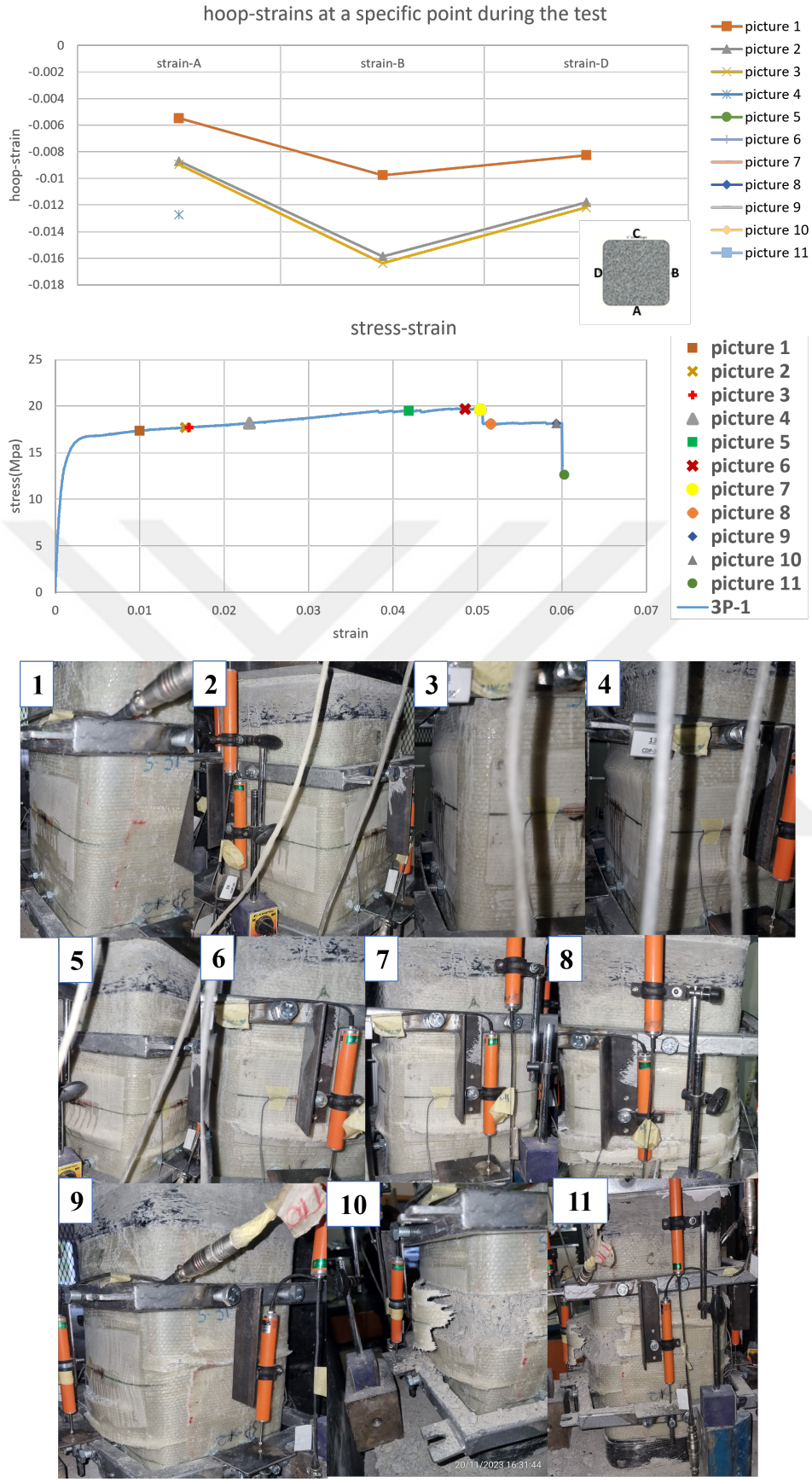

Figure 6.29 : Hoop strain response, stress-strain values, and in-test visuals for PET-wrapped specimens (3P-1) under axial loading.

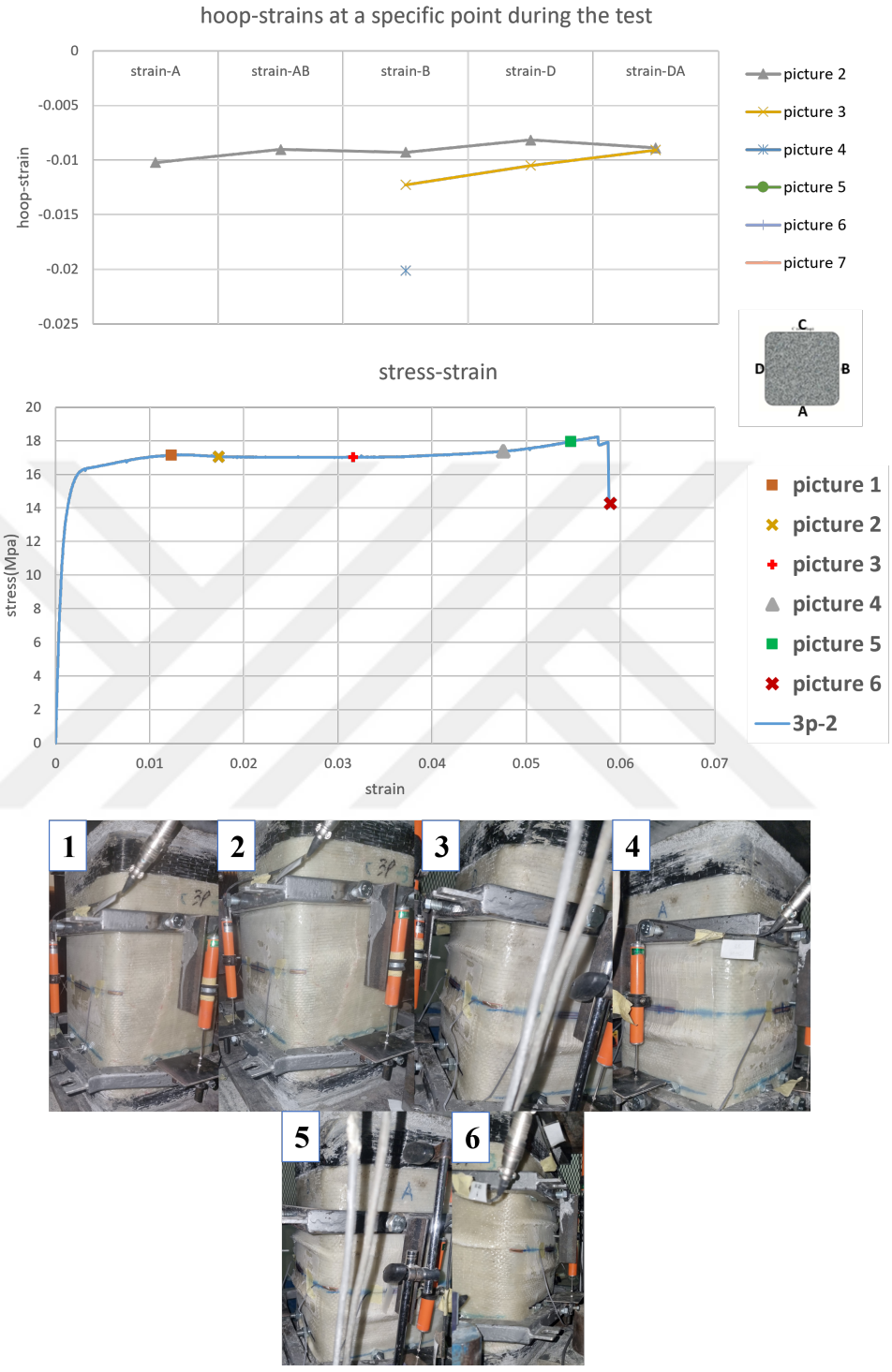

Figure 6.30 : Hoop strain response, stress-strain values, and in-test visuals for PET-wrapped specimens (3P-2) under axial loading.

6.3.4 Group 1C1P & 1C2P & 1C3P

In specimens confined with Hybrid FRP, as shown in Figures 6.31 to 6.33, clicking noises from the concrete and epoxy were common when the FRP confinement started to become active. Before carbon FRP rupture, tearing sounds were audible, followed by minor ruptures before PET-FRP breakage. Post-test, crushed concrete cores were observed in all specimens.

For 1C1P-1, rupture occurred near the BC corner on face B, where strain was highest as per Figure 6.34. In 1C1P-2, failures started on face B and spread to face A, both near corners (Figure 6.35). In 1C2P-1, failure was near the AD corner, while 1C2P-2 first failed at the overlap's end, then extended to face B with the highest strain (Figure 6.36). In 1C3P-1, rupture between faces A and B occurred with a moderate noise level, unlike CFRP-wrapped specimens, and showed a sudden strength drop (Figure 6.37). In 1C3P-2, a small tear at the overlap's end expanded to face B (Figure 6.38).



(a)



(b)

Figure 6.31 : Visual comparison of hybrid-FRP-wrapped specimens 1C1P-1 (a) and 1C1P-2 (b) before and after axial load testing, highlighting failure modes.



(a)



(b)

Figure 6.32 : Visual comparison of hybrid-FRP-wrapped specimens 1C2P-1 (a) and 1C2P-2 (b) before and after axial load testing, highlighting failure modes.



(a)



(b)

Figure 6.33 : Visual comparison of hybrid-FRP-wrapped specimens 1C3P-1 (a) and 1C3P-2 (b) before and after axial load testing, highlighting failure modes.

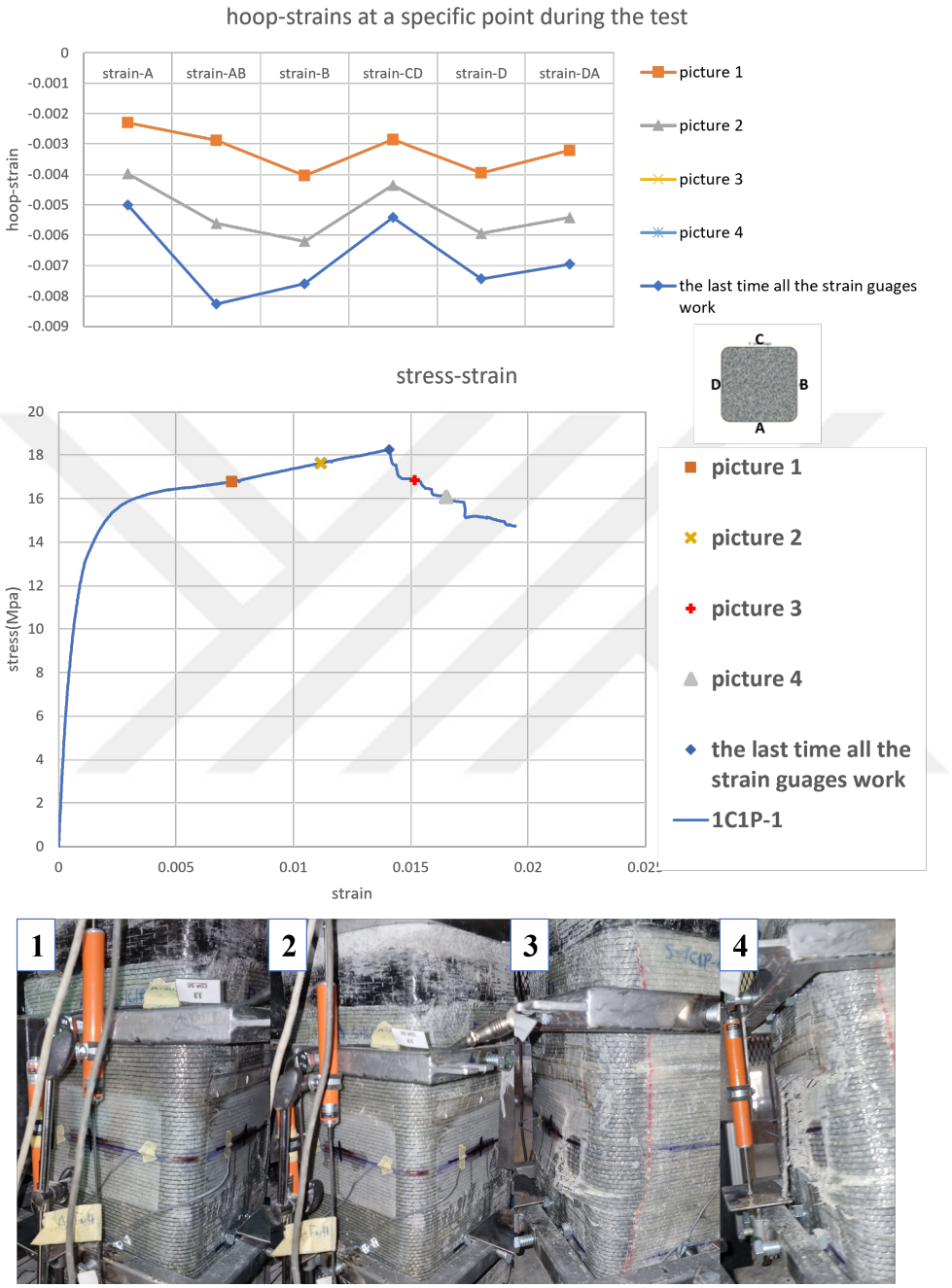

Figure 6.34 : Hoop strain response, stress-strain values, and in-test visuals for hybrid-wrapped specimens (1C1P-1) under axial loading.

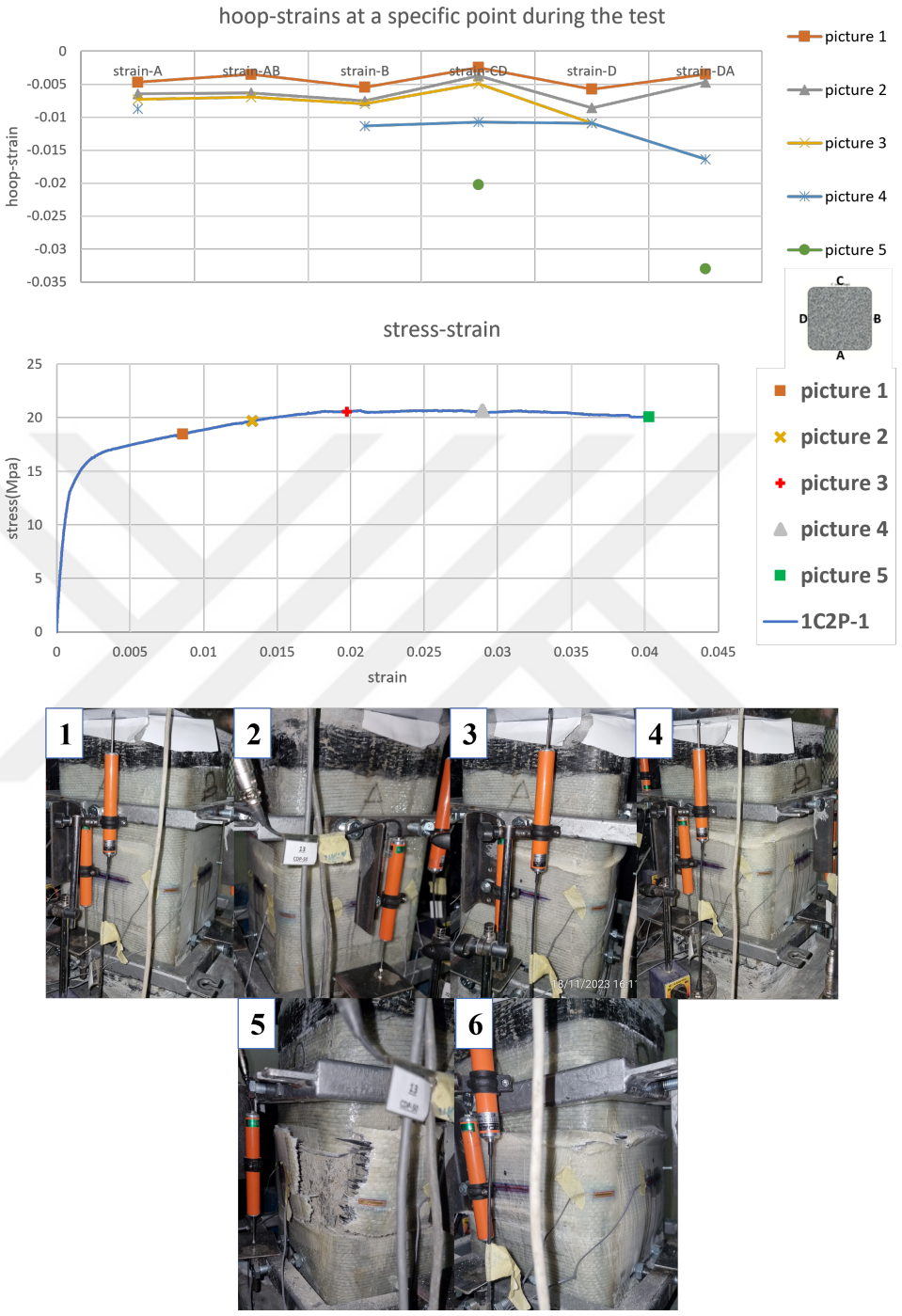

Figure 6.35 : Hoop strain response, stress-strain values, and in-test visuals for hybrid-wrapped specimens (1C2P-1) under axial loading.

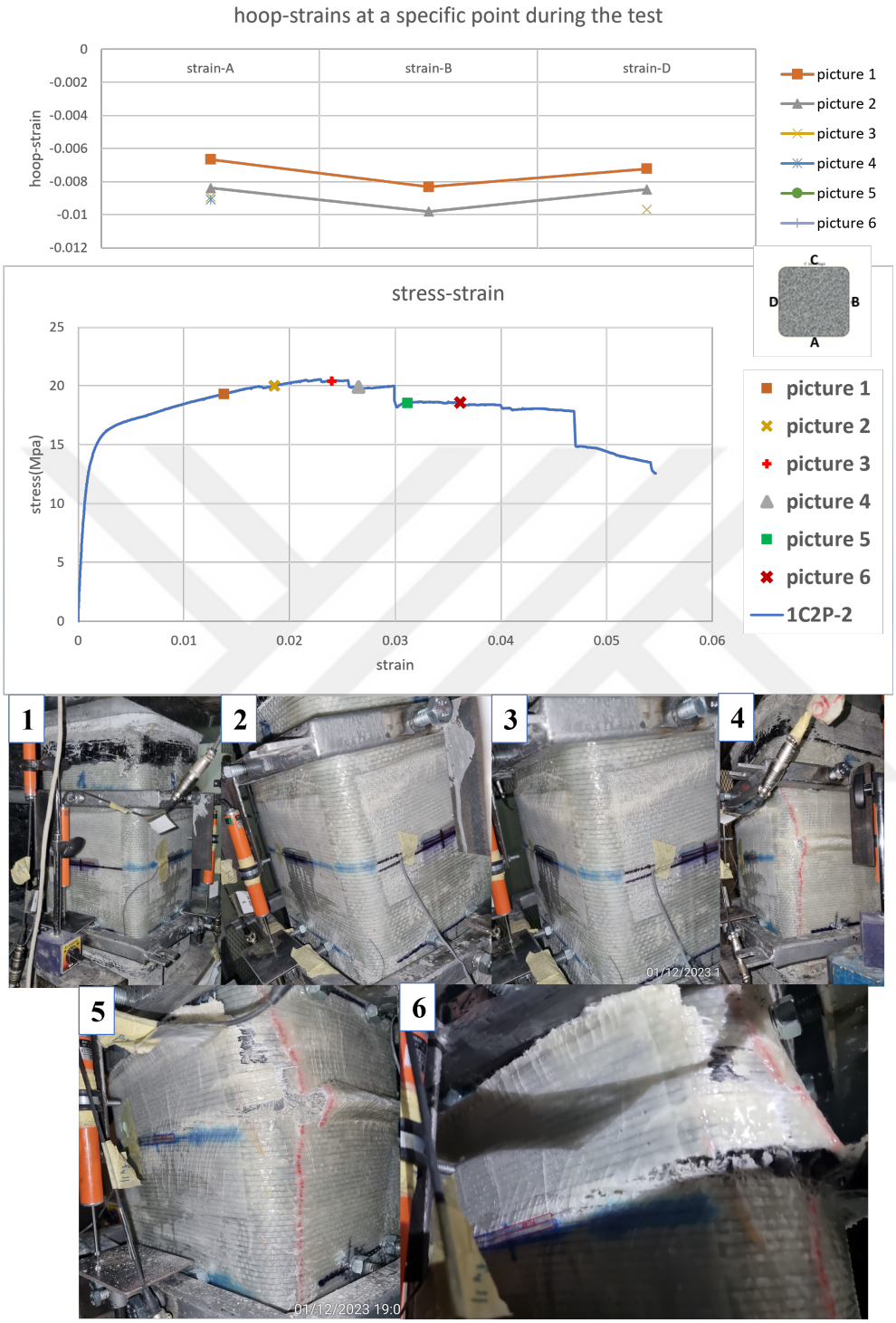

Figure 6.36 : Hoop strain response, stress-strain values, and in-test visuals for hybrid-wrapped specimens (1C2P-2) under axial loading.

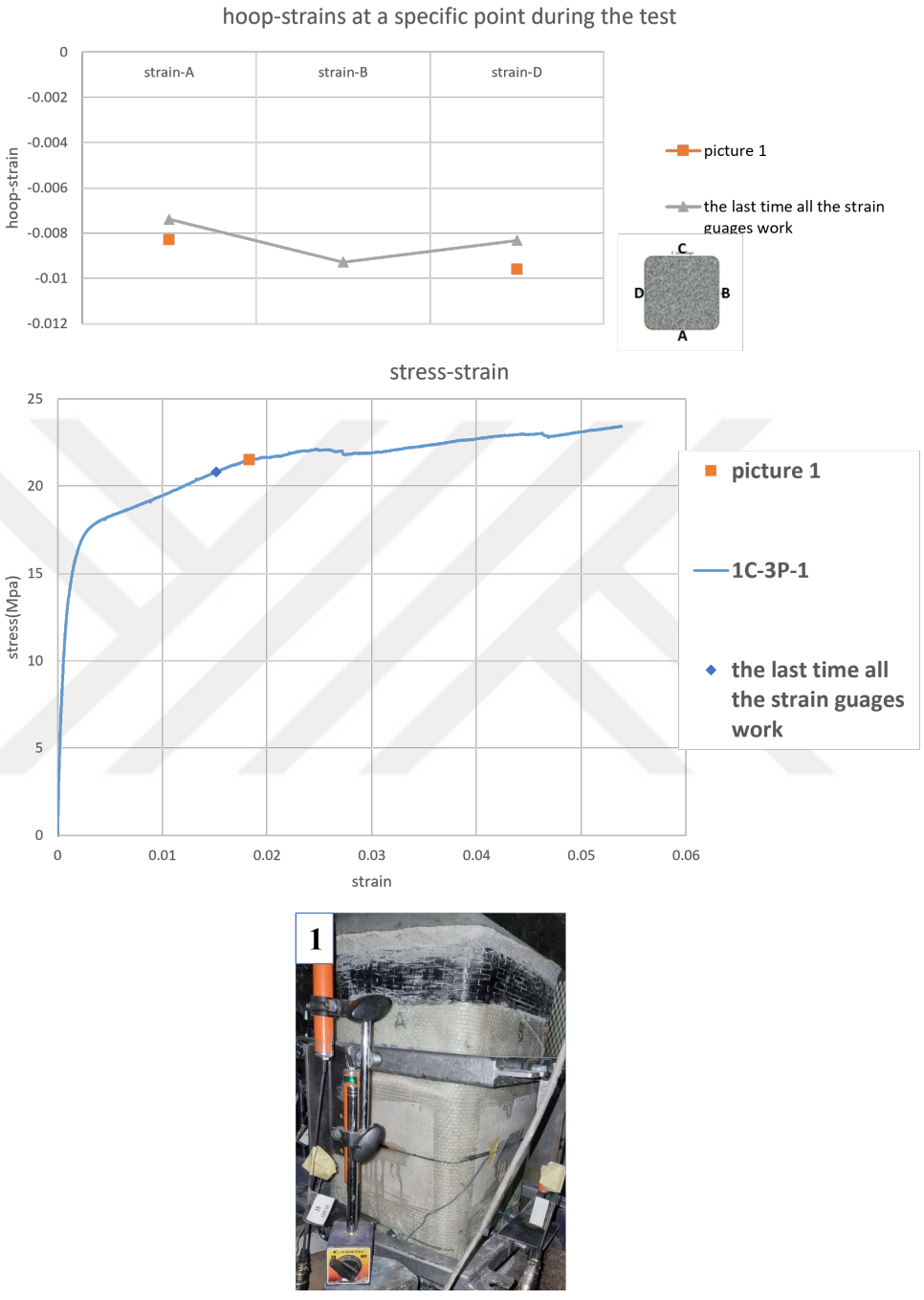

Figure 6.37 : Hoop strain response, stress-strain values, and in-test visuals for hybrid-wrapped specimens (1C3P-1) under axial loading.

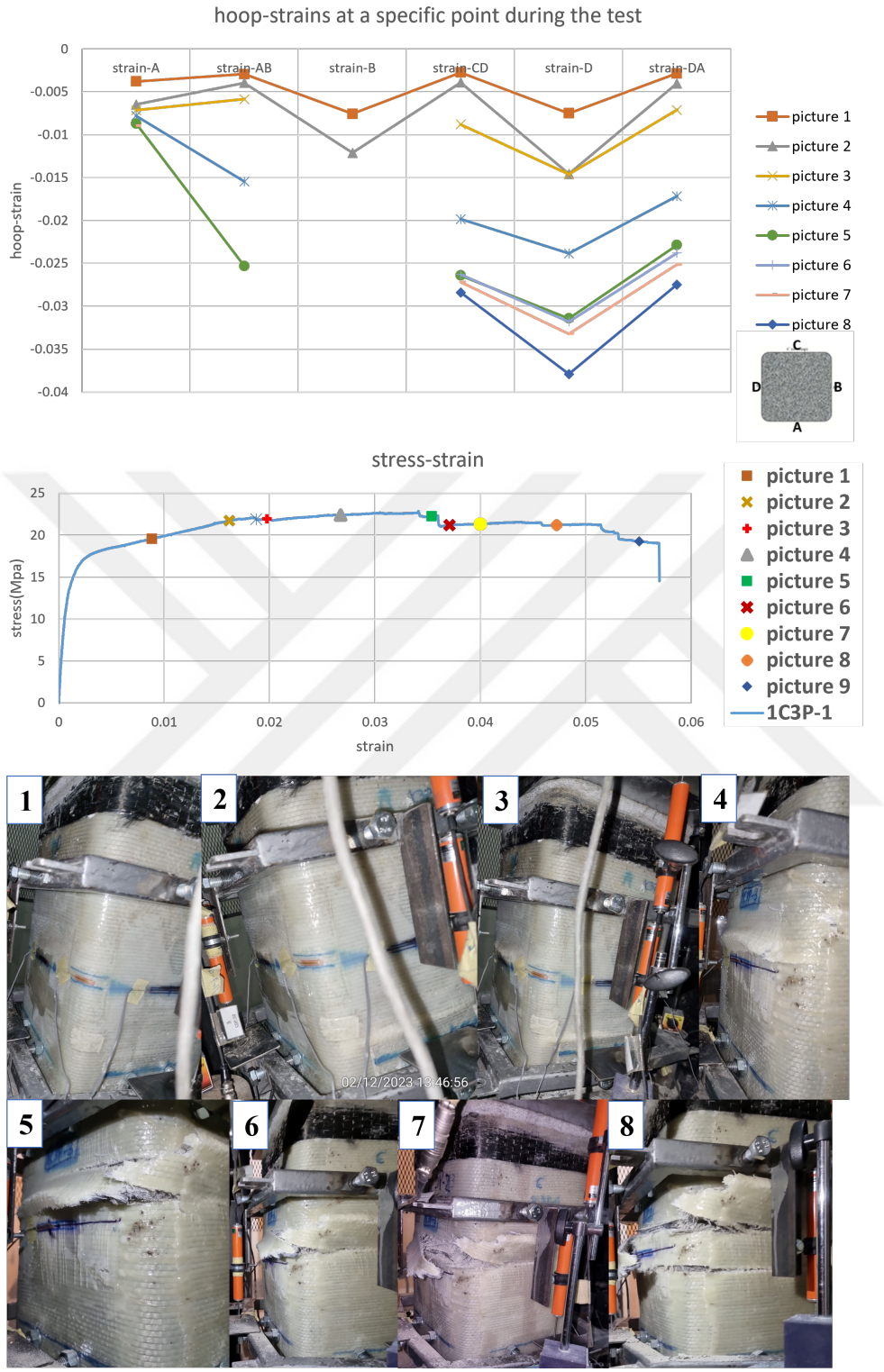

Figure 6.38 : Hoop strain response, stress-strain values, and in-test visuals for hybrid-wrapped specimens (1C3P-2) under axial loading.

6.4 Test Results

The calculation of axial stress is straightforward, achieved by dividing load by the specimen's cross-sectional area. axial strain is determined by dividing displacement , as measured by each LVDTs, by relevant gage length. The experimental results are detailed in Tables 6.1 - 6.4. These results are segmented into multiple tables to reflect the distinct characteristics of each sample group.

Table 6.1 details the ultimate strength (fco) and strain at ultimate strength (εco) of unconfined concrete. Table 6.2 focuses on the results for samples wrapped with CFRP. It includes the ultimate strength of confined concrete (fcc), the axial strain at this ultimate strength (εcc), which also represents the ultimate strain for this group. The table further presents the ratios of strength enhancement (fcc/fco) and strain enhancement ($\varepsilon cc/\varepsilon co$).

Table6.3 displays results for samples wrapped with PET-FRP. It shows the first peak strength of confined concrete ($fccp1$), the strain at this strength ($\varepsilon ccp1$), the second peak strength of the confined concrete with corresponding strain ($fccp2$, represented by $\varepsilon ccp2$) and the strength of the confined concrete at the ultimate strain ($fccp3$, represented by εcu). Additionally, it includes both strength-enhancement ratios ($fccp1/fco$, $fccp2/fco$, $fccp3/fco$) and strain-enhancement ratios ($\varepsilon ccp1/\varepsilon co$, $\varepsilon ccp2/\varepsilon co$,$\varepsilon cu/\varepsilon co$) under the investigated conditions. Figure 6.39 show the investigated points.

Table 6.4 focuses on samples wrapped with hybrid-FRP. It examines three key aspects: the strength at CFRP fracture ($fhcc1$) and its corresponding strain ($\varepsilon hcc1$), the ultimate strength after CFRP fracture ($fhcc2$) and its corresponding strain ($\varepsilon hcc2$), and the strength of confined concrete at ultimate strain ($fhcc3$, represented by $\varepsilon hcc3$). The table also presents strength-enhancement ratios ($fhcc1/fco$, $fhcc2/fco$, $fhcc3/fco$) and strain-enhancement ratios ($\varepsilon hcc1/\varepsilon co$, $\varepsilon hcc2/\varepsilon co$, $\varepsilon hcc3/\varepsilon co$) at these specific points.Figure 6.40 show the investigated points.

A common feature in Tables 6.2-6.4 is the inclusion of $\varepsilon r,s.f$ and $\varepsilon r,s.c$, which represent the rupture hoop strain measured by strain gauges. Capturing this strain

was particularly challenging for PET-FRP and hybrid-FRP samples due to significant deformations occurring at the locations of the strain gauges.

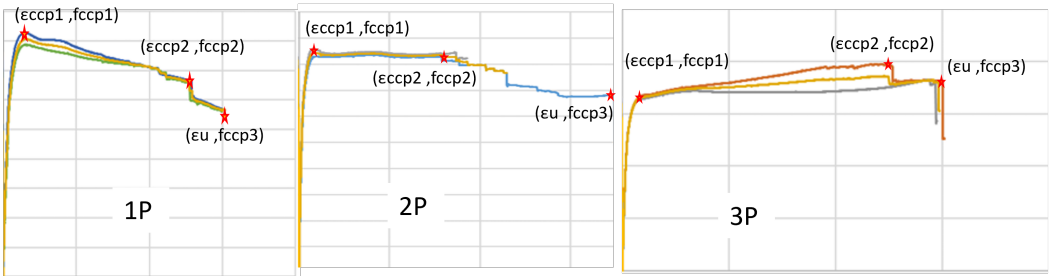

Figure 6.39 : The investigated points of PET-FRP wrapped samples on the stress vs strain curve.

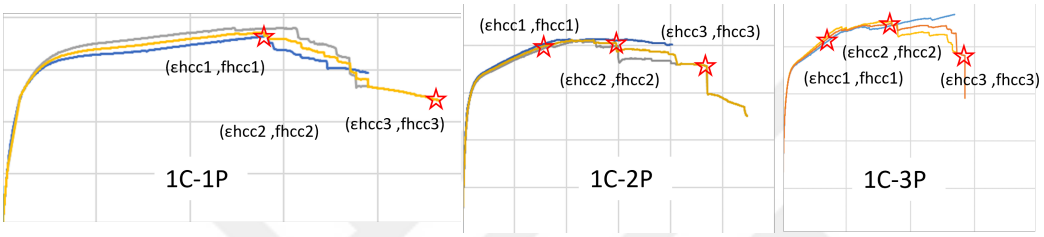

Figure 6.40 : The investigated points of hybrid-FRP wrapped samples on the stress vs strain curve.

Table 6.1 : Ultimate strength and strain characteristics of unconfined concrete.

Specimen	fco (MPa)	Average of fco	εco	Average of εco
R-1	12.87	13.12	0.00192	0.00194
R-2	13.37		0.00196	

Table 6.2 : Test results of CFRP-wrapped concrete.

Specimen	fcc (MPa)	Avg. fcc	fcc/fco	$\varepsilon cu = \varepsilon cc$	Avg. εcc	$\varepsilon cc/\varepsilon co$	$\varepsilon r,s.f$	Avg. $\varepsilon r,s.f$	$\varepsilon r,s.c$	Avg. $\varepsilon r,s.c$
1C-1	16.87	16.59	1.27	0.01289	0.01312	6.75	0.00758	0.00744	0.00619	0.00619
1C-2	16.31			0.01336			0.00731		-	
2C-1	20.75	20.59	1,57	0.02301	0.02123	10,93	0.00859	0.00823	0.00730	0.00730
2C-2	20.44			0.01946			0.00787		-	

Table 6.3 : Test results of PET-FRP-wrapped concrete.

Specimen	$fccp1$ (MPa)	$fccp2$ (MPa)	$fccp3$ (MPa)	$\varepsilon ccp1$	$\varepsilon ccp2$	εcu	$\varepsilon r,s.f$	$\varepsilon r,s.c$	$\frac{fccp1}{fco}$	$\frac{fccp2}{fco}$	$\frac{fccp3}{fco}$	$\frac{\varepsilon ccp1}{\varepsilon co}$	$\frac{\varepsilon ccp2}{\varepsilon co}$	$\frac{\varepsilon cu}{\varepsilon co}$
1P-1	16.54	13.25	11.31	0.0030	0.0257	0.0303	0.0092	0.0123	12.3	1.01	0.86	1.55	13.16	15.51
1P-2	15.75	13.16	11.21	0.0030	0.0254	0.0300	0.0276	0.0300						
2P-1	16.59	16.52	13.63	0.0038	0.0315	0.0697	0.0356	0.0266	1.29	1.27	1.15	1.77	17.03	27.47
2P-2	17.17	16.88	16.45	0.0031	0.0347	0.0371	0.0234	0.0303						
3P-1	16.83	19.49	18.16	0.0051	0.0506	0.0600	0.0179	-	1.27	1.44	1.38	2.42	27.84	30.54
3P-2	16.47	18.25	17.93	0.0043	0.0576	0.0587	0.0327	0.0112						

Table 6.4 : Test results of hybrid-FRP-wrapped Concrete.

Specimen	$fhcc1$ (MPa)	$fhcc2$ (MPa)	$fhcc3$	$\varepsilon hcc1$	$\varepsilon hcc2$	$\varepsilon hcc3$	$\varepsilon r,s.f$	$\varepsilon r,s.c$	$\frac{fhcc1}{fco}$	$\frac{fhcc2}{fco}$	$\frac{fhcc3}{fco}$	$\frac{\varepsilon hcc1}{\varepsilon co}$	$\frac{\varepsilon hcc2}{\varepsilon co}$	$\frac{\varepsilon hcc3}{\varepsilon co}$
1C1P-1	18.26	-	14.75	0.0141	-	0.0195	0.0068	0.0069	14.22	-	1.07	7.49	-	10.93
1C1P-2	19.05	-	13.34	0.0150	-	0.0230	-	-						
1C2P-1	20.62	20.71	20.10	0.0182	0.0262	0.0403	0.0133	0.0266	15.48	1.57	1.45	9.11	12.64	22.43
1C2P-2	19.99	20.57	17.85	0.0172	0.0229	0.0469	0.0096							
1C3P-1	21.56	23.43	23.41	0.0184	0.0537	0.0538	0.0254	-	16.63	1.77	1.71	9.54	22.60	27.76
1C3P-2	22.07	22.87	21.41	0.0186	0.0341	0.0541	0.0405	0.0287						

6.4.1 Analysis and discussion of test results

Based on the data provided in Table 6.2 and Figure 6.41, which displays the test outcomes of concrete samples that were wrapped with CFRP, certain deductions can be made:

1. Increased Ultimate Strength: The concrete specimens covered with CFRP demonstrate a higher ultimate strength (fcc) in comparison to the standard unconfined concrete strength, as shown in Table 6.1. The results indicate that the utilization of CFRP wrapping greatly improves the load-carrying capacity of the concrete specimen. Furthermore, the two-layer specimens had a stronger strength enhancement ratio, suggesting that the extra layer of CFRP has significantly increased strength. as shown in Figure 6.41a.

2. Strain at Ultimate Strength: The CFRP-wrapped specimens exhibit enhanced ductility, as evidenced by their ability to withstand greater strains prior to failure in comparison to unconfined concrete. Furthermore, the strain at ultimate strength for the two-layer specimens is observably greater, indicating that they can withstand a greater amount of elongation before failing. This demonstrates a higher level of axial strain.

3. The strain enhancement ratios ($\varepsilon cc/\varepsilon co$) are considerably greater than 1, indicating that the CFRP wrapping not only boosts the ultimate strength but also significantly improves the strain capacity of the concrete. Additionally, the two-layer specimens demonstrate a higher strain enhancement ratio, suggesting that the extra layer of CFRP substantially increases the strain capacity beyond what a single layer provides. as shown in Figure 6.41b.

In summary, CFRP wrapping significantly improves concrete's mechanical properties, enhancing strength and strain capacities. This makes CFRP an effective material for reinforcing concrete, potentially benefiting structures with improved load-bearing capabilities and ductility. Using two layers of CFRP wrapping enhances ultimate strength and strain capacity, making it ideal for higher performance under load. However, the choice between one and two layers must consider factors like cost,

constructability, and specific project requirements. Ultimately, the decision should be based on a thorough assessment of these factors.

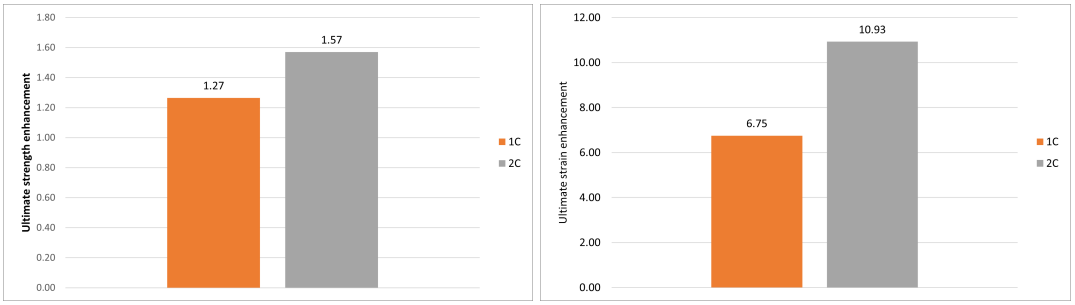

(a) (b)

Figure 6.41 : Enhancement ratios of 1C and 2C wrapped concrete columns: (a) strength enhancement ratios ; (b) strain enhancement ratios.

The results of the tests conducted on concrete specimens that were wrapped with PET-FRP are shown in Table 6.3 and Figure 6.42. Comparing the usage of different layers of PET-FRP is possible using the data supplied in Table 6.3. Each specimen represents a different number of PET-FRP layers, and they are labeled as 1P, 2P, and 3P, respectively. Based on the available data, here is an analysis:

The analysis of the data concerning the enhancement of concrete columns wrapped with PET-FRP layers reveals a direct correlation between the number of layers and the degree of enhancement in both strength and strain. Specifically, columns wrapped with a single layer of PET-FRP, designated as 1P, exhibit an ultimate strength enhancement of 1.23 and an ultimate strain enhancement of 15.51. When a second layer is added, creating 2P specimens, the strength enhancement increases to 1.29, and strain enhancement shows a more pronounced increase to 27.47. This trend continues with 3P specimens, where three layers of PET-FRP wrapping provide the highest recorded enhancements, with strength enhancement reaching 1.44 and strain enhancement escalating to 30.54. These figures suggest that each additional layer of PET-FRP not only contributes to a higher load-bearing capacity but also significantly improves ductility, allowing the column to undergo larger deformations before failure. This is particularly beneficial in seismic zones where energy absorption and ductility are critical for the structural integrity of buildings. When you compare the effects of adding PET-FRP layers to concrete columns, you can see clear trends in terms of how

much strength and strain they increase. There is an increase in strength of about 4.88% when going from a single-layered PET-FRP wrap (1P) to a double-layered wrap (2P). But this improvement is stronger when an extra layer is added to make a 3P specimen; the improvement in strength goes up by about 11.63%. This means that adding the third layer had a bigger effect on strength than adding the second layer. The strain enhancement, on the other hand, shows a different pattern. When the second layer (which changes from 1P to 2P) is added, the strain enhancement goes up by about 77.11%, which means that the material is much more ductile. However, adding the third layer (going from 2P to 3P) only leads to a small increase in strain enhancement of about 11.18 percent. This means that the ductility improves less with each extra layer, which is very different from the strength improvement that gets better over time.

The variation in the failure mechanisms is reflected in the different values of hoop strains for the midpoint on the straight face ($\varepsilon r, s.f$) and corner ($\varepsilon r, s.c$) across specimens. Due to the significant deformation observed in the middle section of the specimens prior to the FRP rupture, it was unfeasible to quantify the rupture strain for nearly all of the specimens. The absence of a distinct trend corresponding to the number of layers is the reason for this.

To summarize, the PET-FRP wrapping significantly improves both the strength and the ability of the concrete specimens to withstand deformation. The utilization of various layers of PET-FRP seems to have a major impact on the strength and strain capabilities of concrete. The addition of many layers of PET-FRP improves both the overall strength and ability to withstand deformation, demonstrating its efficacy as a reinforcement material. Nevertheless, the effect on rupture strain remains uncertain, and an alternate approach is necessary to accurately measure the hoop strain at the point of rupture instead of relying solely on strain gauges. Anyway, the notable augmentation in strain capacity particularly, suggests that PET-FRP is a suitable material for situations that demand improved ductility and deformation capacity.

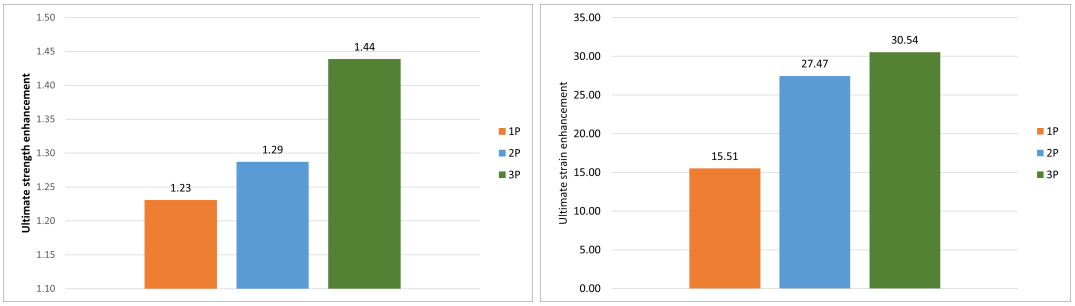

(a) (b)

Figure 6.42 : Enhancement ratios of 1P, 2P and 3P wrapped concrete columns: (a) strength enhancement ratios ; (b) strain enhancement ratios.

Based on the Table 6.3 and Figure 6.43 for Hybrid-FRP-wrapped concrete specimens, The enhancement study of columns that have been wrapped in a hybrid material that contains both carbon and PET-FRP layers gives useful information about the structural advantages that each extra layer brings. After switching from a single hybrid layer configuration (1C1P) to two layers (1C2P), the ultimate strength improvement goes up by about 10.56%. As an extra layer is added, this upward trend continues. The change from 1C2P to 1C3P results in a strength increase of about 12.74 percent. Notably, the strain enhancement metrics are even stronger; going from 1C1P to 1C2P more than doubles the strain enhancement, which means it goes up by about 105.22%. Even though the relative gain slows down when the third layer is added (from 1C2P to 1C3P), it still shows a big improvement of about 23.76%. These numbers show that the hybrid wrapping method works well at improving both the strength and ductility of structural columns. Each extra layer of PET-FRP makes a big difference, especially when it comes to strain capacity, which makes the structure stronger against forces that cause it to deform.

In conclusion, the data suggests that Hybrid-FRP wrapping can significantly enhance the mechanical properties of concrete. The degree of enhancement varies with different configurations, which implies that careful consideration must be given to the design and application of FRP wraps in construction to optimize the performance benefits.

To provide a comprehensive comparison between the results of Hybrid-FRP-wrapped concrete specimens and those wrapped with CFRP and PET-FRP, we would ideally compare the enhancement ratios side by side in a visual way:

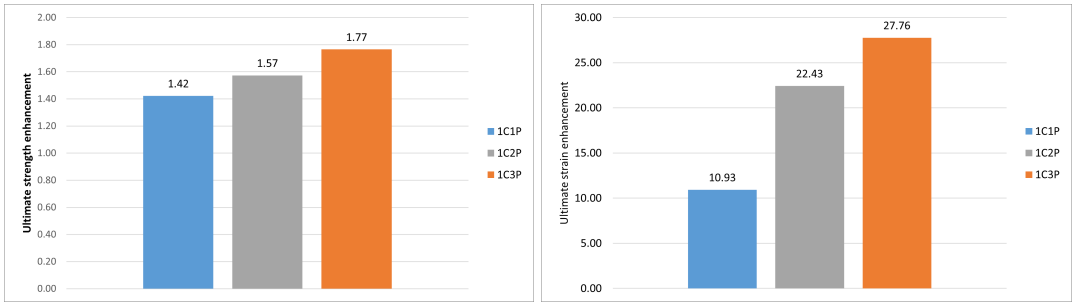

(a) (b)

Figure 6.43 : Enhancement ratios of 1C1P ,1C2P and 1C3P wrapped concrete columns: (a) strength enhancement ratios ; (b) strain enhancement ratios.

1. Figure 6.43 compares the enhancement ratios for different configurations of concrete columns wrapped with CFRP and PET FRP. The specific configurations are: 1C,1P, 1C1P

By conducting a comparative analysis of the performance improvements demonstrated by CFRP (1C) and PET-FRP (1P) separately and in combination (1C1P), it is possible to figure out a complex relationship between ductility and strength in the context of structural reinforcement as shown in figure . On an individual basis, CFRP (1C) exhibits a significant increase in strength (valued at 1.27), while its contribution to strain enhancement is deemed moderate (valued at 6.75). In contrast, PET-FRP (1P) exhibits a moderately increase in strength at 1.23, yet demonstrates exceptional capability in strain enhancement, obtaining a value of 15.51; this underscores the material's remarkable ductility. The hybrid configuration (1C1P), consisting of a single layer of PET-FRP and one layer of CFRP, produces a remarkable interaction that increases the strength to 1.42. This finding highlights the significant increase of 15.45% over 1P and an approximate 11.81% increase over 1C, respectively. These results emphasize the beneficial impact that the hybrid configuration has on boosting strength. Nevertheless, the dynamics of strain enhancement convey a more complicated picture. The hybrid application achieves a strain enhancement of 10.93 percent, which, although significantly greater than the strain enhancement of 1C by approximately 61.93%, falls short of the exceptional ductility demonstrated by 1P in separately, exhibiting a reduction of approximately 29.53%.

2- Figure 6.45 shows the enhancement ratios for different configurations of concrete columns wrapped with CFRP and PET FRP. The specific configurations are: 1C, 2P, 1C2P.

The comparative analysis between the individual applications of CFRP (1C) and PET-FRP (2P) and their hybrid combination (1C2P) unveils a nuanced synergy, particularly pronounced in strength enhancement. Individually, CFRP manifests a robust strength enhancement of 1.27, while two layers of PET-FRP (2P) slightly surpass this with a value of 1.29. However, the hybrid configuration (1C2P) significantly elevates the strength enhancement to 1.57, marking increases of approximately 23.62% over 1C and 21.71% over 2P. This denotes a synergistic interplay in the hybrid application, where the composite effect of CFRP and PET-FRP layers harmoniously augments the structural strength beyond the sum of their individual contributions.

In terms of strain enhancement, the scenario unfolds differently. While CFRP alone offers modest ductility with a strain enhancement of 6.75, two layers of PET-FRP exhibit remarkable ductility, reaching a strain enhancement of 27.47. The hybrid combination (1C2P), however, yields a strain enhancement of 22.43. This represents a substantial improvement of 232.30% over CFRP alone, yet it reflects a decrease of 18.35% from the high ductility provided by two layers of PET-FRP. This divergence underscores the intricate dynamics in hybrid material applications; the introduction of CFRP into the PET-FRP framework significantly reinforces strength but somewhat tempers the exceptional ductility rendered by PET-FRP alone.

3- Figure 6.46 shows the enhancement ratios for different configurations of concrete columns wrapped with CFRP and PET FRP. The specific configurations are: 1C,3P, 1C3P.

The comparative analysis between the individual applications of CFRP (1C) and three layers of PET-FRP (3P) against their hybrid combination (1C3P) illuminates a distinct synergy in strength and ductility enhancements. Individually, CFRP (1C) presents a strength enhancement of 1.27 and a moderate strain enhancement of 6.75, whereas three layers of PET-FRP (3P) exhibit a strength enhancement of 1.44

alongside a substantial strain enhancement of 30.54. The hybrid application (1C3P), integrating one layer of CFRP with three layers of PET-FRP, markedly advances the strength enhancement to 1.77, translating to a significant increase of approximately 39.37% over 1C and 22.92% over 3P. This pronounced improvement underscores the synergistic interplay within the hybrid configuration, where the composite effect of CFRP and PET-FRP layers collectively amplifies the structural strength beyond their individual capabilities.

In terms of strain enhancement, the hybrid application achieves a value of 27.76. While this represents a substantial increment of 311.26% over CFRP alone, it slightly falls short of the exceptional ductility provided by 3P alone by about 9.10%. This nuanced outcome highlights the intricate dynamics within hybrid material applications: while the inclusion of CFRP significantly bolsters strength and contributes to ductility, the peak ductility offered by three layers of PET-FRP alone is marginally moderated in the hybrid configuration.

comprehensive examination of CFRP, PET-FRP, and their hybrid configurations (1C1P, 1C2P, 1C3P) demonstrates strength and strain enhancements in different levels. In contrast to CFRP, which primarily improves strength, PET-FRP contributes substantially to ductility. Hybrid configurations effectively combine these advantageous attributes, typically yielding structural performances that outperform those of their a part applications. However, in hybrid configurations, the remarkable ductility of PET-FRP that is observed when used in solo is slightly decreased. The complicated nature of material dynamics in hybrid systems is emphasized by this interaction, which also emphasizes the need for a strategic approach when selecting materials. When considering the utilization of particular materials or their hybrid configurations, careful consideration should be given to their compatibility with particular structural requirements. The objective should be to achieve an ideal equilibrium between strength and ductility, in order to fulfill the demands of modern structural engineering.

In terms of strain enhancement, hybrid layouts consistently show lower rupture strains than PET-FRP-reinforced systems. This distinction may be due to distinct failure

mechanisms. Specimens wrapped entirely in PET tend to fail at many places during testing, resulting in energy dissipation and reduced confinement, so the specimen takes longer to collapse due to localized failures, and the ultimate rupture strain increases.

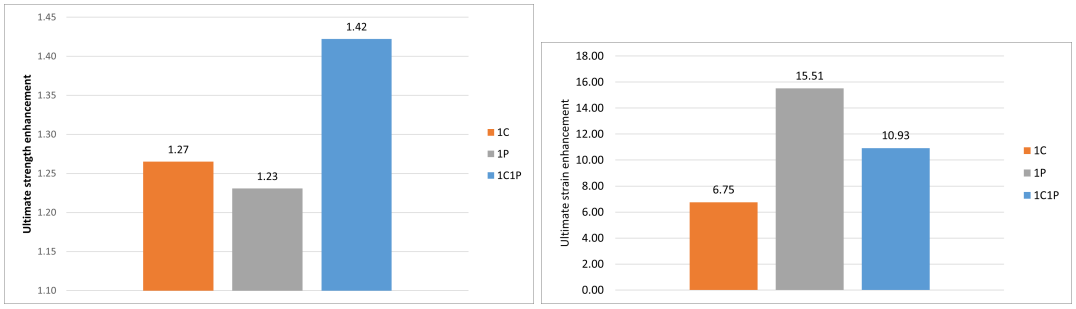

(a) (b)

Figure 6.44 : Enhancement ratios of 1C, 1P and 1C1P Wrapped concrete columns: (a) strength enhancement ratios ; (b) Strain enhancement ratios.

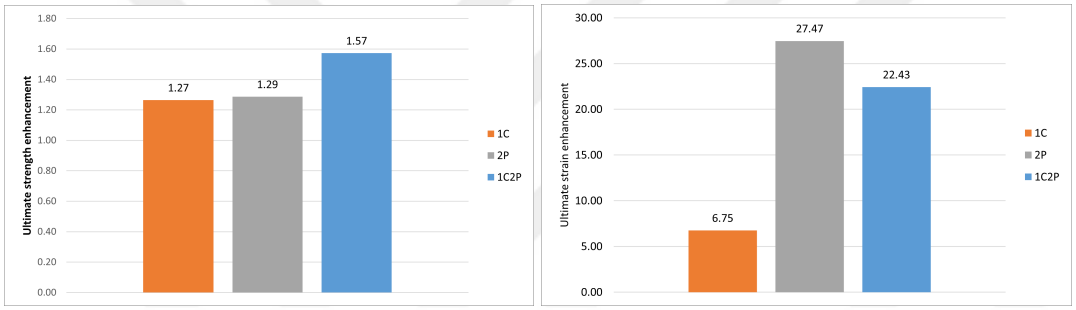

(a) (b)

Figure 6.45 : Enhancement ratios of 1C, 2P and 1C2P wrapped concrete columns: (a) strength enhancement ratios ; (b) strain enhancement ratios.



(a) (b)

Figure 6.46 : Enhancement ratios of 1C , 3P and 1C3P wrapped concrete columns: (a) strength enhancement ratios ; (b) strain enhancement ratios.

7. ANALYTICAL EXPLORATION

7.1 Introduction

Various models have been developed to estimate the ultimate strength and strain capacity of FRP-confined concrete, with some also detailing the overall compressive stress-strain response. These models vary, with certain designs tailored specifically for LRS FRP and others for conventional FRP. In the subsequent sections, we will compare the predictions from these models with the empirical results from our study, focusing on identifying models that accurately predict critical points for CFRP-wrapped and PET-FRP-wrapped specimens. This comparison will then be extended to anticipate the behavior of hybrid FRP-confined samples.

7.2 Evaluation Methodology

This study employs an evaluative approach that involves comparing model-generated predictions to actual data collected using ratios to make sense of the results. More precisely, these ratios are computed by dividing the experimental value (ER) by the predicted results (MP) of the models. In addition, the accuracy of the model's predictions is carefully measured using the Average Absolute Error (AAE), as defined in Equation (1). In this equation, the symbols α_{MP} and α_{ER} represent the model-predicted values and the experimental data, respectively. The variable n represents the number of specimens. The benchmark for this analysis is the Wu and Zhou [67] categorization of model accuracy. It segments accuracy into three distinct classifications: an AAE of 15% or below signifies a model of high precision, an AAE exceeding 15% but not surpassing 30% denotes a model of moderate precision, and an AAE above 30% is indicative of a model with low precision. Using this three-part classification framework, it's easier to see how well the model predicts things based on data from the experiment.

$$\text{AAE} = \frac{\sum_{i=1}^{n} \frac{|\alpha_{MP} - \alpha_{ER}|}{\alpha_{ER}}}{n} \tag{1}$$

7.3 Theoretical Analysis

7.3.1 Estimation of peak axial stress and strain in CFRP-wrapped specimens

For the CFRP-wrapped samples, we'll utilize eight distinct models to estimate the critical points on the stress-strain curve as shown with star symbol in Figure 7.1 . Some models are capable of predicting both the ultimate strength and strain, while others can forecast either strength or strain. The models to estimate the ultimate axial strength of these samples is summarized in Table 7.1.The estimation of ultimate strain is derived from the functions listed in Table 7.2.The outcomes are detailed in Table 7.3 and 7.4 and visualized in Figures 7.2 - 7.4.

Based on the results, Ilki [23], Wang [68], Wu [69], and Nestico's [70] prediction outperformed the other models in estimating strength. The alternative model may exhibit poor predictive performance due to the model equations may be formulated utilizing data mostly representing normal-strength concrete. It is worth mentioning that there are variations in the behavior of normal-strength concrete when it is exposed to CFRP confinement, as opposed to lower-strength concrete [71]. Consequently, the model may fail to appropriately include these differences. Ilki *et al.* [23] and Pham [72] excelled in predicting strain.

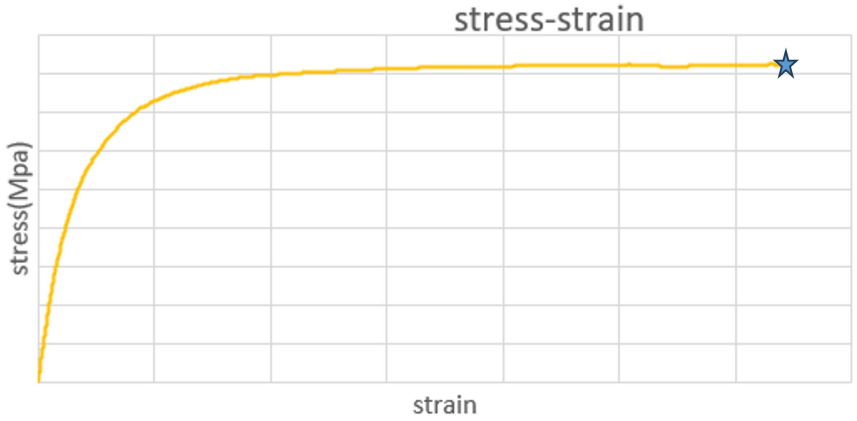

Figure 7.1 : the investigate point of CFRP-wrapped samples stress vs strain curve

Table 7.1 : Compressive strength functions of the models.

Author	Confined compressive strength	Comments[a]
Ilki [23]	$f_{MP} = f_{co}\left[1+2.4\left(\frac{f_{al}}{f_{co}}\right)^{1.2}\right]$	$f_{al} = \frac{2k_a\varepsilon_{f.rup}t_{frp}E_{frp}}{b}$ $k_a = 1-\frac{2(b-2r)^2+r^2(4-\pi)}{4b^2}$
Benzaid [21]	$f_{MP} = f_{co}+0.58f_{al}$	$f_{al} = \frac{2t_{frp}E_{frp}\eta\varepsilon_{f.rup}}{\sqrt{2}b-2Rc(\sqrt{2}-1)}$
Wang [68]	$f_{MP} = f'_{co}+\psi 3.3\kappa f_{al}$	$f_{al} = \frac{2E_{frp}t_{frp}\varepsilon_{f.rup}}{\sqrt{2}b}$
Wu (2010) [69]	$\frac{f_{MP}}{f_{co}} = 1+2.2\left(\frac{2r}{b}\right)^{0.72}\left(\frac{f_{al}}{f_{co}}\right)^{0.94}$	$f_{al} = \frac{2E_{frp}\varepsilon_{f.rup}t_{frp}}{b}$
Hany [73]	$\frac{f_{MP}}{f_{co}} = 0.7+4.62\left(\frac{A_e}{A_g}\right)\left(\frac{f_{al}}{f_{co}}\right)$	$f_{al} = \frac{2E_{frp}t_{frp}\varepsilon_{f.rup}}{\sqrt{2}b}$
Nisticò [70]	$\frac{f_{MP}}{f_{cc}} = 1+2.142\cdot\frac{f_{al}}{f_{co}}$	$f_{al} = \frac{2E_{frp}\varepsilon_{f.rup}t_{frp}}{b}$
Wei (2012) [74]	$\frac{f_{MP}}{f_{cc}} = 0.5+2.7\left(\frac{2r}{b}\right)^{0.4}\left(\frac{f_{al}}{f_{co}}\right)^{0.73}$	$f_{al} = \frac{2E_{frp}\varepsilon_{f.rup}t_{frp}}{b}$

[a] f_{MP}: the predicted maximum compressive strength of confined concrete; f_{al}:the lateral pressure on concrete from confinement;$\varepsilon_{f.rup}$: Lateral strain in FRP sheets at the point of rupture

Table 7.2 : Ultimate strain functions of the models.

Author	Confined compressive strength	Comments[a]
Ilki [23]	$\varepsilon_{MP} = \varepsilon_{co}\left(1+20\left(\frac{f_{al}}{f_{co}}\right)^{0.5}\right)$	$f_{al} = \frac{2k_a\varepsilon_{f.rup}t_{frp}E_{frp}}{b}$ $k_a = 1-\frac{2(b-2r)^2+r^2(4-\pi)}{4b^2}$
Benzaid [21]	$\varepsilon_{MP} = \varepsilon_{co}\left[2+4\left(\frac{f_{al}}{f_{co}}\right)\right]$	$f_{al} = \frac{2t_{frp}E_{frp}\eta'\varepsilon_{f.rup}}{\sqrt{2}b-2Rc(\sqrt{2}-1)}$,
Pham [72]	$\varepsilon_{MP} = \varepsilon_{co}+\frac{t_{frp}k\sqrt{k_c}\Psi f_f\varepsilon_{f.rup}}{k_s(2f_{co}+3.3k_sf_l)}$	$f_{al} = \frac{\sqrt{2tf_f}}{b}$, $k_s = 1-\frac{2(b-2r)^2}{3\left[b^2-r^2(4-\pi)\right]}$ $\Psi = \frac{[4b-r(8-2\pi)]}{b^2-r^2(4-\pi)}$, $k_c = \frac{\pi r}{2b-r(4-\pi)}$, $k = 6.7$
Hany [73]	$\frac{\varepsilon_{MP}}{\varepsilon_{co}} = 3.89+14.76\left(\frac{A_e}{A_g}\right)\left(\frac{f_{al}}{f'_{co}}\right)$	$f_{al} = \frac{2E_{frp}t_{frp}\varepsilon_{f.rup}}{\sqrt{2}b}$ $\frac{A_e}{A_g} = 1-\frac{2(b-2r)^2}{3A_g}$

[a] ε_{MP}: the predicted ultimate axial strain; $\frac{A_e}{A_g}$: sectional aspect ratio

Table 7.3 : Model predictions for ultimate strength of CFRP-specimens

Group	$(\frac{f_{MP}}{f_{c,h1}(ER)})$						
	[23]	[21]	[68]	[69]	[73]	[70]	[74]
1C	0.91	0.85	0.98	0.95	0.78	0.09	0.32
2C	0.86	0.73	0.94	0.88	0.81	0.12	0.30
AAE (%)	11.08	21.33	4.09	8.45	20.15	10.88	30.83

Table 7.4 : Model predictions for ultimate strain of CFRP-specimens

Group	$(\frac{\varepsilon_{cc}(MP)}{\varepsilon_{cc}(ER)})$			
	[23]	[21]	[72]	[73]
1C	1.10	0.37	0.99	0.71
2C	0.92	0.27	1.00	0.53
AAE (%)	8.80	67.96	0.59	38.07

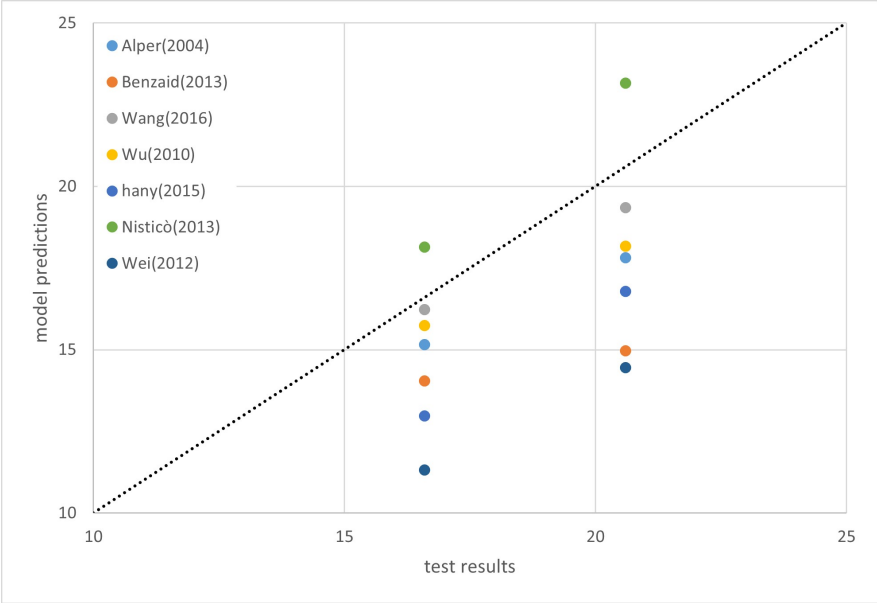

Figure 7.2 : Test results versus model predictions for ultimate axial strength of the CFRP-samples.

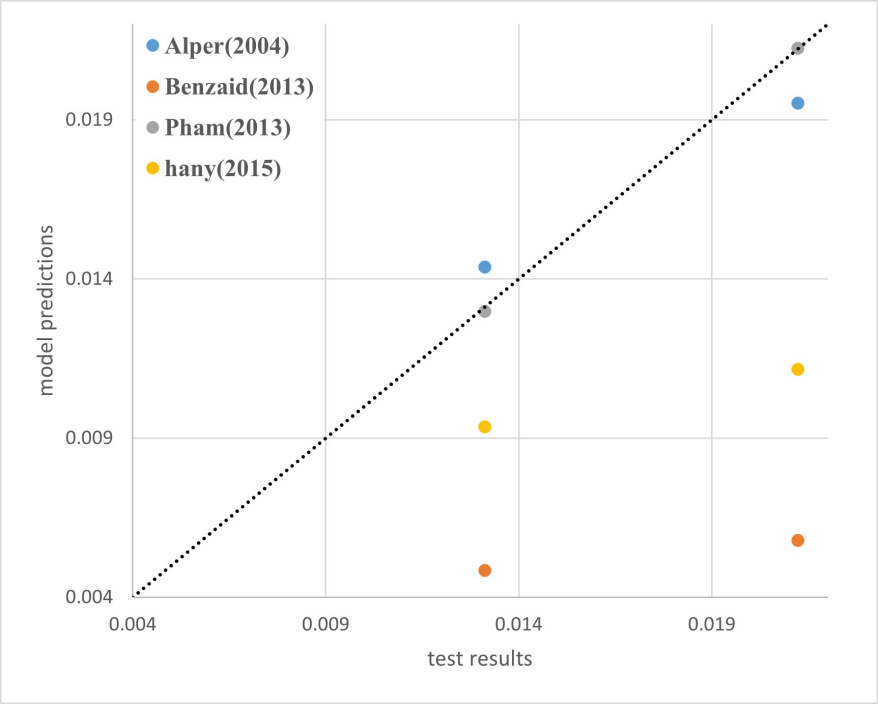

Figure 7.3 : Test results versus model predictions for axial strain of the CFRP-samples.

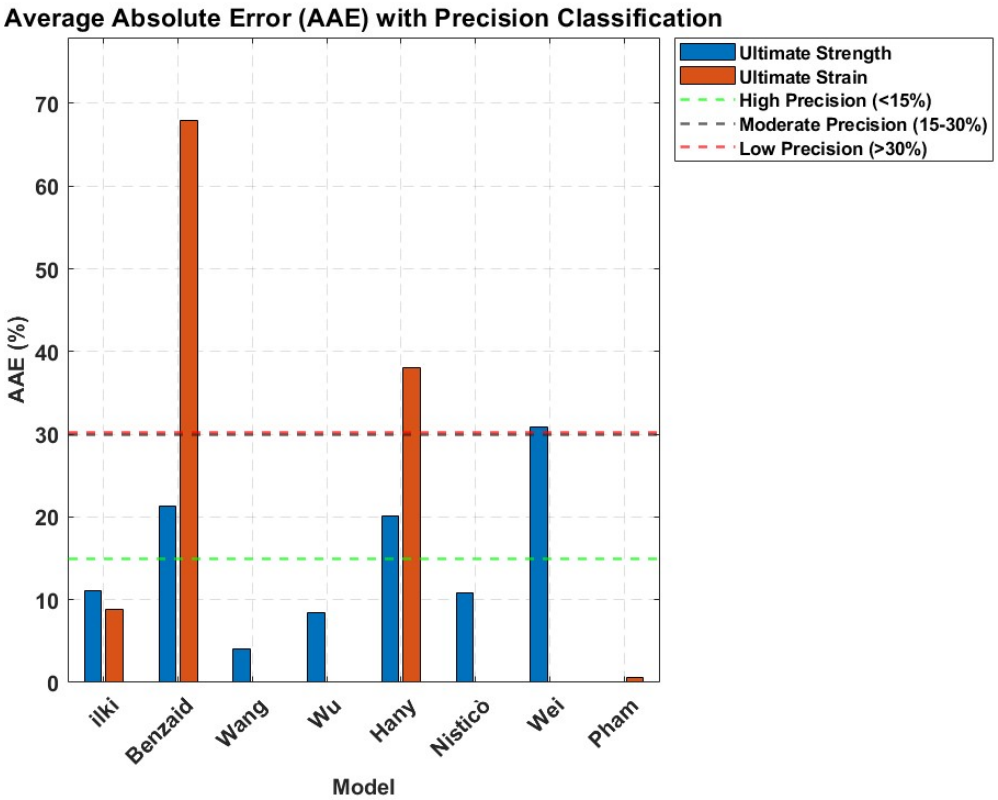

Figure 7.4 : Assessment of Model Accuracy in Predicting Ultimate Strength and Strain: A Comparison Using Average Absolute Error (AAE) of the CFRP-samples.

7.3.2 Estimation of peak axial stress and strain in PET-wrapped specimens

For the PET-wrapped samples, we'll utilize four distinct models to estimate the critical points as shown in Figure 7.5 for the stress-strain curve.The models to estimate the ultimate axial strength of these samples is summarized in Table 7.5.The estimation of ultimate strain is derived from the functions listed in Table 7.6.The outcomes are detailed in Table 7.7-7.10 and visualized in figures 7.6-7.11.

And as can be seen from the results of point 1, Saleem's [75] prediction was superior to that of the other models for both stress and strain prediction. Regarding the final point, Saleem [75], Zeng(2020) [76], and Yuan [77]all achieved a good accuracy in predicting stress, whereas only Yuan [77] accurately predicted strain.

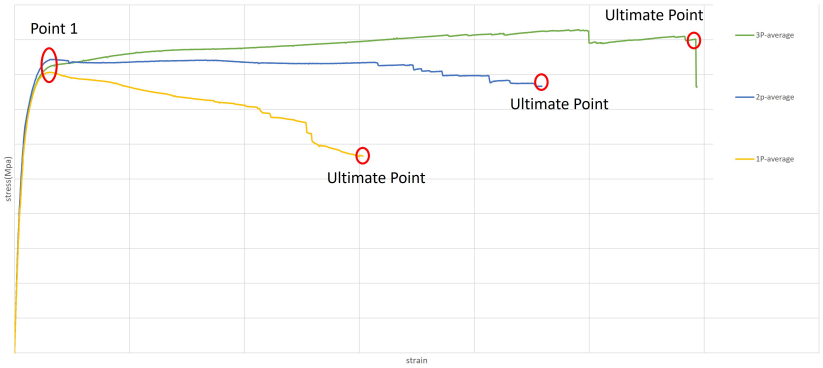

Figure 7.5 : the investigate point of PET-FRP stress vs strain curve

Table 7.5 : Compressive strength functions of the models.

Author	Confined compressive strength	Commends[a]
Saleem [75]	$\frac{f_{MP1}}{f_{co}} = 1 + 0.48\left(\frac{f_{al}}{f'_{co}}\right)^{0.5}$	$f_{al} = \frac{k_a \rho_f e_{f.rup} E_{frp}}{2}$
		$k_a = 1 - \frac{2(b-2r)^2 + r^2(4-\pi)}{4b^2}$
	$\frac{f_{MPu}}{f_{co}} = 0.56 + 3.33\left(\frac{f_{al}}{f_{co}}\right)^{0.5}$	$\rho_f = \frac{2t_{frp}[2(b-2r)+\pi r]}{bh-(4r^2-\pi r^2)}$
Zeng [76]	$f_{MP1} = 1 + 0.5\left(\frac{f_{al}}{f_{co}}\right)$	$f_{al} = \frac{2k_a E_{frp} t_{frp} e_{h,rup}}{\sqrt{2}b}$
		$k_a = 1 - \frac{2(b-2r)^2}{3[b^2-(4-\pi)r^2]}$
	$f_{MPu} = 0.6 + 2\left(\frac{f_{al}}{f'_{co}}\right)^{0.9}\left(\frac{e_{h,rup}}{\varepsilon_{co}}\right)^{0.1}$	
Yuan (softing) [77]	$\frac{f_{MP1}}{f_{co}} = 1.01 + 2.2(0.16 + 0.84\frac{2r}{b})\left(\frac{f_{al}}{f_{co}}\right)$	$f_{al} = \frac{2E_{frp} t_{frp} \varepsilon_{f.rup}}{b}$
	$\frac{f_{MPu}}{f_{co}} = 0.48 + 6.4\left(0.2 + 0.8\frac{2r}{b}\right)\left(\frac{f_{al}}{f_{co}}\right)$	
Yuan (harding) [77]	$\frac{f_{MP1}}{f_{co}} = 1.06 + 0.3\left(2 - \frac{2r}{b}\right)^{3.4}\left(\frac{f_{al}}{f_{co}}\right)$	
	$\frac{f_{MPu}}{f_{co}} = 1 + 2.76\left(2 - \frac{2r}{b}\right)^{1.25}\left(\frac{f_{al}}{f_{co}}\right)$	
Zeng [78]	$\frac{f_{MP1}}{f_{co}} = 1 + 0.761\rho_1\rho_2$	$\rho_1 = \frac{2k_a E_f t_{frp}}{\left(\frac{f_{co}}{\varepsilon_{co}}\right)\sqrt{2}b}$
	$\frac{f_{MPu}}{f_{co}} = \begin{cases} 0.32 + 4.58\rho_{ke}\rho_\varepsilon, & \text{sufficient} \\ 1 + 4.12(\rho_{ke} - 0.004)\rho_\varepsilon, & \text{insufficient} \end{cases}$	$\rho_2 = \frac{e_{h,rup}}{\varepsilon_{co}}$
		$k_a = 1 - \frac{2(b-2r)^2}{3[b^2-(4-\pi)r^2]}$

[a] f_{MP1}: the predicted the peak of compressive strength of confined concrete;f_{MPu}: the predicted compressive strength at the rupture; f_{al}:the lateral pressure on concrete from confinement;$\varepsilon_{f.rup}$: Lateral strain in FRP sheets at the point of rupture

Table 7.6 : strain functions of the PET models.

Author	Confined compressive strength	Commends[a]
Saleem [75]	$\frac{\varepsilon_{MP1}}{\varepsilon_{co}} = 1 + 80\varepsilon_{c,rup}\left(\frac{f_{al}}{f_{co}}\right)$	$f_{al} = \frac{k_a \rho_f e_{f.rup} E_{frp}}{2}$
		$k_a = 1 - \frac{2(b-2r)^2 + r^2(4-\pi)}{4b^2}$
	$\frac{\varepsilon_{MPu}}{\varepsilon_{co}} = 1 + 537\varepsilon_{c,rup}\left(\frac{f_{al}}{f_{co}}\right)^{0.25}\left(0.5 + \frac{2r}{b}\right)^{-1.1}$	$\rho_f = \frac{2t_{frp}[2(b-2r)+\pi r]}{bh-(4r^2-\pi r^2)}$
Zeng [76]	$\frac{\varepsilon_{MP1}}{\varepsilon_{co}} = 1.2 + 1.4\left(\frac{f_{al}}{f_{co}}\right)$	$f_{al} = \frac{2k_a E_{frp} t_{frp} e_{h,rup}}{\sqrt{2}b}$
		$k_a = 1 - \frac{2(b-2r)^2}{3[b^2-(4-\pi)r^2]}$
	$\frac{\varepsilon_{MPu}}{\varepsilon_{co}} = 12 + 0.5\left(\frac{f_{al}}{f'_{co}}\right)^{0.5}\left(\frac{e_{h,rup}}{\varepsilon_{co}}\right)^{1.2}$	
Yuan (softing) [77]	$\frac{\varepsilon_{MP1}}{\varepsilon_{co}} = 2$	$f_{al} = \frac{2E_{frp} t_{frp} \varepsilon_{f.rup}}{b}$
	$\frac{\varepsilon_{MPu}}{\varepsilon_{co}} = 1.75 + 6.1\left(\frac{\varepsilon_{h,rup}}{\varepsilon_{co}}\right)^{0.46}\left(\frac{f_{al}}{f_{co}}\right)^{-0.015}$	
Yuan(harding) [77]	$\frac{\varepsilon_{MP1}}{\varepsilon_{co}} = 2$	
	$\frac{\varepsilon_{MPu}}{\varepsilon_{co}} = 1.75 + 1.5\left(\frac{\varepsilon_{h,rup}}{\varepsilon_{co}}\right)\left(\frac{f_{al}}{f'_{co}}\right)^{0.57}$	
Zeng [78]	$\frac{\varepsilon_{MP1}}{\varepsilon_{co}} = 1 + 0.602\rho_1\rho_2^{1.45}$	$\rho_1 = \frac{2k_a E_f t_{frp}}{\left(\frac{f_{co}}{\varepsilon_{co}}\right)\sqrt{2}b}$
	$\frac{\varepsilon_{MPu}}{\varepsilon_{co}} = 1.75 + 42.99\rho_1^{0.1}\rho_2^{0.1}\left(0.5 + \frac{2r}{b}\right)^{-1.5}$	$\rho_2 = \frac{e_{h,rup}}{\varepsilon_{co}}$
		$k_a = 1 - \frac{2(b-2r)^2}{3[b^2-(4-\pi)r^2]}$

[a] ε_{MP}: the predicted ultimate axial strain; $\frac{A_e}{A_g}$: sectional aspect ratio

Table 7.7 : Model predictions for strength at point 1 of PET-specimens

Group	$\left(\frac{f_{cc}(MP)}{f_{c,h1}(ER)}\right)$				
	[75]	[76]	[77]	[77]	[78]
1p	0.92	0.84	0.91	0.92	0.85
2p	0.92	0.83	0.95	0.93	0.84
3p	0.97	0.87	1.05	0.99	0.89
AAE (%)	6.23	15.14	6.33	5.29	14.17

Table 7.8 : Model predictions for strength at ultimate strain of PET-specimens

Group	$(\frac{f_{cc}(MP)}{f_{c,h1}(ER)})$				
	[75]	[76]	[77]	[77]	[78]
1p	0.95	1.01	0.97	1.38	0.67
2p	0.93	0.96	1.03	1.19	0.72
3p	0.97	0.96	1.11	1.12	0.88
AAE (%)	4.98	3.24	5.72	22.77	24.40

Table 7.9 : Model predictions for strain at point 1 of PET-specimens

Group	$(\frac{\varepsilon_{cc}(MP)}{\varepsilon_{cc}(ER)})$				
	[75]	[76]	[77]	[77]	[78]
1p	0.92	0.84	1.29	1.29	0.74
2p	1.06	0.79	1.13	1.13	0.73
3p	0.95	0.62	0.83	0.83	0.60
AAE (%)	6.04	24.96	19.84	19.84	30.95

Table 7.10 : Model predictions for strain at point 3 of PET-specimens

Group	$(\frac{\varepsilon_{cc}(MP)}{\varepsilon_{cc}(ER)})$				
	[75]	[76]	[77]	[77]	[78]
1p	1.92	1.42	2.07	1.11	3.52
2p	1.28	0.95	1.16	0.90	2.13
3p	1.27	0.96	1.04	1.00	1.99
AAE (%)	48.94	16.97	42.36	7.13	154.47

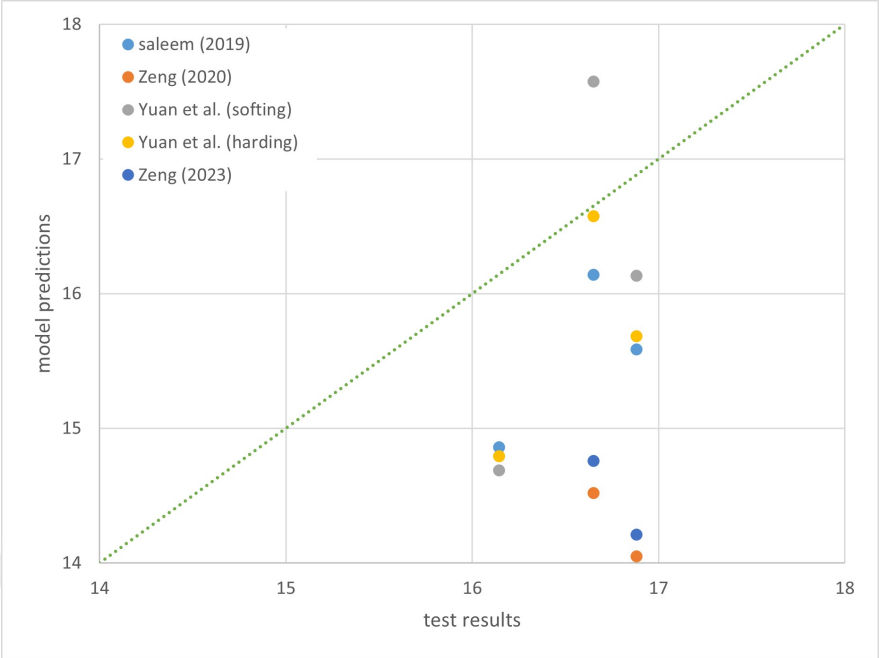

Figure 7.6 : Test results versus model predictions for axial strength of PET-FRP wrapped columns (point 1).

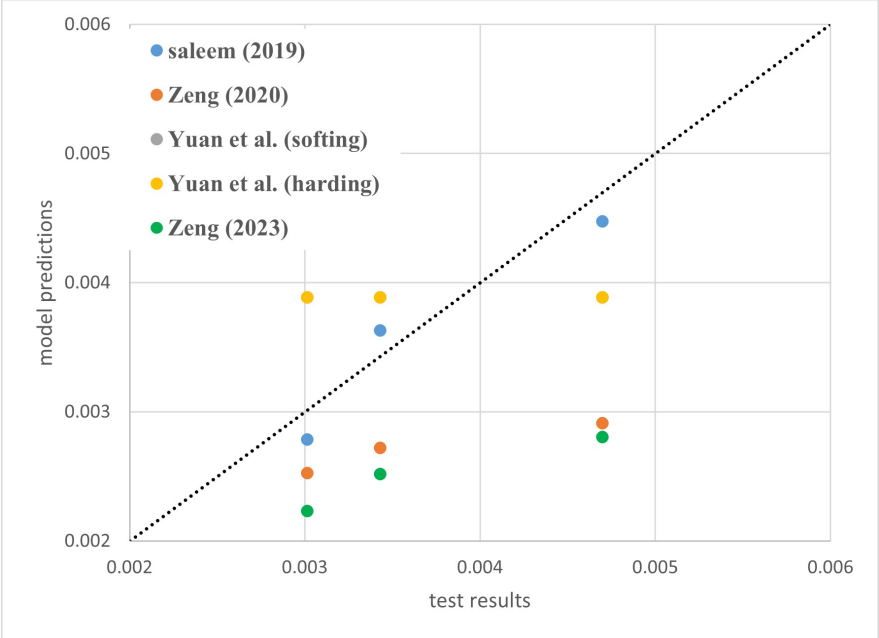

Figure 7.7 : Test results versus model predictions for axial strain of PET-FRP-wrapped columns (point 1).

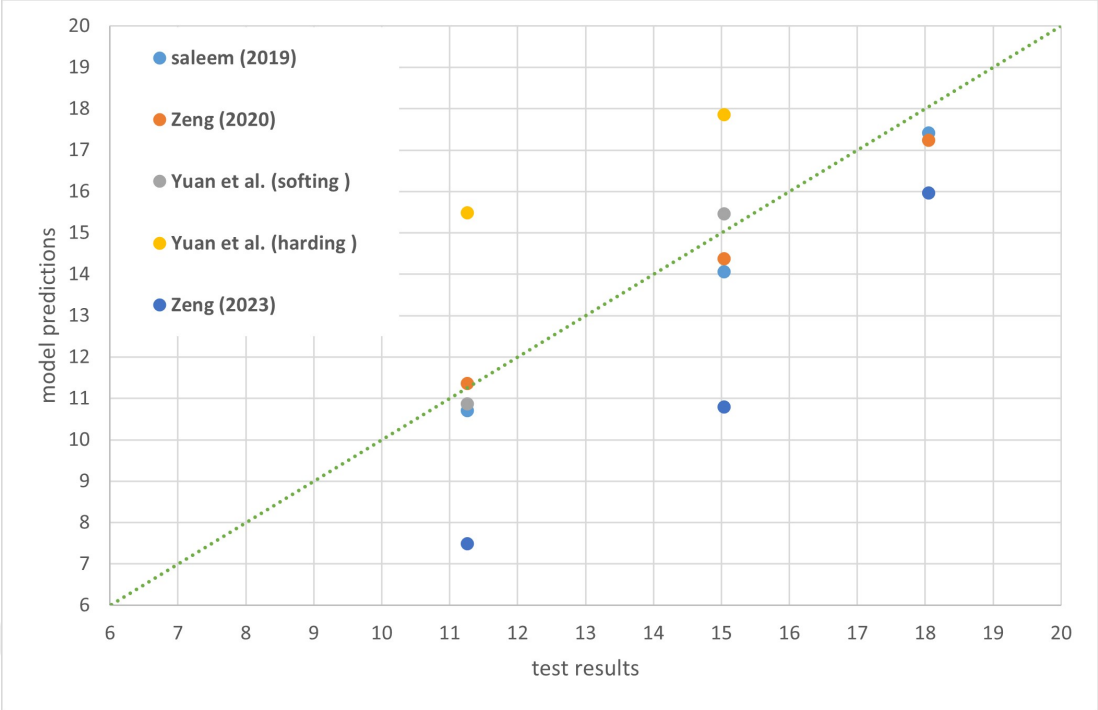

Figure 7.8 : Test results versus model predictions of axial strength at ultimate strain of PET-FRP wrapped specimens.

7.3.3 Estimation of peak axial stress and strain in hybrid-wrapped specimens.

In the study of hybrid-wrapped specimens, we will employ models that have demonstrated proficiency in predicting carbon behavior. This approach is crucial for accurately determining the initial fracture point of carbon. It's essential to take into consideration the confinement pressure of (PET) layers, as highlighted by Ispir *et al.* [58].The outcomes of this approach are detailed in Table 7.11 and demonstrated in figure 7.13-7.15.The models selected to predict the ultimate condition of these specimens are those that effectively forecast the behavior of PET, as discussed in the preceding section. However, a notable modification is the replacement of f_{co} with f_{MP1}, which represents the best estimation of the internal carbon's capture stress. The work of Ispir [58] served as inspiration for this methodology of using models for the hybrid framework. The outcomes of this approach are detailed in Table 7.12.and the results are visualized in figure 7.13,7.14 and 7.16. the critical estimated point shown in figure 7.12.

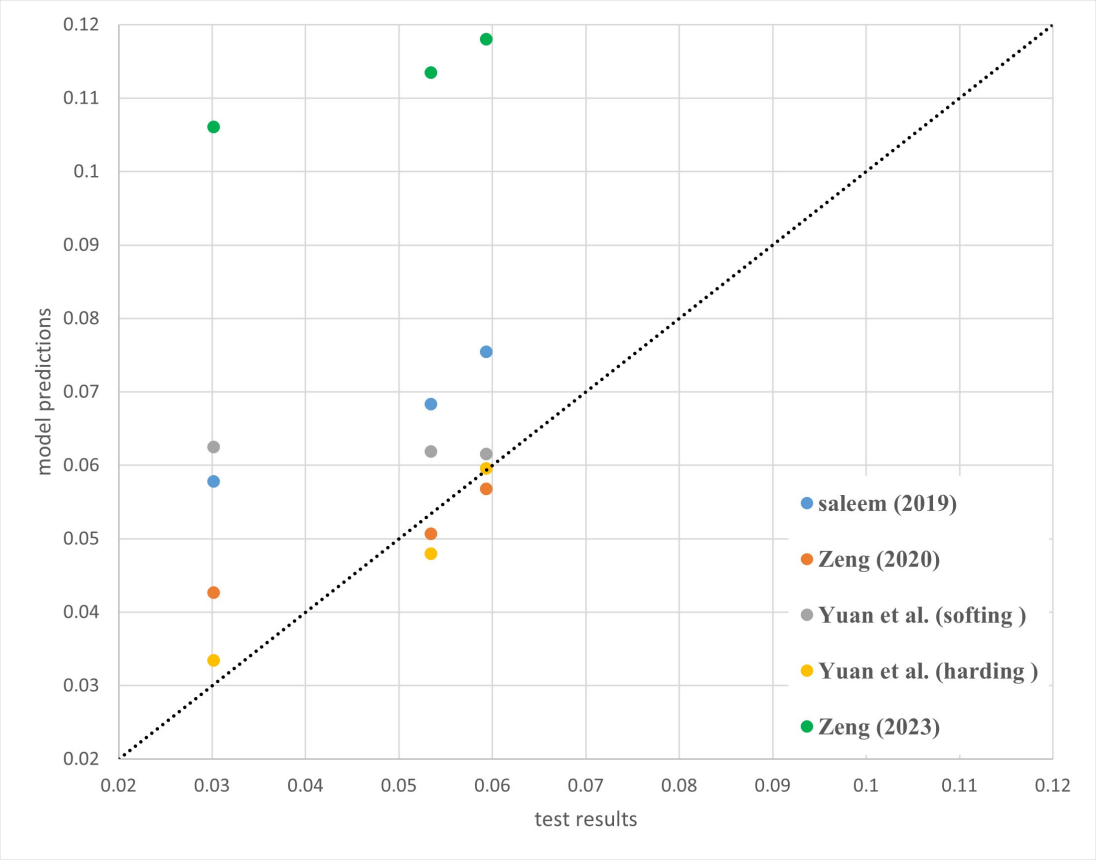

Figure 7.9 : Test results versus model predictions for ultimate axial strain of PET wrapped specimens.

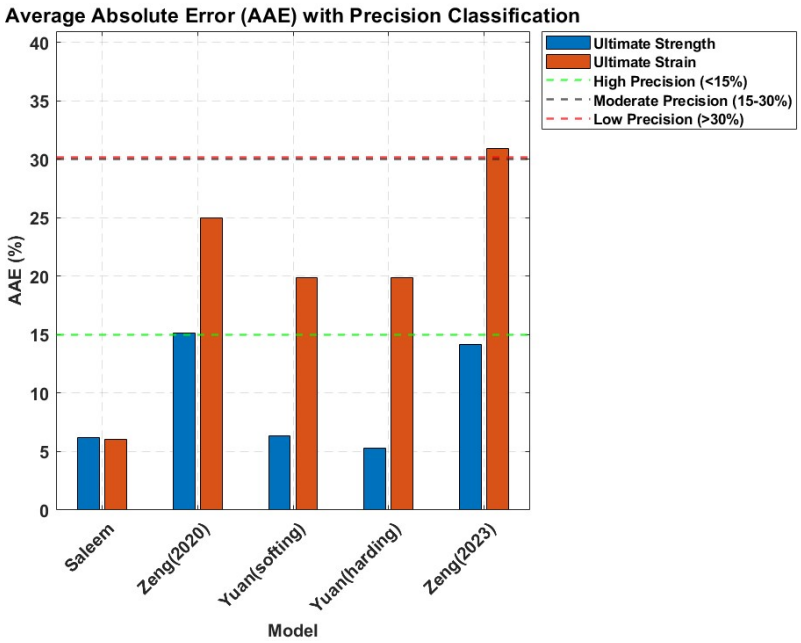

Figure 7.10 : Assessment of Model Accuracy in Predicting First point of PET-FRP Wrapped Specimens

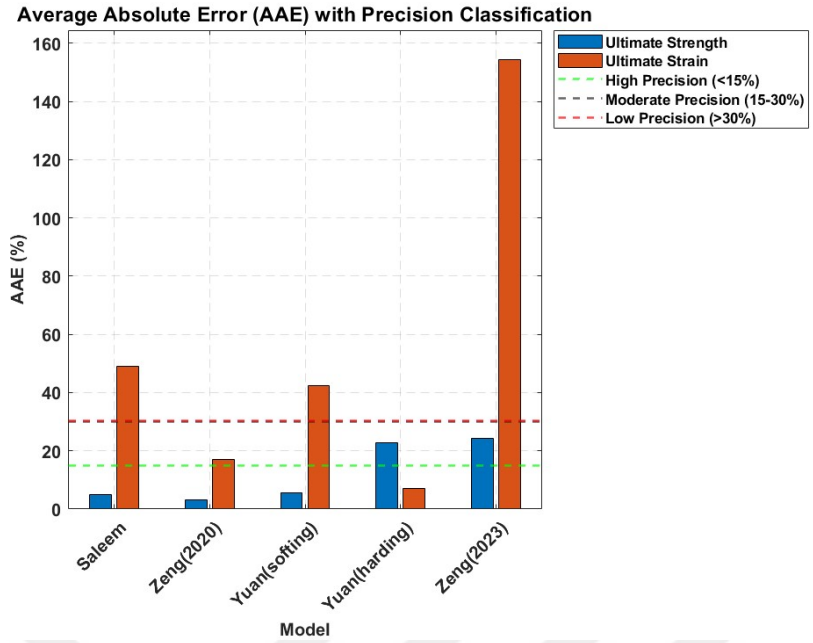

Figure 7.11 : Assessment of Model Accuracy in Predicting second point of PET-FRP Wrapped Specimens

Based on the results of point 1(the point at which the internal layer of carbon ruptures), it is evident that all the selected models [68,69] accurately anticipated stress.However, when it comes to strain, only Ilki [23] demonstrated high accuracy in its predictions. In terms of the estimated final point, all the chosen models [75]–[77] accurately predicted the stress, while only Yuan's [77] model with hardening behaviour moderately predicted the strain. This indicates the necessity of developing a more accurate model that can predict multiple points in the stress-strain relationship.

Table 7.11 : Model predictions at point 1 of hybrid-specimens.

Group	$\left(\frac{f_{MP1}}{f_{ER}}\right)$		$\left(\frac{\varepsilon_{MP1}}{\varepsilon_{ER}}\right)$	
	[68]	[69]	[23]	[72]
1p	0.98	0.93	1.03	1.31
2p	1.01	0.94	0.89	1.36
3p	1.04	0.95	0.88	1.53
AAE (%)	2.05	6.17	7.40	33.32

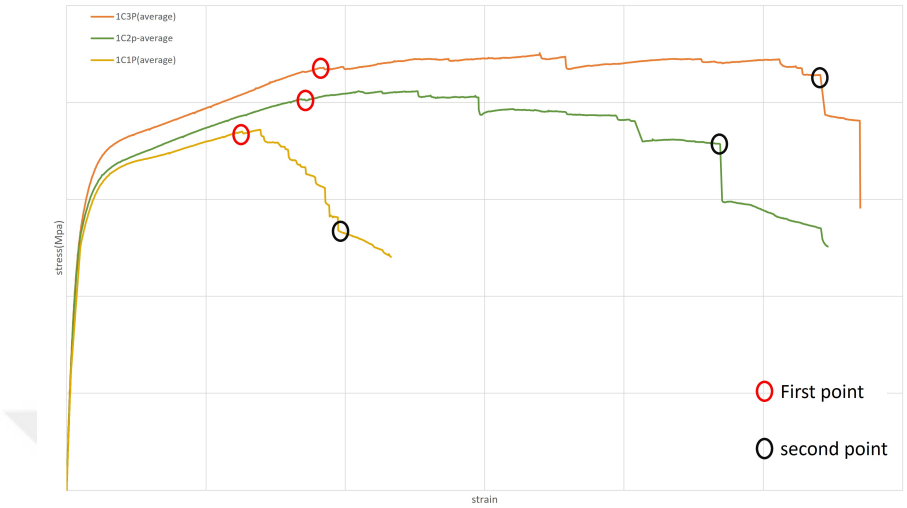

Figure 7.12 : The investigate point of hybrid-FRP stress vs strain curve.

Table 7.12 : Model predictions at the ultimate strain of hybrid-specimens.

Group	$(\frac{f_{MPu}}{f_{ER}})$			$(\frac{\varepsilon_{MPu}}{\varepsilon_{ER}})$
	[75]	[76]	[77]	[77]
1c1p	0.97	1.04	0.95	1.33
1c2p	0.96	1.01	1.00	0.87
1c3p	1.01	1.05	1.10	0.83
AAE (%)	2.82	3.17	4.82	21.01

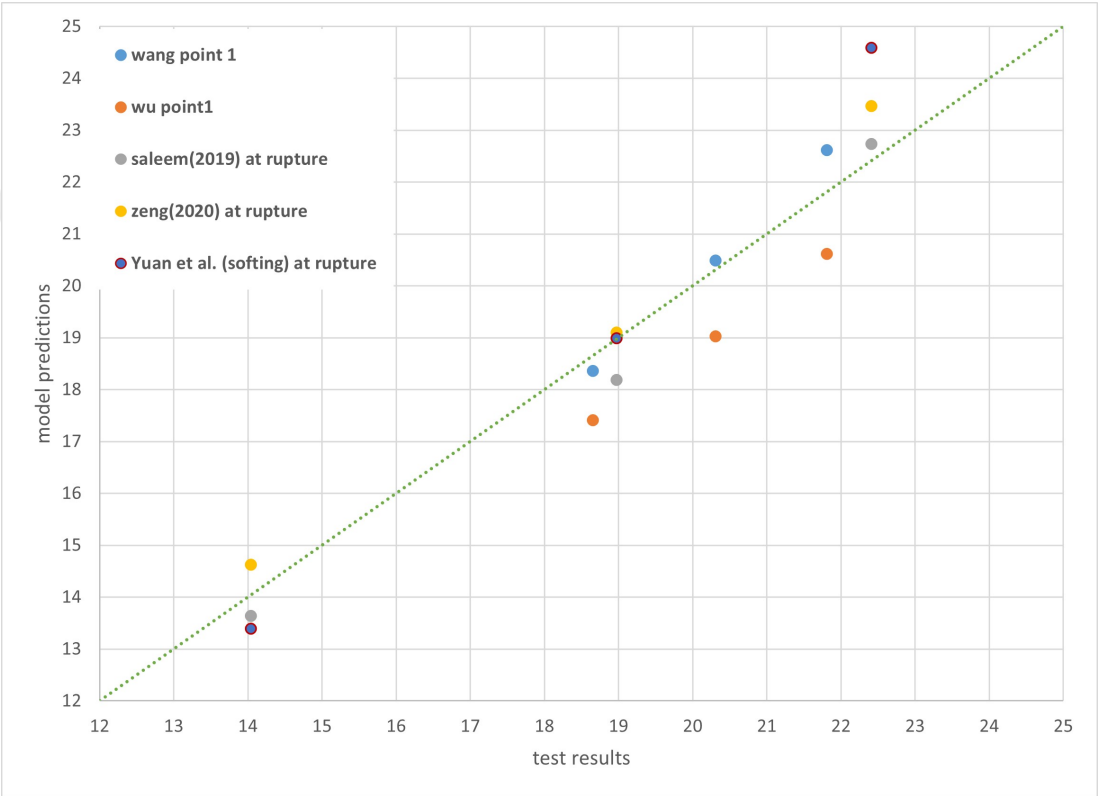

Figure 7.13 : Test results versus model predictions for axial strength of hybrid specimens.

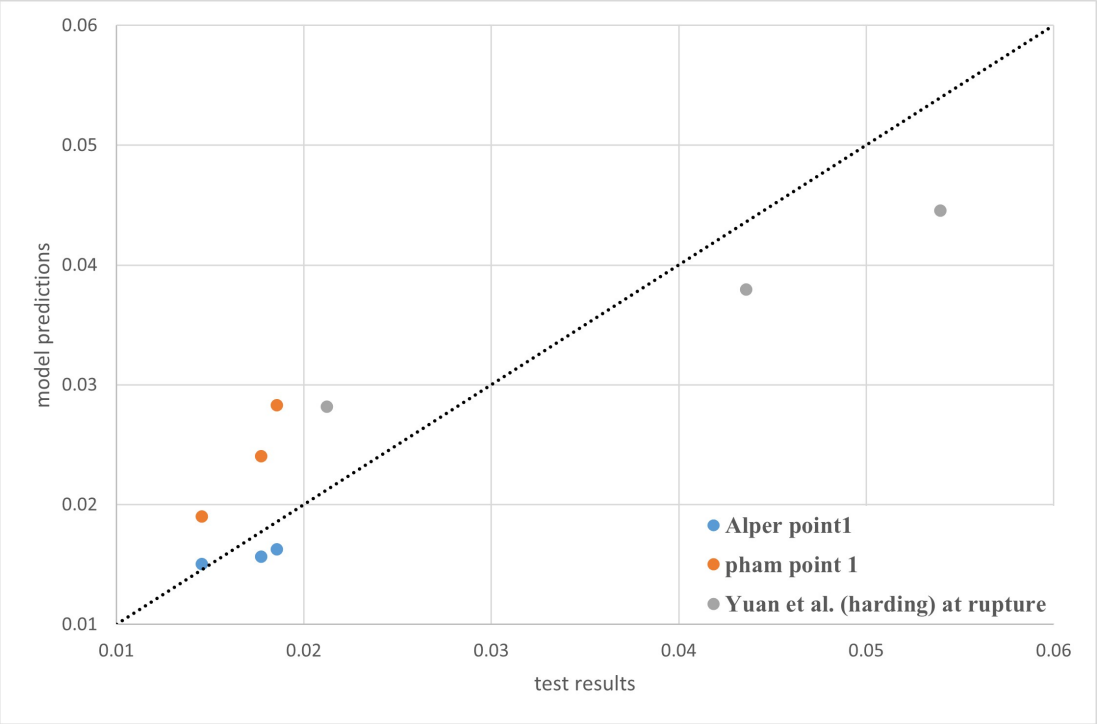

Figure 7.14 : Test results versus model predictions for axial strain of hybrid specimens.

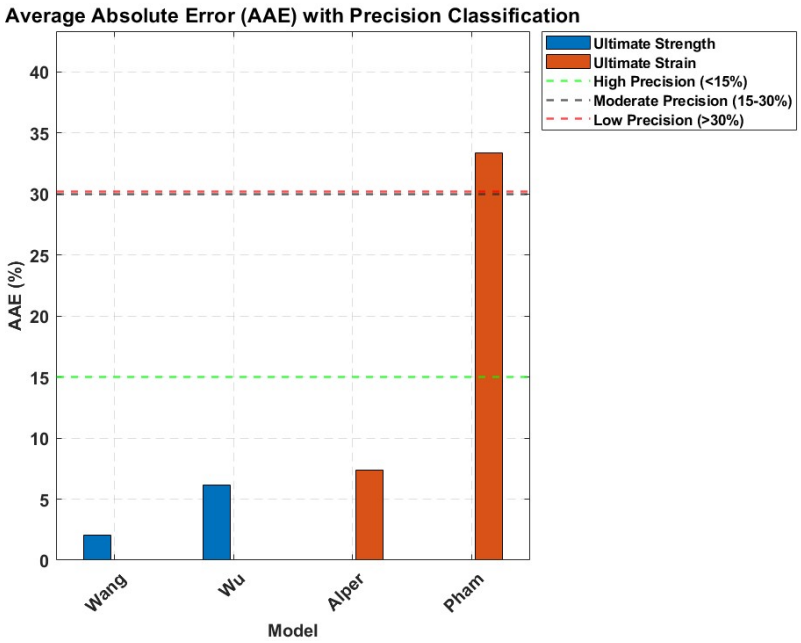

Figure 7.15 : Assessment of model accuracy in predicting ultimate strength and strain at the rupture of the internal CFRP layer: A comparison using AAE.

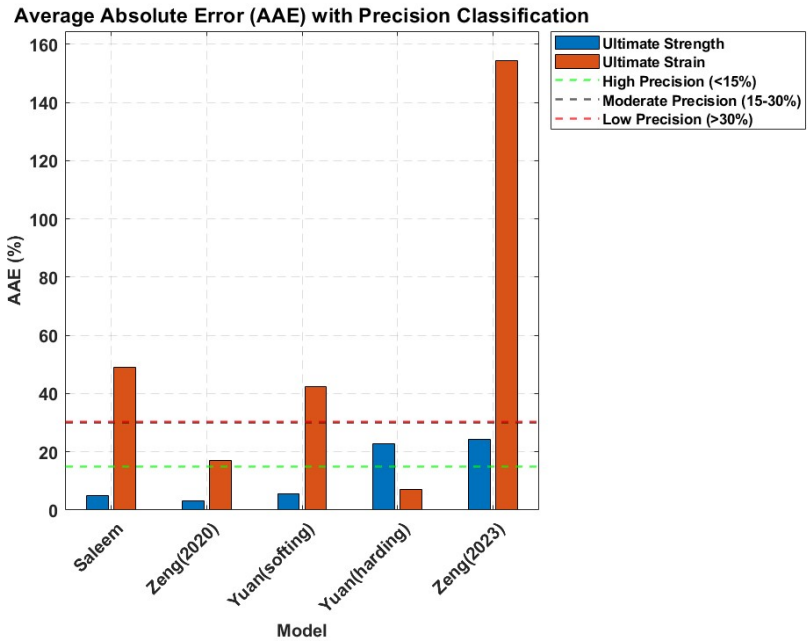

Figure 7.16 : Assessment of model accuracy in predicting ultimate strength and strain: A comparison using AAE.

8. CONCLUSION AND RECOMMENDATION

- The mechanical properties of concrete, such as strength and strain capacities, are significantly improved through the application of CFRP wrapping. This material serves as an efficient reinforcement for structures, providing increased carrying capacity and ductility. Incorporating a second layer of CFRP further amplifies these benefits, although factors like expense, ease of construction, and specific project needs should be considered.

- The study indicates that while PET-FRP layers enhance the strength of concrete specimens, their most significant impact lies in improving ductility. Although the strength increase with PET-FRP is notable, it is less pronounced than with CFRP. The primary benefit of PET-FRP is observed in its substantial contribution to the deformation capabilities of the specimens. This is particularly evident from the significant increase in the ultimate strain and strain at failure, especially in 3P specimens. These findings suggest that PET-FRP is highly effective in scenarios where enhanced ductility and deformation capacity are crucial.

- The research highlights that hybrid-FRP (combining carbon and PET FRP) significantly improves the mechanical properties of concrete. Among the tested groups, the 1C3P configuration demonstrates the most substantial gains in both strength and strain enhancement ratios, indicating the effectiveness of this hybrid approach in strength augmentation. Notably, the benefits in terms of performance become more pronounced with the addition of extra layers of PET-FRP. This suggests a correlation between the number of PET-FRP layers and the extent of mechanical improvements. However, it's important to note that the introduction of a single PET layer does not markedly increase strength following the rupture of the inner carbon layer. In contrast, incorporating two or more PET layers does lead to a modest strength enhancement.

- To accurately measure the hoop strain of PET-FRP, a new method is required. This need arises because strain gauges often lose their functionality before the FRP ruptures. This premature loss of gauge functionality is attributed to the local rupture and high deformability characteristic of this type of fiber. Implementing an alternative measurement technique would ensure more reliable and precise capture of hoop strain data, particularly in the critical phases leading up to the rupture point.". The research conducted by [79] also points out that the utilization of traditional foil strain gauges might result in measurement mistakes, especially because they often separate prior to the collapse of the specimen due to the intricate deformation of spirally wrapped FRP strips. On the other hand, the non-contact technique, notably Particle Image Velocimetry (PIV), has notable benefits in precisely detecting strain. The research has shown a significant connection between the strains detected by the foil strain gauges prior to debonding and the stresses measured using the PIV technique, demonstrating the efficacy of non-contact methods in these types of applications.

- The comprehensive comparison of model predictions with test results for CFRP-wrapped, PET-wrapped, and hybrid-wrapped specimens reveals notable trends and discrepancies that shed light on the predictions of various models and the behavior of these materials under confinement:

  - The models by Ilki [23], Wang [68], Wu [69], and Nestico [70] did a better job of estimating ultimate strength for CFRP-wrapped samples. This shows how reliable they are at capturing the behavior of CFRP confinement, especially in normal-strength concrete settings. Some models, on the other hand, had problems. This could be because they were made using data mostly about normal-strength concrete and didn't take into account how lower-strength concrete behaves differently when it's wrapped with CFRP. Alper [23] and Pham's [72] models were superior in terms of strain prediction, highlighting the need for models that can adjust to the particular stress-strain characteristics of the material.

– In the realm of PET-wrapped samples, Saleem's [75] model outshone others in predicting both stress and strain at critical points, highlighting its comprehensive understanding of PET's behavior under confinement. Other models like Zeng (2020) [76] and Yuan [77] demonstrated excellent accuracy in stress prediction, but only Yuan's [77] model proficiently predicted strain, indicating a gap in the models' ability to predict different aspects of material behavior.

– The study of hybrid-wrapped specimens used models that were good at predicting how carbon would behave to find the initial fracture point of carbon and take into account the pressure of the PET layers. The innovative approach inspired by Ispir *et al.*'s [58] work aimed to refine the prediction of internal carbon's capture stress. While the selected models accurately anticipated stress at the point where the internal layer of carbon ruptures, only Ilki *et al.*'s [23] model showed high accuracy in strain prediction. The final point predictions demonstrated that while stress predictions were generally accurate, strain predictions required refinement, with only Yuan's [77] model moderately capturing the behavior.

  The outcomes highlight the models' varying degrees of predictive success and underscore the complexities of accurately modeling the stress-strain relationship for different material compositions and configurations. Because of the differences in strain predictions, we need to make more complex models that can accurately show how materials behave when they are confined, especially in hybrid frameworks. The insights gained from this comparative analysis are crucial for refining existing models and guiding the development of new predictive models, ensuring a deeper understanding and more accurate prediction of material behavior in structural engineering applications.

REFERENCES

[1] **ASTM** (2002). Standard Test Method for Tensile Properties of Polymer Matrix Composite Materials, **Technical Report**, ASTM International.

[2] **Jain, A.**, **Agrawal, V. and Gupta, R.** (2023). Using serpentine in concrete: A literature review, *Materials Today: Proceedings*.

[3] **Ozturk, M.**, **Arslan, M.H. and Korkmaz, H.H.** (2023). Effect on RC buildings of 6 February 2023 Turkey earthquake doublets and new doctrines for seismic design, *Engineering Failure Analysis*, *153*, 107521.

[4] **Pawlak, A.M.**, **Górny, T.**, **Dopierała, and Paczos, P.** (2022). The Use of CFRP for Structural Reinforcementmdash;Literature Review, *Metals*, *12*(9).

[5] **Natraj, K.**, **Kirthiga, R. and Elavenil, S.** (2023). Structural performance of RCC building and strengthening the structural members with CFRP, *Materials Today: Proceedings*, *84*, 24–32, third International Conference on Sustainable Energy Solutions for a Better Tomorrow.

[6] **Masuelli, M.A.**, (2013). Introduction of fibre-reinforced polymers- polymers and composites: concepts, properties and processes, Fiber reinforced polymers-the technology applied for concrete repair, IntechOpen.

[7] **Tiwary, A.K.**, **Singh, S.**, **Kumar, R.**, **Sharma, K.**, **Chohan, J.S.**, **Sharma, S.**, **Singh, J.**, **Kumar, J. and Deifalla, A.F.** (2022). Comparative Study on the Behavior of Reinforced Concrete Beam Retrofitted with CFRP Strengthening Techniques, *Polymers*, *14*(19).

[8] **Mosallam, A.S. and Mosalam, K.M.** (2003). Strengthening of two-way concrete slabs with FRP composite laminates, *Construction and Building Materials*, *17*(1), 43–54, structural Applications of FRP Compostites.

[9] **Kalyoncuoglu, A.**, **Ghaffari, P.**, **Goksu, C. and Ilki, A.** (2013). Rehabilitation of Corrosion-Damaged Substandard RC Columns Using FRP Sheets, *Advances in Civil Infrastructure Engineering*, volume639 of *Advanced Materials Research*, Trans Tech Publications Ltd, pp.1096–1103.

[10] **Li, B.**, **Qian, K. and Tran, C.T.N.** (2013). Retrofitting Earthquake-Damaged RC Structural Walls with Openings by Externally Bonded FRP Strips and Sheets, *Journal of Composites for Construction*, *17*(2), 259–270.

[11] **Lynn, A.C.**, **Moehle, J.P.**, **Mahin, S.A. and Holmes, W.T.** (1996). Seismic evaluation of existing reinforced concrete building columns, *Earthquake Spectra*, *12*(4), 715–739.

[12] **Cao, Y.G.**, **Jiang, C. and Wu, Y.F.** (2016). Cross-sectional unification on the stress-strain model of concrete subjected to high passive confinement by fiber-reinforced polymer, *Polymers*, *8*(5), 186.

[13] **Jiang, J.**, **Li, P. and Nistico, N.** (2019). Local and global prediction on stress-strain behavior of FRP-confined square concrete sections, *Composite Structures*, *226*, 111205.

[14] **Jin, L.**, **Chen, H.**, **Wang, Z. and Du, X.** (2020). Size effect on axial compressive failure of CFRP-wrapped square concrete columns: Tests and simulations, *Composite Structures*, *254*, 112843.

[15] **Wang, D.**, **Wang, Z.**, **Smith, S. and Yu, T.** (2016). Size effect on axial stress-strain behavior of CFRP-confined square concrete columns, *Construction and Building Materials*, *118*, 116–126.

[16] **Al-Rousan, R.Z. and AL-Tahat, M.F.** (2019). Consequence of surface preparation techniques on the bond behavior between concrete and CFRP composites, *Construction and Building Materials*, *212*, 362–374.

[17] **Gambarelli, S.**, **Nisticò, N. and Ožbolt, J.** (2014). Numerical analysis of compressed concrete columns confined with CFRP: Microplane-based approach, *Composites Part B: Engineering*, *67*, 303–312.

[18] **Nisticò, N.**, **Pallini, F.**, **Rousakis, T.**, **Wu, Y.F. and Karabinis, A.** (2014). Peak strength and ultimate strain prediction for FRP confined square and circular concrete sections, *Composites Part B: Engineering*, *67*, 543–554.

[19] **de Diego, A.**, **Arteaga, Á. and Fernández, J.** (2019). Strengthening of square concrete columns with composite materials. Investigation on the FRP jacket ultimate strain, *Composites Part B: Engineering*, *162*, 454–460.

[20] **Concrete Society** (2012). Design guidance for strengthening concrete structures using fibre composite materials, **Technical Report TR55**, Concrete Society, UK.

[21] **Benzaid, R. and Mesbah, H.A.** (2013). Strength model for square concrete columns confined by external CFRP sheets, *Structural Engineering and Mechanics*, *46*(1), 111–135.

[22] **Benzaid, R.**, **Mesbah, H.A. and Amel, B.** (2016). Experimental investigation of concrete externally confined by CFRP composites, *Proceedings of the 5th International Conference on Integrity-Reliability-Failure (IRF), Porto, Portugal*, pp.24–28.

[23] **Ilki, A.**, **Kumbasar, N. and Koc, V.** (2004). Low Strength Concrete Members Externally Confined with FRP Sheets, *Structural Engineering and Mechanics*, *18*(2), 167–194.

[24] **Smith, S.T.**, **Kim, S.J. and Zhang, H.** (2010). Behavior and Effectiveness of FRP Wrap in the Confinement of Large Concrete Cylinders, *Journal of Composites for Construction*, *14*(5), 573–582.

[25] **Isleem, H.F.**, **Peng, F. and Tayeh, B.A.** (2022). Confinement model for LRS FRP-confined concrete using conventional regression and artificial neural network techniques, *Composite Structures*, *279*, 114779.

[26] **Mohammadi, M.**, **Bai, Y.L.**, **Yang, H.L.**, **Lin, G.**, **Dai, J.G. and Zhang, Y.F.** (2022). FE modeling of Non-circular LRS FRP-confined concrete columns, *Composite Structures*, *286*, 115314.

[27] **Bai, Y.L.**, **Dai, J.G.**, **Mohammadi, M.**, **Lin, G. and Mei, S.J.** (2019). Stiffness-based design-oriented compressive stress-strain model for large-rupture-strain (LRS) FRP-confined concrete, *Composite Structures*, *223*, 110953.

[28] **Bai, Y.L.**, **Bai, S.C.**, **Mei, S.J.**, **Jia, J.F. and Yang, K.** (2023). Seismic behavior of RC square columns strengthened with LRS FRP under high axial load ratio, *Structures*, volume 56, Elsevier, p.104867.

[29] **Saleem, S.**, **Pimanmas, A.**, **Qureshi, M.I. and Rattanapitikon, W.** (2021). Axial Behavior of PET FRP-Confined Reinforced Concrete, *Journal of Composites for Construction*, *25*(1), 04020079.

[30] **Bai, Y.L.**, **Zhang, Y.F.**, **Jia, J.F.**, **Han, Q.**, **Du, X.L. and Ozbakkaloglu, T.** (2022). Compressive behavior of large-scale PEN and PET FRP–confined RC columns with square cross sections, *Journal of Composites for Construction*, *26*(4), 04022034.

[31] **Nain, M.**, **Abdulazeez, M.M. and ElGawady, M.A.** (2020). Behavior of high strength concrete–filled hybrid large–small rupture strains FRP tubes, *Engineering Structures*, *209*, 110264.

[32] **Bai, Y.L.**, **Liu, S.Z. and Mei, S.J.** (2024). Compressive behavior and modeling of concrete wrapped by hybrid low-high elongation capacities FRP, *Engineering Structures*, *300*, 117155.

[33] **Chaiyasarn, K.**, **Hussain, Q.**, **Joyklad, P. and Rodsin, K.** (2021). New hybrid basalt/E-glass FRP jacketing for enhanced confinement of recycled aggregate concrete with clay brick aggregate, *Case Studies in Construction Materials*, *14*, e00507.

[34] **Shen, Z.**, **Liu, W. and Zhang, Q.** (2023). Tensile behavior of high-performance interlayer hybrid composites of polypropylene and glass fiber for civil engineering, *Construction and Building Materials*, *403*, 133017.

[35] **Tang, W.**, **Liu, Z.**, **Lu, Y. and Li, S.** (2022). Hybrid confinement mechanism of large-small rupture strain FRP on concrete cylinder, *Journal of Building Engineering*, *51*, 104335.

[36] **Ispir, M.**, **Dalgic, K.D. and Ilki, A.** (2021). Cyclic Compressive Behavior of Hybrid FRP-Confined Concrete, *Journal of Composites for Construction*, *25*(5), 04021045.

[37] **Türk Standardı** (2010). ASTM C469/C469M-10Standard test method for static modulus of elasticity and poisson's ratio of concrete in compression., **Technical Report**, ASTM International, West Conshohocken, PA, USA.

[38] **Al-Nimry, H.S. and Ghanem, A.M.** (2017). FRP confinement of heat-damaged circular RC columns, *International Journal of Concrete Structures and Materials*, *11*, 115–133.

[39] **Qaidi, S.**, **Al-Kamaki, Y.S.**, **Al-Mahaidi, R.**, **Mohammed, A.S.**, **Ahmed, H.U.**, **Zaid, O.**, **Althoey, F.**, **Ahmad, J.**, **Isleem, H.F. and Bennetts, I.** (2022). Investigation of the effectiveness of CFRP strengthening of concrete made with recycled waste PET fine plastic aggregate, *PLoS One*, *17*(7), e0269664.

[40] **Motavalli, M.**, **Czaderski, C.**, **Schumacher, A. and Gsell, D.**, (2010). 4 - Fibre reinforced polymer composite materials for building and construction, **G. Pohl**, editor, Textiles, Polymers and Composites for Buildings, Woodhead Publishing Series in Textiles, Woodhead Publishing, pp.69–128.

[41] **Soutis, C.** (2005). Fibre reinforced composites in aircraft construction, *Progress in aerospace sciences*, *41*(2), 143–151.

[42] **Zeng, J.J.**, **Gao, W.Y.**, **Duan, Z.J.**, **Bai, Y.L.**, **Guo, Y.C. and Ouyang, L.J.** (2020). Axial compressive behavior of polyethylene terephthalate/carbon FRP-confined seawater sea-sand concrete in circular columns, *Construction and Building Materials*, *234*, 117383.

[43] **Kitane, Y.**, **Aref, A.J. and Lee, G.C.** (2004). Static and fatigue testing of hybrid fiber-reinforced polymer-concrete bridge superstructure, *Journal of Composites for Construction*, *8*(2), 182–190.

[44] **Van Krevelen, D. and Te Nijenhuis, K.**, (2009). Chapter 13 - Mechanical Properties of Solid Polymers, **D. Van Krevelen and K. Te Nijenhuis**, editors, Properties of Polymers (Fourth Edition), Elsevier, Amsterdam, fourth edition edition, pp.383–503.

[45] **American Concrete Institute** (2012). *Guide test methods for fiber-reinforced polymers (FRPs) for reinforcing or strengthening concrete structures*.

[46] **Adams, D.O. and Adams, D.F.** (2002). Tabbing Guide for Composite Test Specimens, **Technical Report**, Federal Aviation Administration.

[47] **Lechat, C.**, **Bunsell, A.R. and Davies, P.** (2011). Tensile and creep behaviour of polyethylene terephthalate and polyethylene naphthalate fibres, *Journal of Materials Science*, *46*, 528–533.

[48] **Hawileh, R.A.**, **Mhanna, H.H.**, **Al Rashed, A.**, **Abdalla, J.A. and Naser, M.** (2022). Flexural behavior of RC beams externally bonded with polyethylene terephthalate (PET) fiber reinforced polymer (FRP) laminates, *Engineering Structures*, *256*, 114036.

[49] **Mhanna, H.H.**, **Hawileh, R.A.**, **Abuzaid, W.**, **Naser, M. and Abdalla, J.A.** (2020). Experimental investigation and modeling of the thermal effect on the mechanical properties of polyethylene-terephthalate FRP laminates, *Journal of Materials in Civil Engineering*, *32*(10), 04020296.

[50] **C09 Committee** (2014). Test method for static modulus of elasticity and poissons ratio of concrete in compression, **Technical Report**, ASTM International, West Conshohocken, PA.

[51] **Türk Standardı** (2014). TS500 Betonarme Yapıların Tasarım ve Yapım Kuralları, **Technical Report**, Türk Standardı Enstitüsü, Ankara, Türkiye.

[52] **CEN/TC 104** (2013). SIST EN 12390-13:2014 - Testing hardened concrete - Part 13: Determination of secant modulus of elasticity in compression, **Technical Report**, European Committee for Standardization, Brussels.

[53] **abd allah Abd elaty, M.** (2014). Compressive strength prediction of Portland cement concrete with age using a new model, *HBRC Journal*, *10*(2), 145–155.

[54] **Ispir, M.**, **Ates, A.O. and Ilki, A.** (2022). Low strength concrete: Stress-strain curve, modulus of elasticity and tensile strength, *Structures*, *38*, 1615–1632.

[55] **Lam, L. and Teng, J.G.** (2003). Design-oriented stress–strain model for FRP-confined concrete, *Construction and building materials*, *17*(6-7), 471–489.

[56] **Pekgöz, M.**, **uslu, M. and Tekin, İ.** (2020). An In-Situ Study on The Specimen Size Effects on Compressive Strength for Different Strength Concretes, *Journal of Cement Based Composites*, *3*, 7–10.

[57] **Yi, S.T.**, **Yang, E.I. and Choi, J.C.** (2006). Effect of specimen sizes, specimen shapes, and placement directions on compressive strength of concrete, *Nuclear Engineering and Design*, *236*(2), 115–127.

[58] **Ispir, M.**, **Dalgic, K.D. and Ilki, A.** (2018). Hybrid confinement of concrete through use of low and high rupture strain FRP, *Composites Part B: Engineering*, *153*, 243–255.

[59] **Asad-ur Rehman Khan, S.F. and Zahid, B.** (2022). Use of high strength technical textiles in strengthening of reinforced concrete structural elements, *The Journal of The Textile Institute*, *113*(2), 281–291.

[60] **Mier, J.G.M.V.** (1998). Failure of Concrete under Uniaxial Compression: An Overview, *FraMCoS-3*, Aedificatio, Gifu, pp.1169–1183.

[61] **Wang, L.M. and Wu, Y.F.** (2008). Effect of corner radius on the performance of CFRP-confined square concrete columns: Test, *Engineering Structures*, *30*(2), 493–505.

[62] **Chaallal, O.**, **Shahawy, M. and Hassan, M.** (2003). Performance of Axially Loaded Short Rectangular Columns Strengthened with Carbon Fiber-Reinforced Polymer Wrapping, *Journal of Composites for Construction*, *7*(3), 200–208.

[63] **Rochette, P. and Labossière, P.** (2000). Axial Testing of Rectangular Column Models Confined with Composites, *Journal of Composites for Construction*, *4*(3), 129–136.

[64] **Wang, Z.**, **Wang, D. and Smith, S.T.** (2012). Size effect of square concrete columns confined with CFRP wraps, *Proceedings of the 3rd Asia-Pacific Conference on FRP in Structures*, Sapporo.

[65] **Lim, J.C. and Ozbakkaloglu, T.** (2014). Hoop strains in FRP-confined concrete columns: experimental observations, *Materials and Structures*, *48*(9), 2839–2854.

[66] **Chen, J.F.**, **Ai, J. and Stratford, T.J.** (2010). Effect of Geometric Discontinuities on Strains in FRP-Wrapped Columns, *Journal of Composites for Construction*, *14*(2), 136–145.

[67] **Wu, Y.F. and Zhou, Y.W.** (2010). Unified strength model based on Hoek-Brown failure criterion for circular and square concrete columns confined by FRP, *Journal of Composites for Construction*, *14*(2), 175–184.

[68] **Wang, D.**, **Wang, Z.**, **Smith, S.T. and Yu, T.** (2016). Size effect on axial stress-strain behavior of CFRP-confined square concrete columns, *Construction and Building Materials*, *118*, 116–126.

[69] **Wu, Y.F. and Wei, Y.Y.** (2010). Effect of cross-sectional aspect ratio on the strength of CFRP-confined rectangular concrete columns, *Engineering Structures*, *32*(1), 32–45.

[70] **Nisticò, N. and Monti, G.** (2013). RC square sections confined by FRP: Analytical prediction of peak strength, *Composites Part B: Engineering*, *45*(1), 127–137.

[71] **Ilki, A.**, **Peker, O.**, **Karamuk, E.**, **Demir, C. and Kumbasar, N.** (2008). FRP retrofit of low and medium strength circular and rectangular reinforced concrete columns, *Journal of Materials in Civil Engineering*, *20*(2), 169–188.

[72] **Pham, T.M. and Hadi, M.N.** (2013). Strain estimation of CFRP-confined concrete columns using energy approach, *Journal of Composites for Construction*, *17*(6), 04013001.

[73] **Hany, N.F.**, **Hantouche, E.G. and Harajli, M.H.** (2015). Axial stress-strain model of CFRP-confined concrete under monotonic and cyclic loading, *Journal of Composites for Construction*, *19*(6), 04015004.

[74] **Wei, Y.Y. and Wu, Y.F.** (2012). Unified stress–strain model of concrete for FRP-confined columns, *Construction and Building Materials*, *26*(1), 381–392.

[75] **Pimanmas, A. and Saleem, S.** (2019). Evaluation of existing stress–strain models and modeling of PET FRP–confined concrete, *Journal of Materials in Civil Engineering*, *31*(12), 04019303.

[76] **Zeng, J.J.**, **Duan, Z.J.**, **Gao, W.Y.**, **Bai, Y.L. and Ouyang, L.J.** (2020). Compressive behavior of FRP-wrapped seawater sea-sand concrete with a square cross-section, *Construction and Building Materials*, *262*, 120881.

[77] **Yuan, W.Y.**, **Han, Q. and Bai, Y.L.** (2022). A unified stress-strain model for LRS FRP-confined concrete columns with square and circular cross-sections, *Engineering Structures*, *255*, 113900.

[78] **Zeng, J.J.**, **Liao, J.**, **Zhu, D.H. and Li, P.D.** (2023). Axial compressive behavior and design-oriented model for large-rupture-strain (LRS) FRP-confined concrete in rectangular columns, *Journal of Building Engineering*, 106925.

[79] **Chen, G.**, **Fu, M.**, **Zhang, J.**, **Lin, G.**, **Chen, J. and Jiang, T.** (2023). FRP spiral strip-confined concrete columns: Stress-strain behavior and size effect, *Structures*, *57*, 105223.

CURRICULUM VITAE

Bilal Ibrahim Majeed AL-OUBAIDI

EDUCATION:

- **M.Sc.:** 2024, Istanbul Technical University (Turkiye), Graduate School, Structural Engineering.
- **B.Sc.:** 2018, University of Technology, Civil Engineering

RESEARCH EXPERIENCE:

- 2022 - present, Graduate research in Tubitak Project No. 221M159

PUBLICATIONS, PRESENTATIONS AND PATENTS:

- Khattab, M. M., **Al-Oubaidi, B.**, and Abduljaleel, Y. W. .The Prediction of Compressive Strength of Concrete Containing Recycled Aggregate with Different Machine Learning Algorithms.

- **Bilal Al-Oubaidi**, İsmail Sencar, Ali Gürkan Genç, Medine Ispir, Korhan Deniz Dalgıç, and Alper Ilki. Mechanical Properties of Hybrid FRP Composites Used for Confinement of Concrete. INTERNATIONAL GRADUATE RESEARCH SYMPOSIUM - IGRS'23.
- Khattab, M. M., **Al-Oubaidi, B.**, and Abduljaleel, Y. W. . The Prediction of Compressive Strength of Concrete Containing Recycled Aggregate with Different Machine Learning Algorithms. 6TH INTERNATIONAL CONFERENCE ON ENGINEERING SCIENCES - ICES'23